The Effect of Nickel and Nitrogen on Void Formation in Vanadium

Randy George Lott

July 1979

UWFDM-280

Ph.D. thesis.

FUSION TECHNOLOGY INSTITUTE

UNIVERSITY OF WISCONSIN

MADISON WISCONSIN

The Effect of Nickel and Nitrogen on Void Formation in Vanadium

Randy George Lott

Fusion Technology Institute
University of Wisconsin
1500 Engineering Drive
Madison, WI 53706

http://fti.neep.wisc.edu

July 1979

UWFDM-280

Ph.D. thesis.

THE EFFECT OF NICKEL AND NITROGEN ON VOID FORMATION IN VANADIUM

BY

RANDY GEORGE LOTT

A thesis submitted in partial fulfillment of the

requirements for the degree of

DOCTOR OF PHILOSOPHY

(Nuclear Engineering)

at the

UNIVERSITY OF WISCONSIN-MADISON

1979

TABLE OF CONTENTS

TABLE OF CONTENTS (continued)

ABSTRACT

THE EFFECT OF NICKEL AND NITROGEN ON VOID FORMATION IN VANADIUM

Randy George Lott

Under the supervision of Professor Gerald L. Kulcinski

Vanadium alloys are being considered for structural materials in fusion reactors because they combine good mechanical properties with an apparent resistance to radiation damage. The objective of this thesis is to demonstrate how alloying additions affect the microstructural response of vanadium to irradiation. The effects of 1 atomic percent nickel and 1 atomic percent nitrogen additions on void and precipitate formation in copper ion irradiated vanadium were determined. Nickel and nitrogen were chosen for this study because they represent two different classes of alloys and because they are both important contaminants in vanadium systems. These results are compared to current theories of void nucleation and void growth.

No neutron source presently available can reproduce the intense fluxes of high energy that will occur in fusion reactor environments. It is, therefore, crucial to the fusion program that alternative methods of irradiation be developed to evaluate the behavior of materials in high damage states. In this study, a high temperature, high vacuum facility was designed and constructed for heavy ion irradiation using the University of Wisconsin tandem accelerator. This facility provides the well characterized, high vacuum environment required for irradiations of vanadium and other refractory metals.

Samples of high purity vanadium, V-1% Ni and V-1% N were irradiated to doses between 1 dpa and 10 dpa at 450°C, 550°C and 650°C. The displacement rate for these irradiations was approximately 5×10^{-4} dpa/sec. All of the irradiations were performed in a high vacuum of less than 10^{-8} Torr. Subsequent analysis was performed using transmission electron microscopy and energy dispersive X-ray analysis.

Voids were observed in all of the irradiated pure vanadium specimens. A decrease in void swelling and density was observed in specimens irradiated at 450°C and 550°C to doses in excess of 2 dpa. This decrease in swelling can be attributed to the formation of a void coating which inhibits vacancy migration to the void. Voids were also observed in pure vanadium specimens irradiated to 2.5 dpa at 450°C. The void density in the 250°C specimens was lower than the void density in the specimens irradiated to 2.5 dpa at 450°C.

Vanadium-1% nitrogen specimens exhibited only sparse void populations when irradiated under conditions identical to the pure vanadium irradiations. When void nucleation was assisted by hydrogen doping, voids grew rapidly in the V-1% N alloy. The suppression of void nucleation by nitrogen can be explained by an increase in the nucleation barrier caused by segregation of nitrogen to the void nuclei.

Evidence of an incubation dose required for void nucleation was observed in the vanadium-1% nickel alloy. No voids were observed in the V-1% Ni specimens irradiated at 650°C to 1 dpa and 5 dpa and at 550°C to 1 dpa. Evidence of coherent precipitation was observed in these low dose, high temperature speciments. However, specimens

irradiated at 550°C to 5 dpa and at 450°C to 1 dpa and 5 dpa all exhibited voids and incoherent precipitates. Void nucleation in the V-1% Ni alloy apparently occurs heterogeneously. The incubation dose observed in this alloy was a consequence of the time required for irradiation induced solute segregation to produce incoherent precipitates.

Approved: _____
G.L. Kulcinski

ACKNOWLEDGEMENTS

During the past seven years, I have enjoyed the support of more people than it is possible to mention in this space. This work would have been impossible without that support and I want to express my sincere gratitude to everyone who has helped me.

My wife, Charlotte, deserves a special word of thanks. Her support and editorial assistance are an essential part of this work.

The guidance and encouragement of Professor Gerald L. Kulcinski, who supervised this work, was also very important to me. During the course of this work, I also had many stimulating discussions (both technical and non-technical) with Professor Peter Wilkes. I would also like to acknowledge the advice of Professor W.G. Wolfer.

A number of people worked on the construction and operation of the heavy ion irradiation facility. I would particularly like to acknowledge the work of Dr. H.V. Smith in this regard. R.C. Walsh machined most of the sample chamber and provided invaluable advice. The many graduate students with whom I have worked so closely during the years were important to me, Dr. W.J. Weber, Dr. J.B. Whitley, Dr. K.Y. Liou, S.K. McLaurin, R.W. Knoll, C.A. O'Donnell, R.L. Jackson, E.K. Opperman and M.A. Sherman. Dr. J.H. Billen also assisted with the irradiations. I would like to acknowledge the cooperation of Professors H.T. Richards and P.A. Quinn and the other members of the University of Wisconsin nuclear physics group.

I am also grateful to Diana Reuschlein who typed this thesis and helped to keep me organized.

This work was supported in part by the Department of Energy, Basic Energy Sciences, under contract number EY-76-S-02-2206.

LIST OF FIGURES

LIST OF FIGURES (continued)

LIST OF FIGURES (continued)

LIST OF FIGURES (continued)

LIST OF TABLES

CHAPTER I INTRODUCTION

I. Introduction

The successful operation of commercial reactors will require the development of advanced alloys that combine favorable mechanical and nuclear properties with a strong resistance to radiation damage. Swelling due to void formation under irradiation is a serious problem in reactor design. A number of different vanadium base alloy systems have the potential of satisfying this broad range of requirements. In order to develop alloys that meet the requirements of specific reactor designs, it is necessary to understand how alloying additions affect the irradiation behavior of the metals. The objective of this study is to characterize void formation in V, V-1% Ni and V-1% N.

I-A. Vanadium and Vanadium Alloys

Vanadium and vanadium alloys have been considered as structural materials in both fast breeder[1] and fusion [2] reactors. The initial interest of the fast breeder reactor program in these vanadium systems has waned because of their extremely high corrosion rates in liquid sodium environments contaminated with small amounts of oxygen. In order to use vanadium in a liquid sodium cooled system, an oxygen level of less than one part per million would have to be maintained in the sodium.[3] However, lithium has a higher affinity for oxygen[4] and the vanadium alloys may be used in a liquid lithium environment. Therefore, vanadium alloys may be used in fusion reactors, where their nuclear properties give them a clear advantage over other possible structural materials. In a typical fusion reactor spectrum, essentially no long-lived isotopes of vanadium are produced; and the biological hazard of the radioactive waste will fall to a minimal level within twenty years

after reactor shutdown.[5] The after-heat generated at shutdown in the vanadium structure of a fusion reactor would be comparable to other proposed structural materials, such as stainless steel and niobium. Within a few months, however, the after-heat in a vanadium structure will have decayed to negligible levels. If a neutron wall loading of 1 MW/m^2 was incident on the vanadium first wall of a fusion reactor, the helium and hydrogen production rates would be approximately 60 and 120 appm per year respectively.[5] These calculated gas production rates are higher than those obtained in a niobium wall but lower than those obtained in a stainless steel wall.

The vanadium alloys that have received the most attention as structural materials are the substitutional solid solution hardeners. Mechanical property data has been compiled for vandium alloys containing Ti, Nb, Ta, Cr, Mo, W, Ni and Fe.[1] A number of studies have shown that the V-Ti system is resistant to void swelling. Initial data obtained at Argonne National Laboratory[118] on the V-Cr system indicates that chromium enhances void formation. No irradiation data exists for the other vanadium alloys that use substitutional solutes as matrix hardeners.

Any commercial vanadium alloy will contain significant levels of interstitial impurities (> 2000 appm). In addition, it is also possible to use interstitial solutes as matrix hardeners. The effect of interstitial impurities on swelling may be important to all studies of void formation in BCC refractory metals. At a temperature of 700°C, a 0.1 mm thick sample of vanadium exposed to an oxygen atmosphere of 10^{-6} Torr for 10 hours will increase its oxygen content by 1600 appm.[6] The

amount of contamination from any vacuum environment depends upon the residual gasses in that environment. Unfortunately, the contamination rates have not been measured in vanadium for gasses other than oxygen. It is obvious that the vacuum environment must be well-characterized in any high temperature irradiation study.

I-B. Heavy Ion Bombardment

In the past ten years the study of radiation damage with heavy ions has gained wide acceptance. The use of energetic heavy ions to simulate neutron damage in reactor materials was first reported in 1969 by Nelson and Mazey.[7] In that study, the Harwell 150 KeV Heavy Ion Accelerator was used to irradiate specimens of type 316 stainless steel with protons, carbon ions, oxygen ions and iron ions. The microstructure produced in these ion irradiated specimens consisted of voids and dislocation loops similar to those observed in neutron irradiated specimens. The relatively low energy ions used in that study produced damage in a relatively thin region near the irradiated surface. For this reason the irradiations were soon shifted to the Harwell Variable Energy Cyclotron, where 20 MeV carbon ions were used to irradiate specimens of 316 stainless steel.[8] These high energy carbon ions have a range of 7.5 microns in steel. Keefer, Neely, Robinson, Pard, and Kramer[9] then used 1.2 MeV protons to produce damage in stainless steel. Also in that study, the first serious attempt to calculate the number of displaced atoms per atom using the Rutherford differential cross section and a Kinchen and Pease displacement model was made. While the use of high energy carbon ions and protons extended the volume of damaged material

produced, significant amounts of impurities were also introduced in the damaged region as the ions were stopped in the material. The first use of high energy metal ions to produce damage without altering the composition of the irradiated material was made by Kulcinski, Laidler and Doran.[10] Specimens of type 316 stainless steel were irradiated with 5 MeV Cu ions from a tandem accelerator. The theory of Lindhard and co-workers[11,12,13] was first applied to the calculation of the number of displaced atoms per atom in this study. This simulation process has spread throughout the radiation damage community. It is now used by over 10 major laboratories and has been a topic of discussion at a number of conferences.[14-24]

There are two primary advantages to using heavy ions to produce damage similar to that introduced by high neutron fluences: (1) the damage can be produced in a relatively short time period; and (2) the damage can be produced in a well controlled experiment. Several years of irradiation are required to produce a high energy neutron fluence of 10^{23} n/cm^2 in any existing nuclear facility, while an equivalent damage state may be produced in a matter of hours with heavy ions. Furthermore, it is difficult to control the irradiation environment in a nuclear reactor and the specimens are subjected to complex thermal histories, while heavy ion irradiations may be performed under high vacuum and at constant temperatures.

Although the advantages of ion bombardment are clear, there are a number of questions about its validity as a simulation technique which remain to be answered. These questions will be outlined here to provide

a proper perspective for the rest of this study. The most fundamental question that may be asked of the entire simulation process is: how can damage be compared on the basis of the total number of displaced atoms in two experiments where the damage rates differ by several orders of magnitude? Theoretical studies of void nucleation (described in section II-B) indicate that the radiation damage produced in low dose rate experiments is much more sensitive to the presence of impurity atoms than the radiation damage produced in high dose rate experiments. It can also be predicted theoretically that measurements of void growth made in a high dose rate simulation study at one temperature are equivalent to measurements made in a lower dose rate neutron irradiation performed at a lower temperature (see section II-C). This shift in the temperature dependence of void swelling has been observed qualitatively; but the calculation of the temperature shift is based on a particular relationship between irradiation dose and swelling, which does not adequately describe void growth under all conditions.

The total number of displaced atoms is also an inadequate basis for comparison of experiments because void formation is actually controlled by the number of displaced atoms and vacant lattice sites that survive the displacement cascade. Although most of the displaced atoms created by both neutrons and heavy ions are produced in displacement cascades, the average size of the cascade may differ significantly in the two cases. The size of the displacement cascade depends on the energy of the primary knock-on atom created by the neutron or heavy ion. The energy spectrum of primary knock-on atoms may be calculated for both

neutron and heavy ion irradiations, but there is not at present any satisfactory way to measure the number of surviving defects.

Impurity gas atoms, such as hydrogen and helium, which are continuously produced through (n,p) and (n,α) reactions in neutron irradiations, play an important role in void formation. In many ion bombardment studies, the samples are pre-doped with helium (this procedure was used by Nelson and Mazey); but a constantly changing helium concentration may give different results. This difficulty may be overcome by simultaneous bombardment of the specimens with heavy ion and helium ion beams. Systems for simultaneous bombardment have been constructed at Argonne National Laboratory, Westinghouse, Oak Ridge National Laboratory and Battelle Northwest Laboratory.

Although the damage zone can be extended by the use of higher energy heavy ions, the region of analysis is still limited to a few microns from the irradiated surface and there may still be a residual effect of that free surface, especially with respect to the impurity concentration and stress state in the sample. Because heavy ion irradiations are limited to small regions surrounded by unirradiated material, large stresses may be generated in the material when it begins to swell. This induced stress may effect the swelling behavior of the material.

It is currently believed that void formation is driven by a small imbalance between the number of interstitial atoms and vacant lattice sites. When a sample is bombarded with self ions, excess interstitial atoms are continually injected into the region where the ions are stopped, which may upset this delicate imbalance.

Despite all of these difficulties, the short time required to perform irradiations and the ability to perform well controlled experiments still make heavy ion bombardment an attractive technique for screening potential alloys and performing fundamental studies of void formation. Until these difficulties are resolved, it will be impossible to predict quantitatively the swelling in neutron irradiated materials from heavy ion irradiations with any confidence. However, heavy ion bombardment is still a legitimate tool for studying the process of void formation and growth.

I-C. Objectives

In this study heavy ion irradiations of pure vanadium and two solid solution alloys have been performed. Three primary objectives were outlined for this study:

1. to evaluate previous results[25] obtained in heavy ion irradiations of pure vanadium and extend them to higher doses;
2. to determine how a 1% nickel alloy behaves under irradiation;
3. to study the effect of the addition of 1% nitrogen on void swelling in vanadium.

All of the irradiations were performed in the University of Wisconsin Heavy Ion Irradiation Facility[26] using 14 MeV Cu^{3+} ions. The post irradiation analysis was based primarily on microstructural observations in the transmission electron microscope.

In 1977 W.J. Weber[25] completed two series of irradiations of pure vanadium using the same facility. This previous study is reviewed in detail in Section IV-C. In the first series of irradiations, Weber

demonstrated that it is possible to produce a surface related nickel contamination during the preirradiation anneal. This contamination produced a high density of radiation induced precipitates. The specimens for the second series of irradiations were annealed in an improved high vacuum furnace, and the amount of irradiation induced precipitation was drastically reduced. In the second series, void formation was studied as a function of temperature over the range 150°C to 700°C at 1 dpa.

In the present study the dose rate has been increased by a factor of three over those in Weber's investigation, and the results in pure vanadium have been extended to higher doses. The objective of this work was to gain more information about void formation in pure vanadium by studying the microstructural evolution between 1 dpa and 10 dpa at 450°C 550°C and 650°C. The data obtained in pure vanadium was then used as a basis for comparison in the vanadium-1% nickel and vanadium-1% nitrogen alloys.

The vanadium-1% nickel alloy was chosen because initial results[27] indicated that nickel suppresses swelling in vanadium at low doses. Also, more information was needed to describe the irradiation induced precipitation process first observed by Weber. These samples were irradiated to doses of 1 and 5 dpa at 450 °C, 550°C and 650 °C.

The irradiations of the vanadium-1% N alloy were performed to determine the effect of an interstitial alloying addition on void formation. This alloy was irradiated over the same temperature and dose ranges as the pure material. This segment of the study was designed to determine how certain solutes affect void formation. The effects of

a substitutional solute, N, were compared through observations of microstructural evolution during irradiation.

CHAPTER II THEORY OF VOID FORMATION

II-A. Production of Point Defects by Energetic Charged Particles

An energetic heavy ion incident on a metal target undergoes collisions with target atom nuclei producing vacancies and interstitials. During this process, the incident ion is continually losing energy through inelastic, dissipative interactions with electrons and elastic collisions with the target atom nuclei. The primary knock-on atoms (PKA's) which are created through the elastic collisions, will undergo similar elastic and inelastic interactions creating more displaced atoms in a cascading effect. Because the cross section for elastic nuclear interactions increases sharply with decreasing energy, the number of PKA's created by the incident ion (and hence the number of displaced atoms) increases near the end of the range of the incident ions. For the same reason, the energetic knock-on atoms will produce highly localized collision cascades near the end of their range.

In order to compare the damage obtained with different bombarding species (i.e. neutrons, electrons and various ions), dose is measured in terms of the number of displacements per atom (dpa). A dose of 1 dpa is defined such that the integral number of atoms that have been theoretically displaced in any region is equal to the total number of atoms in that region. In the case of heavy ion bombardment, the dpa level is a function of distance, x, along the projected ion range. The displacement level is calculated by using a modified Kinchen and Pease [28] model according to the equation

$$dpa = \frac{J}{N} \frac{\kappa \, S_D(x)}{2 \, E_d} ,$$

where J is the fluence of ions and N is the atomic density of the target. It is assumed here that all displacements occur at the position where the PKA is created. The parameter, κ, depends on the exact form of the interatomic potential and is a measure of how efficiently the energy is used in displacing atoms. Torrens and Robinson[29] have found $\kappa = 0.8$ from computer studies. The displacement energy, E_d, is an effective threshold energy for displacement. E_d is actually larger than the threshold energy, E_{th}, due to the effects of spontaneous recombination, focusing and the directional dependence of the threshold energy. Experiments by Erginsoy[30] and computer simulations by Beeler[31] indicate the $E_d = 5/3 \, E_{th}$ for iron. In low energy electron irradiations, Miller and Chaplin[32] have found that $E_{th} = 26$ eV for vanadium. Therefore, a value of $E_d = 43$ eV will be used for this work analogous to the work in iron.

The function $S_D(x)$ represents the amount of energy expended in elastic collisions per unit path length at position x. The basis for the calculation of $S_D(x)$ is given by Lindhard and co-workers,[11,12,13] who developed a generalized stopping power theory for the slowing down of energetic ions in amorphous materials. The first application of this work to heavy ion simulation studies was made by Kulcinski, Laidler, and Doran.[10] Computer programs expanding on that earlier work have been prepared by Manning and Mueller[33] and Brice[34] to calculate $S_D(x)$. Both computer codes use essentially the same logic. The energy loss

is related to the projected range of the particle such that,

$$S_D(x) = \int_0^x f(x') \; S_L(E_1(x'-x)) \; \frac{dR(x'-x)}{dx'} \, dx' \; . \qquad (2\text{-}2)$$

The function of $f(x')$ is the distribution in range (the two codes use a slightly different formulation for this quantity), and $\frac{dR(x'-x)}{dx'}$ relates the projected range to the actual path length. The energy $E_1(x'-x)$ is the average energy of an ion whose projected range is $(x'-x)$. The range-energy relationship is determined by both the electronic and nuclear stopping power. In this analysis, it is assumed that these two mechanisms are completely independent. The function $S_L(E)$ may be expressed as

$$S_L(E) = N \int_{T=T_1}^{T_m} T \, \eta(T) \, d\sigma(T), \qquad (2\text{-}3)$$

where T_m is the maximum energy that can be transferred by an incident ion of energy, E, to a PKA and T_1 is the lowest energy of interest, which can be assumed to be zero for the case of heavy ion bombardment. The fraction of PKA energy which is eventually spent in elastic collisions in the cascade is given by $\eta(T)$. Lindhard, Nielsen, Scharff and Thomsen[13] have provided a numerical evaluation of $\eta(T)$. The differential cross section, $d\sigma(T)$, for the production of primary knock-on atoms of energy T by the incident ion was reduced by Lindhard, Nielsen, and Scharff[11] to be a function of a single variable, t, where

$$t^{\frac{1}{2}} = \varepsilon \sin \psi/2. \qquad (2\text{-}4)$$

ψ is the center of mass scattering angle; and ε is a dimensionless

energy defined to be

$$\varepsilon = E/E_L , \tag{2-5}$$

where

$$E_L = \frac{Z_1 Z_2 \, e^2 (A_1+A_2)}{a \, M_2} \tag{2-6}$$

and

$$a = 0.8853 \, (\hbar^2/mc) \, (Z_1^{2/3}+Z_2^{2/3})^{-\frac{1}{2}} . \tag{2-7}$$

The subscripts 1 and 2 refer to the incident ion and target atom respectively. A is the atomic mass; Z is the atomic number; and m is the electron mass. The evaluation of Lindhard et al. is used for the differential cross section assuming a Thomas-Fermi potential.

Equation (2-2) is only valid for bombarding ion energies greater than 0.01 times the Lindhard energy, E_L. An upper limit, E_{lim}, for the validity of Manning and Mueller's analysis is determined by the assumption that the electronic stopping power is proportional to the velocity. In this case it is possible to show that

$$E_{lim} = 0.025 \, A_1 Z^{4/3} \quad (\text{MeV}) . \tag{2-8}$$

The energy limits of the Manning and Mueller theory for several different ions on vanadium have been compiled in Table II-1. Brice's formulation extends the upper limit by using a three parameter fit to the electronic stopping power. This is most useful for low Z materials.

In the range of energies relevant to this study, both codes give similar results for Cu ions incident on V. The dpa levels in this study are calculated using the computer code developed by Brice,[34] which has

TABLE II-1 Energy Limits Defining the Validity of the Manning and Mueller[21] Computer Code for a Range of Ions Striking a Vanadium Target. (All energies given in MeV.)

Incident Ion	Lower Limit MeV	Upper Limit MeV
He	4.74×10^{-5}	0.25
C	1.77×10^{-4}	3.27
V	1.31×10^{-3}	83
Cu	1.93×10^{-3}	141
Nb	3.63×10^{-3}	325
Ta	1.19×10^{-2}	1380

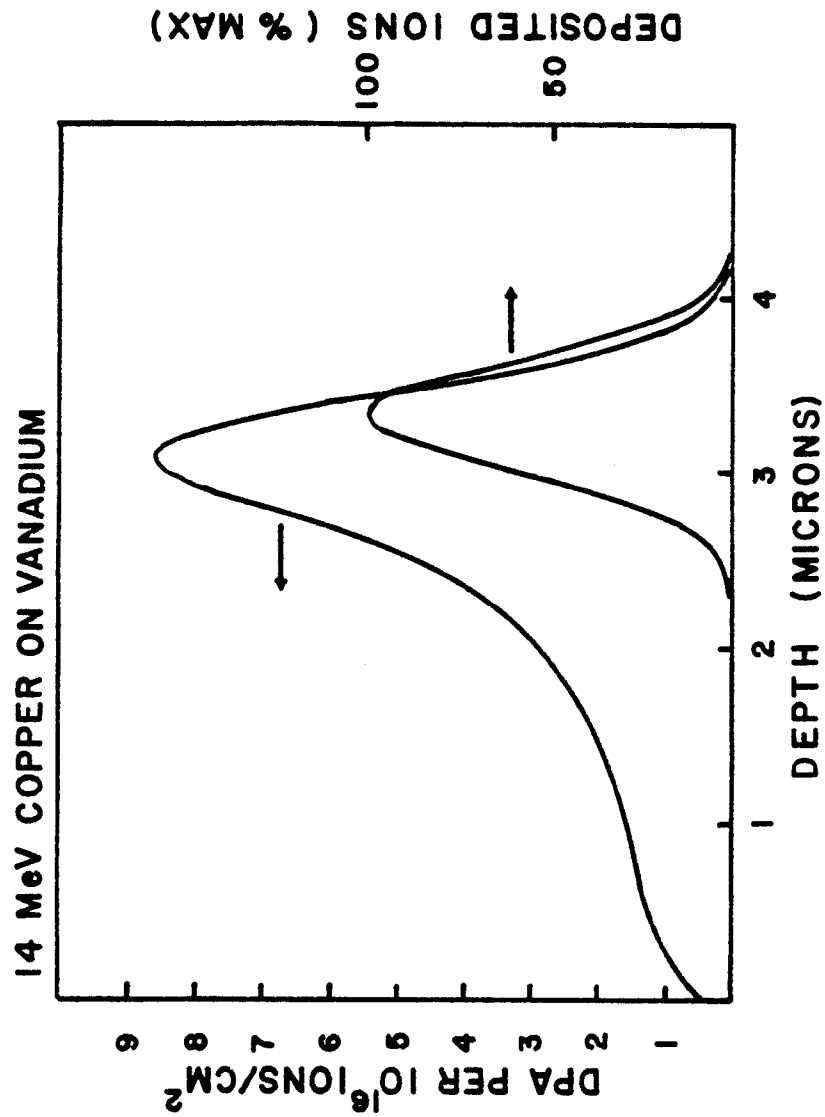

Figure II-1. Distribution of displacement damage and deposited copper ions for vanadium irradiated with 14 MeV Cu^{3+} ions. This calculation was made with Brice's computer model[34] using an effective displacement energy of 43 eV.

been adapted for use on the University of Wisconsin computer system. The results of a typical calculation for 14 MeV copper ions incident on vanadium are illustrated in Figure II-1.

II-B. Void Nucleation

The nucleation and growth of voids is dependent upon having a steady state supersaturation of vacancies. Although this supersaturation is an extremely important quantity, it is difficult to measure experimentally or predict theoretically. The calculation of the steady state vacancy concentration is central to the rate theory of void growth and is discussed in section II-C of this paper. The primary focus of this section is void nucleation theory, and it is assumed that the vacancy and interstitial concentrations are known from separate calculations. Although the final void density is the observed quantity, nucleation theory is limited to the calculation of nucleation rates. If the nucleation rate is too low, it will serve as a barrier to void production. For example, void nucleation rates of at least 10^{10} voids per cubic centimeter per second are required to produce void densities of 10^{15} voids per cubic centimeter in reasonable times for accelerator experiments. In power or test reactors, the irradiation times are measured in years and void nucleation rates of 10^{8} voids per cubic centimeter per second are sufficient. Important variables in void nucleation theory are damage rate, impurity gas concentration and temperature. As the theory is refined, it will have to be expanded to include the effects of displacement cascades on both the number of surviving defects in the system and the direct production of void nuclei.

The precipitation of second phases in a medium can usually be explained by classical nucleation theory.[35] Unfortunately, the nucleation of voids in materials supersaturated with vacancies and interstitials cannot be described by direct application of classical nucleation theory because such a formalism assumes that nuclei will grow by the addition of individual units of the constitutent species and shrink by the loss of individual units of the constituent species. Void nuclei grow by both the addition of vacancies and the emission of interstitials (although the latter process is relatively improbable), and they shrink by the emission of vacancies and capture of interstitials. Katz and Wiedersich[36] refer to this phenomenon as nucleation in the presence of matter and anti-matter. Attempts to extend classical nucleation theory to include void nucleation have been made by Russell[37,38] as well as Katz and Wiedersich.[36,39,40]

The advantage of classical nucleation theory is that it reduces a large system of equations to a much simpler analytic expression. In the case of void formation, however, the assumptions of classical nucleation theory become restrictive. Modifications must be made to include the effect of interstitials. When the effect of mobile gas atoms is included, the assumption of one dimensional flow breaks down and fundamental difficulties arise in classical nucleation theory.

In classical nucleation theory, the concentration of all species are assumed to be kept at a constant level and the rate of flow between species of neighboring sizes is calculated. Only reactions with immediate neighbors in size space may be included, and nucleation must proceed

along a one dimensional path. In this case, the net rate at which precipitates of size x flow to size x + 1, J, may be expressed

$$J = \beta_v(x)\ C(x) - \delta_v(x+1)\ C(x+1) - \beta_i(x+1)\ C(x+1), \qquad (2\text{-}9)$$

where C(x) is the concentration of void nuclei of size x, $\beta_v(x)$ is the vacancy arrival rate, $\delta_v(x)$ is the vacancy emission rate and $\beta_i(x)$ is the interstitial arrival rate. The interstitial emission rate is assumed to be zero.

The vacancy emission rate is determined by considering the hypothetical case where there are no interstitials ($\beta_i(x) = 0$ for all x) and the void embryo distribution is in equilibrium with the vacancy concentration, (J = 0). For this case, it can be shown that[36]

$$C(x) = \frac{C_v^{eq}}{C_v} \exp[-\gamma \mathcal{A}(x)/kT], \qquad (2\text{-}10)$$

where C_v^{eq} is the thermal equilibrium concentration of vacancies, γ is the surface energy and $\mathcal{A}(x)$ is the surface area of a void embryo containing x vacancies. Equation (2-9) may then be rearranged to give

$$\delta_v(x+1) = \beta_v(x) \frac{C_v^{eq}}{C_v} \exp[\gamma(\mathcal{A}(x+1) - \mathcal{A}(x))/kT]. \qquad (2\text{-}11)$$

As an intermediate step to calculating the nucleation rate, it is helpful to define the constrained embryo distribution, $C^o(x)$. The constrained embryo distribution is derived from Equation (2-9) by setting J = 0. A recursive relation for $C^o(x)$ is then

$$C^o(x+1) = C^o(x) \left(\frac{\beta_v(x)}{\delta_v(x+1) + \beta_i(x+1)} \right). \qquad (2\text{-}12)$$

An effective free energy, $\Delta G(x)$, may be defined in a manner analagous to more conventional nucleation theories such that

$$C^{o}(x) = C_{v}\, e^{-\Delta G(x)/kT}. \qquad (2\text{-}13)$$

In a conventional precipitation problem, such as the nucleation of a second phase from solid solution, $\Delta G(x)$ would correspond to the free energy of formation for a cluster of size x. However, for void nucleation, the effective free energy is sharply dependent on the irradiation parameters and loses its simple physical significance. The definition of the effective free energy becomes even more nebulous when an additional constituent, such as an insoluble gas, is included, because the entire formalism breaks down.

The nucleation rate may be expressed in terms of the constrained embryo distribution by making two assumptions: (1) the vacancy concentration is independent of the nucleation rate; and (2) the concentration of precipitates of very large size is essentially zero. The nucleation rate is then determined from Equation (2-9) to be

$$J = \left[\sum_{x=1}^{n} [\beta_{v}(x)\; C^{o}(x)]^{-1} \right]^{-1}, \qquad (2\text{-}14)$$

where n has a large value such that J is independent of n.

In order to calculate the nucleation rate, it is necessary to determine the vacancy and interstitial arrival rates, $\beta_{v}(x)$ and $\beta_{i}(x)$, from theoretical considerations. Both Russell[37] and Katz and Wiedersich[36] assumed arrival rates for point defects of type k were of the form

$$\beta_k(x) = C_k D_k \frac{x^{2/3}}{b^2}, \qquad (2\text{-}15)$$

where b is the lattice constant. However, in more detailed calculations, Wolfer and Yoo[41] have shown that

$$\beta_k(x) = 4\pi b x^{1/3} Z_k^o(x) D_k C_k, \qquad (2\text{-}16)$$

where Z_k^o is a bias factor which approaches 1 for large voids. Wolfer's derivation is consistent with the void sink strengths, which are derived in Section II-C. For a pure material, Wolfer and Yoo derived two contributions to the bias factor. The first contribution arises from the image interaction between the point defect and the void surface and has the form

$$Z_k^{im} \cong 1 + \left[\frac{Gb^3}{kT} \frac{(1+\nu)}{36\pi(1-\nu)}\right]^{1/3} \left(\frac{V_k}{b^3}\right)^{2/3} \frac{b}{a}, \qquad (2\text{-}17)$$

where a is the void radius, V_k is the relaxation volume for the point defect, G is the shear modulus and ν is Poisson's ratio. The interaction between the shear strain field of the void and the point defect gives rise to the second contribution. The bias factor for this modulus effect is

$$Z_k^s = 1 - \frac{3}{56} \frac{\alpha_k}{kT} \left(\frac{2\gamma}{rG}\right)^2, \qquad (2\text{-}18)$$

where α_k is the polarizability for point defects of type k. The compound bias factor is given by the product of the contributions:

$$Z_k^o = Z_k^{im} Z_k^s . \qquad (2\text{-}19)$$

For this study, a computer program has been written based on Wolfer and Yoo's calculation of bias factors. The results of these calculations are reported in Chapter VII.

II-C. Void Growth

The theories of void growth have traditionally been divided into two categories--the cellular models as outlined by Bullough and Perrin[42,43] and the rate theory models as outlined by Wiedersich,[44] Harkness and Li,[45] and Brailsford and Bullough.[46] The rate theory models have gained greater acceptance because they lead to simpler, analytic solutions, which give more insight into the void formation process. In order to illustrate the basic assumptions of the models and the inherent similarity of all of the models, a comparison is made here of the cellular model of Bullough and Perrin[43] and the rate theory model of Brailsford and Bullough.[46] Both models attempt to determine the rate of swelling increase by calculating void growth for a pre-existing distribution of voids.

In the cellular model, the vacancy and interstitial concentrations must be determined in a region of space directly surrounding a single void. The basic equations used by Bullough and Perrin[43] to describe this situation are

$$D_v \nabla^2 C_v + K - \alpha C_v C_i - D_v Z_v \rho_D C_v = 0 \qquad (2\text{-}20)$$

and

$$D_i \nabla^2 C_i + K - \alpha C_v C_i - D_i Z_i \rho_D C_i = 0 \ , \qquad (2\text{-}21)$$

where the subscripts v and i refer to vacancies and interstitials respectively, the D's are the corresponding diffusion coefficients, the C's are concentrations in atomic fraction, K is the defect production rate, α is a recombination coefficient, the Z's are the numbers representing the capture volume of a dislocation (note $Z_i > Z_v$ implies a bias for interstitials) and ρ_o is the dislocation density. The defect production rate is generally taken as the displacement rate, but it must be kept in mind that most displacements occur in cascades and it is only the free or surviving defects that should be counted in this formulation. These two coupled, non-linear differential equations must be solved according to the boundary conditions indicated in Figure II-2a. The net defect flux across the outer boundary, R, where R is determined by the void density, is set equal to zero implying that

$$\left.\frac{dC_v}{dr}\right|_R = 0 \qquad (2\text{-}22)$$

and

$$\left.\frac{dC_i}{dr}\right|_R = 0. \qquad (2\text{-}23)$$

At the void surface, r_v, the defect flux is determined by the transfer velocities, of vacancies and interstitials, S_v and S_i, across the void surface. The net fluxes of defects across the void surface may be written as

$$D_v \left.\frac{dC_v}{dr}\right|_{r_v} = S_v[C_v - \bar{C}_v] \qquad (2\text{-}24)$$

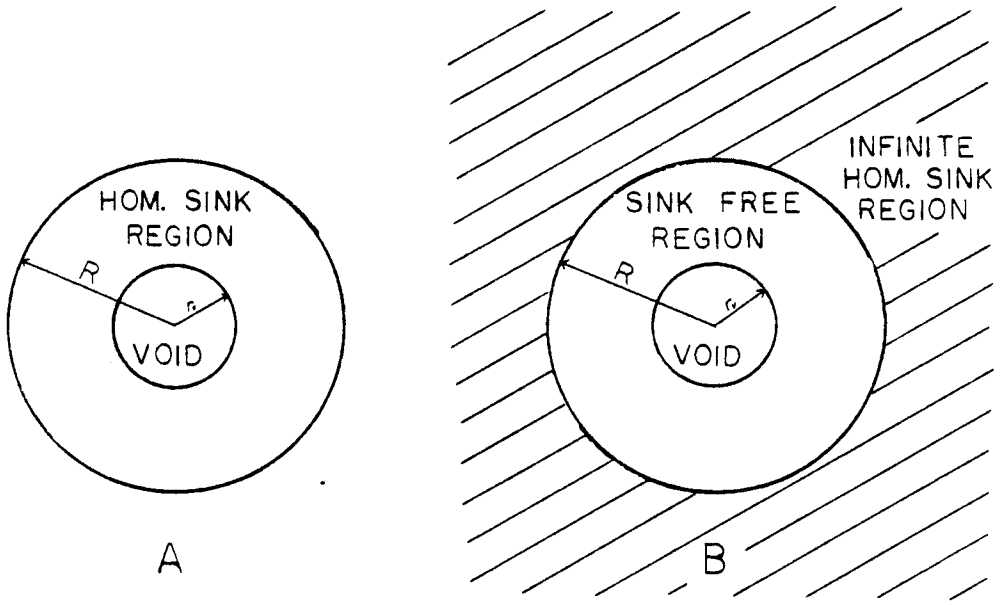

CELLULAR MODEL

RATE THEORY MODEL

Boundary Conditions

1.) Net flow of defects across surface at r=R is zero.

2.) Net flow of defects across void surface ($r=r_v$) is determined by transfer velocity.

1.) Defect concentration and defect flux continuous at r= R.

2.) Net flow of defects across void surface ($r=r_v$) is determined by transfer velocity.

Figure II-2. Comparison of boundary conditions used in cellular and rate theory models for void growth. The boundary conditions are used in the rate theory model to calculate the void sink strength.

and

$$D_i \left.\frac{dC_i}{dr}\right|_{r_v} = S_i C_i, \tag{2-25}$$

where $S_v \bar{C}_v$ is the emission rate of vacancies from the void. The rate of change of void radius may then be found by equating the net flow of vacancies to the void and the rate of change of void volume, which, after some manipulation, gives

$$\frac{dr_v}{dt} = \left(D_v \frac{dC_v}{dr} - D_i \frac{dC_i}{dr}\right)\Big|_{r = r_v}. \tag{2-26}$$

Bullough and Perrin assume that the transfer velocity is the same at the void surface as the diffusion rate in the matrix, such that

$$S = D/b. \tag{2-27}$$

By applying the boundary conditions, equation (2-20) can be rewritten as

$$\frac{dr_v}{dt} = \frac{1}{b}\left[D_v(C_v(r)-\bar{C}_v) - D_i C_i(r)\right]\Big|_{r = r_v}. \tag{2-28}$$

The swelling is computed by starting with an initial value of r_v, solving equations (2-20) and (2-21) numerically, finding the increment in r_v from equation (2-28) and then continuing the iteration. The volume swelling may then be found through the relation

$$\frac{\Delta V}{V} = \frac{r_v^3}{R^3}. \tag{2-29}$$

The rate theory of swelling is based on the chemical rate equations for the steady state concentrations of vacancies and interstitials in a homogeneous medium, so that

$$K' - D_v C_v k_v^2 - \alpha C_v C_i = 0 \qquad (2\text{-}30)$$

and

$$K - D_i C_i k_i^2 - \alpha C_v C_i = 0, \qquad (2\text{-}31)$$

where K' is the effective vacancy production rate including the emission of vacancies from voids and other sinks and α is the recombination coefficient. A rough estimate[44] of the recombination coefficient can be made from the jump frequencies, ν_i and ν_v, of interstitials and vacancies and the number of sites, a, surrounding each defect which will lead to direct recombination. Taking values of $\nu_v = 9.6 \times 10^4$ sec^{-1}, $\nu_i = 1.1 \times 10^{13}$ sec^{-1} and a = 10, which are characteristic of nickel at 525°C, yields $\alpha = 10^{14}$/sec. The parameters k_v^2 and k_i^2 are effective vacancy and interstitial sink strengths for the homogenized medium. The sink strength for each type of sink is determined separately, and the effective sink strength is the sum over all types of sinks in the system. The rate theory models are distinguished by the methods used for determining sink strengths. The calculations of Brailsford and Bullough,[46] which include three types of sinks, are the most sophisticated. The first type of sink considered is the neutral sink, which has no preference for vacancies or interstitials. The most common types of neutral sinks are voids and incoherent precipitates. The second type of sink is the fixed bias sink, such as a dislocation, which is more effective

in annihilating interstitials than vacancies. These sinks are responsible for the overall excess of vacancies necessary for void formation. Coherent precipitates which have a limited capacity for vacancies or interstitials form the third type of sink. These variable bias sinks must adopt a bias similar to that of the fixed bias sinks to avoid a net accumulation of defects. Once all of the relevant coefficients have been determined, the steady state vacancy and interstitial concentrations may be found by analytically solving the two simultaneous quadratic equations (2-30) and (2-31).

The relationship to cellular theory is shown in the method of calculating the void sink strength. The geometry used by Brailsford and Bullough[45] is illustrated in Figure II-2b. The volume outside of the void is divided into two regions. The first region between the void radius, r_v, and R is a sink free region (recombination in this region is also ignored) in which the steady state defect (both vacancy and interstitial) concentration is described by the equation

$$D\nabla^2 C + K = 0. \qquad (2\text{-}32)$$

Outside of the sink free region is a second region, which has a homogeneous distribution of sinks in which the steady state defect concentration is given by the equation

$$D\nabla^2 C + K - k^2 C = 0. \qquad (2\text{-}33)$$

This may be a more realistic model than the cellular model because the matrix is sink free on the scale of the void radius. The boundary conditions at the void surface are identical to those used in cellular theory.

At the surface separating the two regions, both the defect concentration and its first derivative must be continuous. The asymptotic solution for the defect concentration must match the rate equation solution. The net flow rate of both types of defects (J_v or J_i) may be described by equations of the form

$$J_x = \frac{4\pi r_v^2}{b^3} D_x \left.\frac{dC_x}{dr}\right|_{r = r_v}. \tag{2-34}$$

If ρ_v is the concentration of voids, then $J_x\rho_v$ is the total flow rate of defects to voids in the system. This quantity may also be expressed in terms of the original chemical rate equations, to give the relation

$$J_x\rho_v = \frac{1}{b^3}\left[-K_x + D_x C_{mx} k_{vx}^2\right], \tag{2-35}$$

where K_x is the defect emission rate from the voids (this quantity is negligible for interstitials), k_{vx}^2 is the effective sink strength of voids for defects of type x and C_{mx} is the asymptotic solution of equation (2-33) for large r. By assuming voids are unbiased sinks, Brailsford and Bullough solve equation (2-35) to show that

$$k_v^2 = 4\pi r_v \rho_v \tag{2-36}$$

and

$$K_v = 4\pi r_v \rho_v D_v \bar{C}_v. \tag{2-37}$$

Similar calculations of sink strengths must be made for all types of sinks in the system.

The volume swelling rate, which is equal to the net accumulation rate of vacancies at voids in the system, is given by rate theory as

$$\frac{d}{dt}\left(\frac{\Delta V}{V}\right) = \left\{ D_v C_v - D_i C_i - D_v \bar{C}_v \right\} 4\pi r_v \rho_v . \qquad (2\text{-}38)$$

For comparison, equation (2-28) of the cellular theory may be rewritten

$$\frac{d}{dt}\left(\frac{\Delta V}{V}\right) = \left\{ D_v C_v - D_i C_i - D_v \bar{C}_v \right\}\Bigg|_{r = r_v} \frac{4\pi \rho_v r_v^2}{b} . \qquad (2\text{-}39)$$

Although the similarity between equations (2-38) and (2-39) is striking, there are also some important differences. The extra factor of r_v/b in the calculation of Bullough and Perrin arises largely because the vacancy and interstitial concentrations are evaluated at the void surface, while the rate theory model evaluates them in the homogeneous medium. Also, rather than making an assumption about the time dependence of the right hand side of equations (2-38) and (2-39) as Brailsford and Bullough do,[46] Bullough and Perrin[43] use an iterative technique. The calculations of C_v and C_i in the two models differ because of the different methods and geometries used. Because it does not involve the solution of coupled non-linear differential equations, the rate theory model does not require complex numerical analysis. There is no clear advantage to the cellular model, and the rate theory model has gained greater acceptance because it can be applied to a wider range of problems.

In order to compute the time dependence of swelling, Brailsford and Bullough[45] assume a linear dose dependence after an incubation period of t_o in order to derive the relation

$$\frac{\Delta V}{V} = \frac{K\,(t-t_o)\,(Z_i-Z_v)\,\rho_o 4\pi r_v \rho_v}{(\rho_o+4\pi r_v\rho_v)\,(\rho_o+4\pi r_v\rho_v+4\pi r_p\rho_p)}\,F(\eta)\,, \qquad (2\text{-}40)$$

where r_p is the radius of the coherent precipitates and ρ_o and ρ_p are the densities of dislocations and coherent precipitates respectively. The function, $F(\eta)$, contains all of the information on temperature dependent processes such as recombination and thermal emission.

Brailsford and Bullough have calculated $F(\eta)$ for two different dose rates in nickel. The low dose rate, 10^{-6} dpa/sec, is typical of a reactor environment, while 10^{-3} dpa/sec is typical of a simulation experiment. The results of this calculation along with the material parameters used are presented in Figure II-3. The shift in peak swelling temperature is predicted in all theories. The low temperature limit is determined by recombination effects, which become more important with higher steady state vacancy and interstitial concentrations (higher dpa rates). The swelling decreases at higher temperatures when the thermal emission rate of vacancies is comparable to the irradiation production rate of vacancies.

Bullough and Perrin[47] indicate that damage produced at different dose rates may be compared through a shift in effective radiation temperature from the relation

$$K_1/D(T_1) = K_2/D(T_2). \qquad (2\text{-}41)$$

Damage produced at temperature, T_2, with a dose rate equal to K_2 is then roughly equivalent to damage produced at temperature, T_1, with dose rate

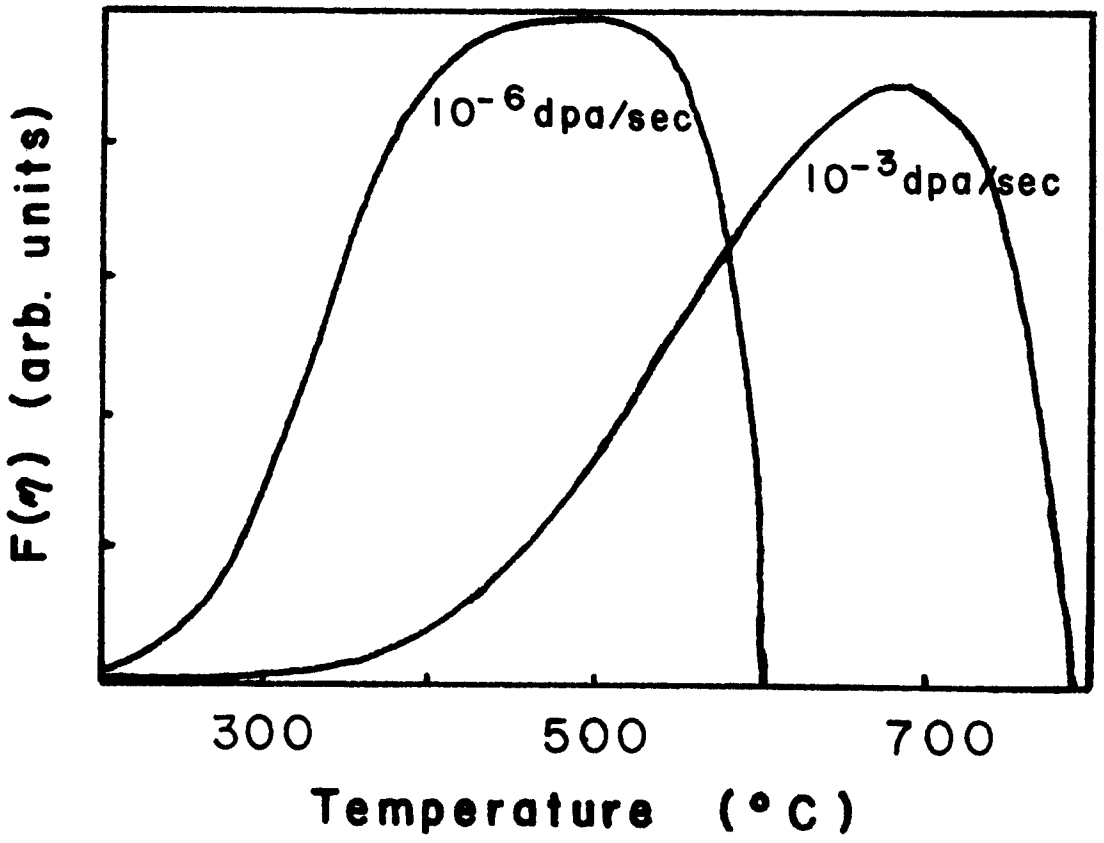

Figure II-3. Dose rate induced temperature shift in calculated void growth rate. The function $F(\eta)$ contains all of the temperature dependent quantities used in Brailsford and Bullough's rate theory model. The parameters used for this calculation were $k_v^2 = 10^{11} cm^{-2}$, $k_i^2/k_v^2 = 1.01$, $E_m^v = 1.4$ eV, $E_f^v = 1.6$ eV and $\alpha/D_i = 10^{17} cm^{-2}$.

equal to K_1, where

$$T_1 = T_2 + \frac{T_2^2 \ln(K_2/K_1)}{E_v/k + T_2 \ln(K_2/K_1)} \quad . \qquad (2\text{-}42)$$

E_v is the diffusion energy, and K is the Boltzman constant. It should also be noted that the preceding discussion is predicated on a temperature and time independent sink density. The temperature shift may be drastically affected by changes in sink density, which are expected to occur in irradiated materials.

The actual dose dependence of void growth is a complicated function of the overall microstructural evolution. For instance, the formation of radiation induced precipitates can change the point defect sink density. During irradiation, the dislocation structure may change as small dislocation loops nucleate and grow to form a dislocation network. Bullough, Eyre and Krishan[48] suggest that small vacancy loops may be continually forming in displacement cascades and decaying by thermal emission. These small vacancy loops, which would be irresolvable by conventional transmission electron microscopy, could have significant effects on void growth. TRANSWEL, a computer program to calculate time dependent void growth rates based on this theory, has been develped by N. Ghoniem[49] at the University of Wisconsin.

II-D. Specialized Alloying Effects

It is of primary importance to this study to understand the effects of solute atoms and precipitates on radiation damage. Although the significance of small compositional changes has long been recognized (see

for instance Ref. 50), there is to date no way of predicting a priori the behavior of any alloy. The materials used in the construction of any reactor will probably be alloys, and they will certainly not be of extremely high purity. The large number of possible alloy systems provides a complexity that defies a complete theoretical treatment. There have, however, been several attempts to incorporate specialized alloying effects into the theory of void formation.

Perhaps the most important and least understood effects of alloying additions occur in the area of void nucleation. There are many different mechanisms through which alloying additions may affect void nucleation. The magnitude of each effect may be very sensitive to dose rate. Therefore, simulation studies, which have high dose rates, may give very different results from lower dose rate neutron irradiations. The presence of precipitates can affect the nucleation process by providing sites for heterogeneous nucleation. There is no consistent theory to describe heterogeneous void nucleation. As indicated in section II-B, the theory of homogeneous void nucleation in the absence of impurities has been developed. The extension of the theory to include impurity atoms is currently an area of primary interest.

Although much of the work on void nucleation has concentrated on the effect of helium on void nucleation, the effects of other constituents may also be incorporated. Internal pressure caused by insoluble gas atoms and decreased surface energy caused by surface coatings can both inhibit vacancy emission and enhance the void nucleation rate. The bias factors derived in Section II-B may also be affected by changes in the void surface energy or the shear modulus. The last few point

defect jumps into the void embryo may be inhibited by thin void coatings. Wolfer[50] has suggested that the effect of void coatings be modeled by an additional contribution to the void embryo bias factor, Z_k^c, of the form

$$Z_k^c(x) = \frac{1}{1 + Z_k^{im} Z_k^s x^{-1/3} e^{E_k^*/kT}}, \qquad (2\text{-}42)$$

where E_k^* is the difference between the average interaction potential for the bare void in the near surface region and the increase in this potential due to the void coating. When the bias factors are included in the nucleation equations, the nucleation barrier becomes prohibitively high unless void coatings are included. This theory implies that residual impurities are important to void nucleation even in pure materials.

The segregation of impurities to voids can also affect void growth. This segregation effect has been observed in a number of materials including vanadium (see section IV-B). Okamoto, Santhanam, Wiedersich and Taylor[51] attribute this behavior to the dragging of solute atoms to the void by diffusing point defects. A gradient of solute atoms will then be set up near the void surface to counter balance the incoming flux. Okamoto and Wiedersich[52] have shown that solute drag can result in significant solute concentrations around the void. Brailsford[53] treats the solute segregation phenomenon by assuming that there is a force which inhibits solute emission from the segregated region. He further suggests that this force is a result of the lowering of void surface energy by solute atoms. The solute concentration around

the void is then found by balancing the arrival rate of solutes at the segregated region with the loss rates due to diffusion and direct emission by the bombarding particles. The diffusion rates of point defects in the matrix and in the segregated region may be different.[53] Brailsford has shown that if the diffusion rates of vacancies and interstitials within a segregated region of thickness δ are D_v^c and D_i^c, the rate theory equation for the swelling rate (equation 2-37), neglecting thermal emission of vacancies from voids, may be rewritten as

$$\frac{d}{dt}\left(\frac{\Delta V}{V}\right) = \left(W_v D_v C_v - W_i D_i C_i\right) 4\pi r_v \rho_v, \qquad (2\text{-}43)$$

where

$$W_x = \left(1+\frac{\delta}{r_v}\right)/\left(1+\frac{D_x \delta}{D_x^c r_v}\right). \qquad (2\text{-}44)$$

If the vacancy diffusivity is significantly reduced relative to the interstitial diffusivity, segregation may inhibit or even reverse swelling. If the void surface energy is changed by the segregating species, the thermal emission rate of vacancies from the void surface will also be affected, which would either increase or decrease the swelling rate. In addition, the presence of solute atoms can remove the bias of dislocations for interstitials. This possibility is discussed by Norris,[55] who suggests that oversized substitutional or interstitial solutes may interact with the strain field of a dislocation to reduce the interaction with self interstitials. There is, however, no hydrostatic interaction between the impurity atoms and the point defects.[56] This strain field induced attraction of dislocations for impurities was first suggested by

Cottrell[57] and is a well known effect. Norris calculates that an impurity content of 1000 atomic ppm can significantly reduce the void growth rate by reducing the dislocation bias. It is also possible that precipitates may pin dislocations, prohibiting climb and hence reducing the dislocation bias for interstitials.[58]

The presence of solute impurities and precipitates can also affect the steady state point defect concentration. The change in point defect concentration will in turn affect both void nucleation and void growth. Precipitates may act as fixed or variable bias sinks, which can be included in equations (2-29) and (2-30).

Solute atoms may also act as trapping sites for point defects, slowing diffusion. Schilling and Schroeder[59] have described the trapping of vacancies in terms of an effective diffusion constant, D_v^+, such that

$$D_v^+ = \frac{1}{1 + a_t \tau} \quad , \tag{2-45}$$

where τ is the average time that the vacancy is trapped and a_t is the trapping rate. In an alternative approach, Mansur[60] has solved three coupled equations for the concentrations of free vacancies, trapped vacancies and free interstitials. Mansur has also shown that vacancy trapping and interstitial trapping are equivalent when

$$E_i^b = E_v^m - E_i^m + E_v^b + kT \ln \left(\frac{D_i r_v^o}{D_v r_i^o}\right) \quad , \tag{2-46}$$

where E_x^b, E_x^m, r_x^o and D_x are respectively the point defect-trap binding energy, migration energy, trap radius and diffusion coefficient for point defects of type x.

In this study a model similar to that developed by Mansur[60] has been used. A common problem for all trapping models has been the unusually high trapping energies (>0.2 eV) required to produce significant effects. Recent experiments have shown these trapping energies are far in excess of the measured values for vacancy-solute atom trapping.[54] However, clusters of solute atoms may trap vacancies with trapping energies in excess of 0.2 eV. For this reason a concentration of vacancy traps, C_T, equal to a fraction of the total alloying concentration has been assumed. These vacancy traps are further assumed to be immobile. In this case the rate at which vacancies are trapped is

$$A_1(C_T - C_p)C_v, \tag{2-47}$$

where C_p is the concentration of occupied vacancy traps. The vacancy-empty trap combination coefficient, A_1, is determined by the rate at which vacancies diffuse to traps and has been taken to be equal to $a_1 D_v$, where a_1 is a constant. The rate at which vacancies detrap is equal to

$$f\,\nu_o\, e^{-(E_v^m + E_v^b)/kT}, \tag{2-48}$$

where f is a geometrical factor, ν_o is the vibrational frequency of the trapped vacancy, E_v^m is the vacancy migration energy and E_v^b is the binding energy. Interstitials may also encounter trapped vacancies and undergo recombination at the trap. The interstitial-filled trap combination coefficient, A_2, is used to calculate the rate that recombination events occur at trapped sites:

$$A_2\, C_p\, C_i. \tag{2-49}$$

This rate constant, A_2 is determined by the rate at which interstitials diffuse to trapped vacancies and is taken to be equal to $a_2 D_i$, where a_2 is a constant. When the rate theory equations (2-29) and (2-30) are modified to include vacancy trapping, they then take the form

$$K - k_i^2 D_i C_i - \alpha C_i C_v - A_2 C_p C_i = 0 \qquad (2\text{-}50)$$

and

$$K^c + K - k_v^2 D_v C_v - \alpha C_i C_v + C_p f \nu_o e^{-(E_v^m + E_v^b)/kT}$$

$$- A_1 C_v (C_T - C_p) = 0. \qquad (2\text{-}51)$$

The steady state concentration of trapped vacancies is determined by a third rate theory relation:

$$A_1 C_v (C_T - C_p) - A_2 C_p C_i - C_p f \nu_o e^{-(E_v^m + E_v^b)/kT} = 0. \qquad (2\text{-}52)$$

For this study a computer program using an iterative technique to solve equations (2-50), (2-51) and (2-52) has been developed. The results of this calculation are reported in Chapter VII.

Closely coupled to the void formation process in alloy systems is the effect of irradiation on the precipitation process. Nelson, Hudson and Mazey[61] suggest that irradiation induced resolution will produce an equilibrium size of precipitates in an irradiation environment. This effect, however, has been shown[62] to be an artifact of the calculation rather than a true physical mechanism. Russell[63] has pointed out that the precipitation rate in quenching experiments can be increased by

several orders of magnitude due to the presence of excess vacancies. This effect might also be expected in irradiation experiments, where the vacancy supersaturation is maintained continuously.

The presence of excess vacancies may also be important in determining the phase stability during irradiation. The amount of energy required to displace atoms in the matrix is very large compared to the free energy of transformation in metallic systems. Any mechanism which can couple the point defect production to phase stability, such as solute drag, can potentially have a large effect. If vacancy formation affects one phase more than another, the relative stability of those phases will also be affected. This shift in relative stability will manifest itself in the phase diagram, which will be different for this steady state non-equilibrium situation. The free energy increase associated with the steady state vacancy concentration under irradiation is important only in high dose rate experiments. This process has been described by Wilkes, Liou and Lott[64] and Liou and Wilkes.[65]

CHAPTER III VANADIUM ALLOY SYSTEMS

A knowledge of precipitation and phase equilibria in the V-Ni and V-N alloy systems is a necessary prerequisite to a study of irradiation effects in these alloys. There are a large number of possible stable and metastable phases that can be formed in these systems. Before any conclusions can be drawn about the effect of irradiation on an alloy, the equilibrium composition of that alloy must be known. As noted in the previous section, irradiation may affect the process of precipitation as well as the equilibrium condition. Changes in precipitate morphology and distribution may then also be caused by irradiation. In the following sections, a brief review of the work done on phase equilibria and precipitation in the dilute alloy systems of Ni and N in vanadium will be given.

III-A. Vanadium-Nickel

Studies of phase equilibria in the V rich region of the V-Ni diagram have been limited to temperatures above 800°C because of the sluggish nature of the precipitation reactions. The phase diagram proposed by Stevens and Carlson[66] is presented in Figure III-1. The vanadium solvus was determined by x-ray parametric studies. Two intermetallic phases form in the vanadium rich region of this diagram.

The β phase, which is stable to 900°C, was first reported by Rostoker and Yamamoto.[67] Although it has a nominal V_3Ni composition, the β phase forms homogeneously over the substoichometric range of 22.0 to 23.0 at% Ni. This phase has a body centered cubic W-A-15 structure

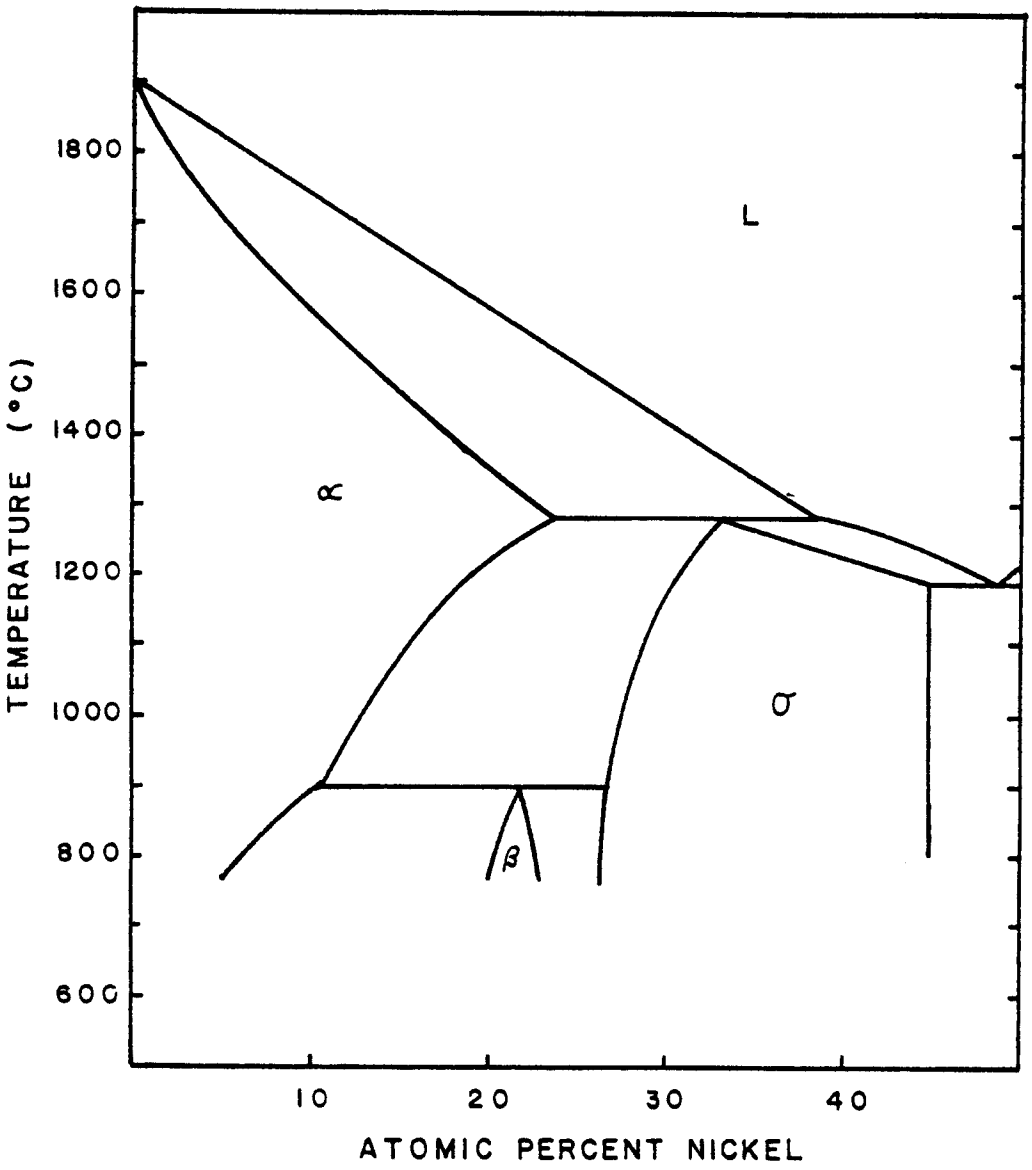

Figure III-1. Vanadium rich portion of V-Ni phase diagram proposed by Stevens and Carlson.[66]

with a lattice parameter of 4.712 Å at 25 at% Ni.

The σ phase is stable over the range 26 at% to 45 at% Ni.[66] This phase forms peritectiсly at 1280°C. The σ phase has a complicated tetragonal structure with a = 8.954 Å and c = 4.635 Å. Other high Ni composition phases include VNi_2[68] with an orthorhombic structure and $V Ni_3$[69] with a cubic structure.

In a series of splat cooling experiments in V-Ni alloys containing 33 at% to 53 at% Ni, Ruhl et al.[70] have identified two metastable phases. The first metastable phase is a body centered cubic W-A2 phase with a lattice parameter of 2.91 Å. This first metastable phase forms in all of the alloys studied. In the range of 33 at% Ni to 47 at% Ni, a microcrystalline phase was also observed. Although the structure of this microcrystalline phase is not determined, it is believed to be similar to the first metastable stage.

III-B. Vanadium Nitrogen

The terminal solubility of nitrogen in vanadium in the temperature range from 275°C to 575°C has been measured by Monroe and Cost[71] using internal friction techniques. They found that the concentration of the saturated solution, C, in atomic percent is

$$C = 50 \exp(-0.24/kT) \text{ (eV/atom)}. \qquad (3\text{-}1)$$

In a later study, Henry, O'Hare, McCune and Krug[72] determined that the terminal solubility in the range 600°C to 1200°C is

$$C = 33 \exp(-0.16/kT) \text{ (eV/atom)}. \qquad (3\text{-}2)$$

These high temperature measurements have been confirmed by both Horz[73] and

and Potter, Epstein and Goldstein.[74] A compilation of all these measurements is given in Figure III-2. The low temperature results of an electron microscopy study reported by Potter, Epstein and Goldstein are also included in Figure III-2. Data points indicated by x's are in a two phase region, while those indicated by o's are in a one phase region. This data is in rough agreement with work of Monroe and Cost.[71]

The study of phase equilibria in the vanadium-nitrogen system has been complicated by the existence of intermediate, metastable phases which form during the aging of quenched specimens. At temperatures above 600°C, the V_3N phase exists in equilibrium with the α solid solution. Although V_3N is still stable at 550°C, Potter, Epstein and Goldstein[74] have shown that precipitation from the supersaturated solution at this temperature follows the path

$$\alpha \text{ Vanadium} \rightarrow V_{16}N \rightarrow V_yN + V_xN \rightarrow V_3N. \qquad (3\text{-}3)$$

Aging studies at lower temperatures observe only the $V_{16}N$ phase; and, although the kinetics of precipitation may be much slower at lower temperatures, it seems reasonable to assume that $V_{16}N$ is a stable phase. The existence of this new stable phase could explain the change in slope of the terminal solubility curve. Henry et al.[72] suggest that there may be a peretectoid horizontal between 500°C and 600°C but cannot identify a transformation temperature using differential thermal analysis. Potter et al.[71] indicate that all measurements made between 450° and 650° are uncertain because of the sensitivity to aging conditions, but their results do show that the peretectoid must take place below 550°C. The broken line in Figure III-2 suggests a possible low

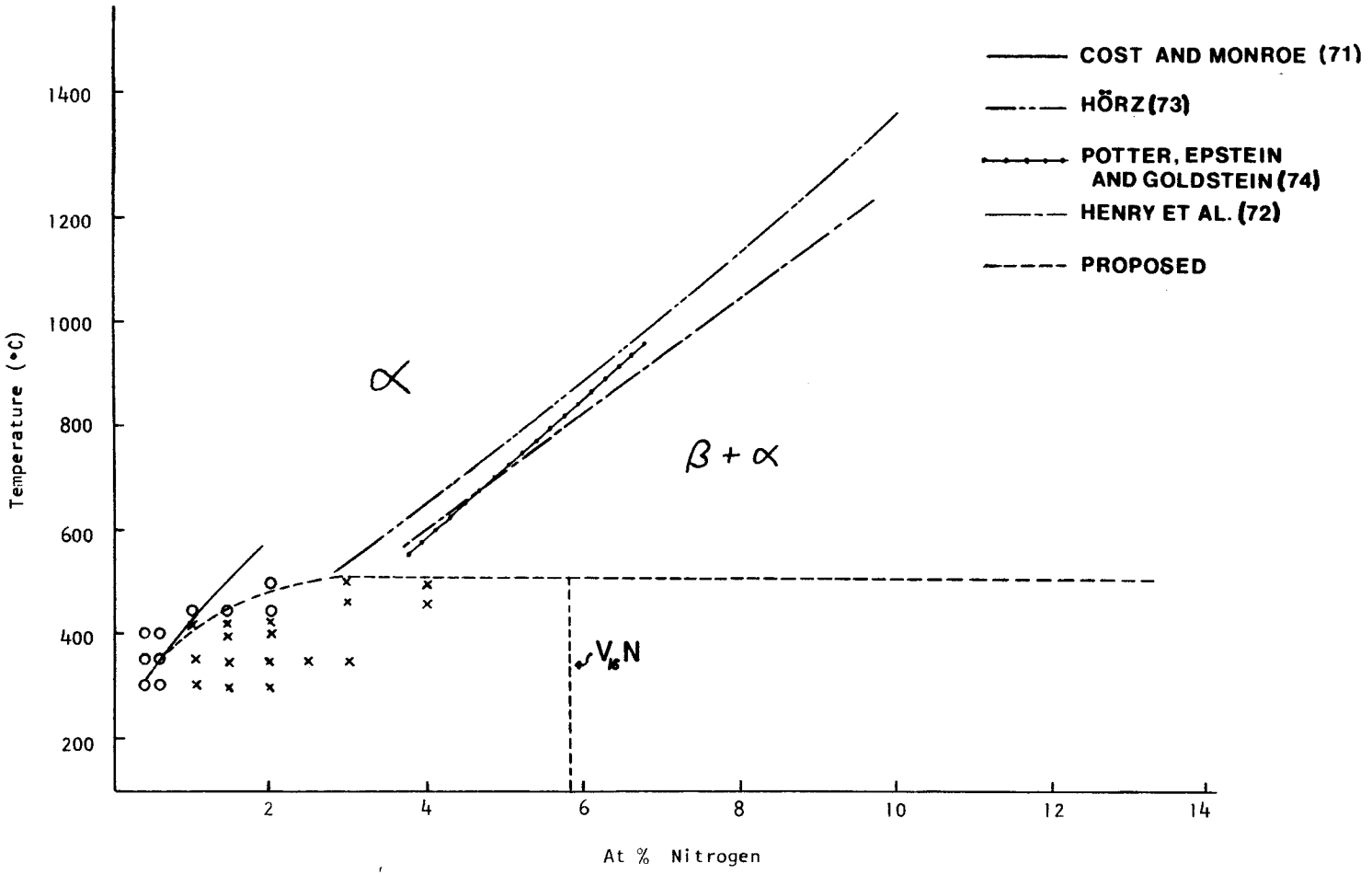

Figure III-2. Compilation of work on the vanadium rich portion of the V-N phase diagram. The data points indicated by x's (two phase) and o's (one phase) were obtained in a transmission electron microscopy study by Potter, Epstein and Goldstein.[74]

temperature peretectoid transformation and a readjustment of the low temperature terminal solubility of the α phase consistent with Potter et al.'s[71] measurements and the rest of the phase diagram.

The $\beta(V_3N)$ phase of this system has a plate-like morphology and a habit plane near (112).[75] The metal atoms in this precipitate have a close packed hexagonal structure rotated 30^{o} around the "c" axis with a lattice parameter 3 times that of the metal atom sublattice. The $V_{16}N$ phase forms with a plate-like morphology on the (100) planes of the vanadium matrix.[76] This phase also has a nitrogen atom superlattice based on a 4 x 4 x 1 array of BCT vanadium atom sub cells.[77] The metal atoms in the metastable V_yN phase are arranged on a BCC lattice only slightly larger than the matrix. The unit cell of the V_yN phase is also BCC containing a 3 x 3 x 3 superlattice of metal atom sub cells.[67] The V_xN phase forms in discs on (100) planes of the α matrix, which are twinned along planes exactly parallel to the (100) planes of the matrix. This phase is analagous to the V_9O phase in the vanadium-oxygen system with the vanadium atoms occupying a BCT lattice. At higher nitrogen contents, the VN phase, which has a NaCl structure, is stable.[78]

CHAPTER IV PREVIOUS STUDIES OF VOID FORMATION IN VANADIUM AND VANADIUM ALLOYS

IV-A. Neutron Irradiation

IV-A-1. Pure Vanadium

The formation of voids in neutron irradiated vanadium has been observed by several experimenters.[79-91] A summary of these results is presented in Table IV-1. In these studies, the total neutron dose ranges from the extremely low value of 1.6×10^{20} n/cm^2 to 6×10^{22} n/cm^2. The conversion from neutron fluence to dpa is determined by the shape of the flux spectrum. For a thermal reactor, such as HFIR, a neutron fluence of 10^{21} n/cm^2 (E > 0.1 MeV) produces approximately 1 dpa, while in a fast reactor, such as FFTF, the same neutron fluence corresponds to 1.4 dpa.[83] Helium production by (n,α) reactions is also important in determining swelling behavior. For both types of fission reactor, a neutron fluence of 1×10^{21} n/cm^2 will produce less than 0.05 appm He.[83] In the first wall of a fusion reactor with a wall loading of 1 MW/m^2, one year of operation will produce $\sim$ 10 dpa and $\sim$50 appm He.[89] Even the low dose studies are, however, important, because they provide a base of comparison for simulation studies. The major drawbacks to neutron irradiations are the extremely long irradiation times required to produce significant dpa levels and the difficulty of properly controlling the irradiation conditions.

Voids were first observed in neutron irradiated vanadium by Wiffen and Steigler,[79,80] who examined specimens irradiated in EBR-II to a fluence of 1.7×10^{22} n/cm^2 at 600°C. In addition to the voids, they

TABLE IV-1 Void Formation in Vanadium and Vanadium Alloys--Neutron Studies

Material	Interstitial Impurities (appm)	Fluence n/cm^2 E > 0.1 MeV	Temperature (^{o}C)	$N_v \times 10^{15}$ (cm^{-3})	d (A)	Swelling (%)	Precipitation Reported	Reference
V	N.G.	1.7×10^{22}[a]	630	5.3×10^{15}	117	0.37	Yes	80
V	5000	5×10^{20}	335	0.34	140	0.05	No	85
V	5000	5×10^{20}	435	0.2	280	0.22	No	85
V	5000	5×10^{20}	600	0.015	780	0.38	No	85
V	5000	5×10^{20}	800	0	-	-	No	85
V	800	4.9×10^{21}	385	12	50	0.08	No	81
V	4500	5.7×10^{21}	385	120	45	0.56	No	81
V	1000	9.7×10^{21}	475	10.6	82	0.34	No	81
V	1000	1.4×10^{22}	550	5.9	170	1.77	No	81
V	1000	1.4×10^{22}	600	2.0	230	1.47	No	81
V	4000	3×10^{21}	450	30	50	0.2	No	86
V	920	1.6×10^{20}	150	0.94	68	0.3	No	82

TABLE IV-1 (continued)

Material	Interstitial Impurities (appm)	Fluence n/cm^2 $E > 0.1$ MeV	Temperature (°C)	$N_v \times 10^{15}$ (cm^{-3})	d (Å)	Swelling (%)	Precipitation Reported	Reference
V	1400	1.6×10^{20}	150	0.035	283	1.4	No	82
V	3000	1.6×10^{20}	150	0.5	110	0.9	No	82
V	600	2.2×10^{20}[b]	420	6.0	35	0.01	Yes	84
V	600	3.7×10^{20}[b]	630	1.0	70	0.02	No	84
V	600	2.7×10^{20}[b]	750	0.1	110	0.007	No	84
V	C.P.	1.1×10^{22}	465	16.0	98	1.04	No	87
V	C.P.	1.1×10^{22}	525	1.2-8.0	102-168	0.3-1.10	No	87
V	C.P.	2.5×10^{22}	625	9.0	138	0.005-0.011	No	87
V	28400[c]	1.1×10^{22}	525	0.74	182	0.6	No	87
V	ZR	3.6×10^{22}	450	13.5	60	0.2	No	88

TABLE IV-1 (continued)

Material	Interstitial Impurities (appm)	Fluence n/cm^2 E > 0.1 MeV	Temperature (°C)	$N_v \times 10^{15}$ (cm^{-3})	d_o (A)	Swelling (%)	Precipitation Reported	Reference
V	ZR	3.6×10^{22}	550	1.25	213	0.6	No	88
V	ZR	3.6×10^{22}	600	0.94	258	0.8	No	88
V	CP	3.6×10^{22}	450	10.6	110	0.7	No	88
V	CP	3.6×10^{22}	550	1.6	224	0.9	No	88
V	CP	3.6×10^{22}	600	0.32	281	0.4	No	88
V-20% Ti	N.G.	9.7×10^{21}	475	0	-	0	Yes	81
V-20% Ti	N.G.	2.0×10^{22}	525	0	-	0	Yes	81
V-20% Ti	Various	1.6×10^{20}	150	0	-	0	Yes	81
V-2.8% Ti	3000	2.2×10^{20}	400	0	-	0	Yes	82
V-1% Ti	1300	1.1×10^{22}	525	0.04-0.5	60-120	0.005-0.011	Yes	87

TABLE IV-1 (continued)

Material	Interstitial Impurities (appm)	Fluence n/cm^2 E> 0.1 MeV	Temperature (^oC)	$N_v \times 10^{15}$ (cm^{-3})	d ($\AA$)	Swelling (%)	Precipitation Reported	Reference
V-3% Ti-V-20% Ti	1300	1.1×10^{22}	525	0	-	0	Yes	87
V-1% Ti	17500[c]	2.5×10^{22}	625	3.5	173	1.36	Yes	87
V-15% Cr-5% Ti	N.G.	3.6×10^{22}	450	0	-	0	No	88
V-15% Cr-5% Ti	N.G.	3.6×10^{22}	550	0	-	0	No	88
V-15% Cr-5% Ti	N.G.	3.6×10^{22}	600	0	-	0	No	88
V-10% Cr	N.G.	1.5×10^{22}	496	0.11	80	0.003	Yes	91
V-10% Cr	N.G.	1.5×10^{22}	580	0.14	93	0.006	Yes	91
V-10% Cr	N.G.	1.5×10^{22}	690	0.005	1580	1.06	No	91
V-10% Cr	N.G.	1.5×10^{22}	805	0.005	1690	1.35	No	91
VANSTAR-7	N.G.	1.5×10^{22}	496	0.9	98	0.045	Yes	91
VANSTAR-7	N.G.	1.5×10^{22}	580	0.3	129	0.040	Yes	91

TABLE IV-1 (continued)

Material	Interstitial Impurities (appm)	Fluence n/cm^2 E>0.1 MeV	Temperature (^oC)	$N_v \times 10^{15}$ (cm^{-3})	d (Å)	Swelling (%)	Precipitation Reported	Reference
VANSTAR-7	N.G.	1.5×10^{22}	690	0	-	≈0	Yes	91
VANSTAR-7	N.G.	1.5×10^{22}	805	0	-	≈0	Yes	91
V-20% Ti	N.G.	1.3×10^{22}	470	0	-	0	Yes	91
V-20% Ti	N.G.	3.5×10^{22}	700	0	-	0	Yes	91
V-20% Ti	N.G.	4.0×10^{22}	440	0	-	0	Yes	91
V-20% Ti	N.G.	4.0×10^{22}	580	0	-	0	Yes	91
V-20% Ti	N.G.	6.1×10^{22}	780	0	-	0	Yes	91

C.P. -- Commercial Purity
N.G. -- Not Given
Z.R. -- Zone Refined

a.) E > 0 MeV
b.) E > 1 MeV
c.) Oxygen Doped

observed that irradiation produced plate-like precipitates, which were attributed to interstitial impurities. Essentially all of the subsequent studies of neutron irradiated vanadium have attempted to determine the effect of interstitial impurities on void formation. In a follow up study, Wiffen[81] found that at 385°C a sample containing 4500 appm interstitial impurities had an order of magnitude higher void density than a sample containing 1000 appm. Elen[82,83,84] attempted to study this effect systematically by irradiating specimens containing three different impurity levels. He found that there was a significant effect but was unable to categorize that effect. Plate-like precipitates similar to those observed by Wiffen and Steigler were observed in the samples irradiated at 420°C but not in those irradiated at 650°C or 750°C. Another study of the effects of interstitial impurities was performed by Carlander, Harkness and Santhanam.[87] The interpretation of their results is complicated by the extremely inhomogeneous void distribution that they observed. However, increasing the oxygen content from 0.64 at% to 2.8 at% did result in a double peaked void size distribution. Bartlett et al.[88] also noted that the void distribution exhibited extreme spatial inhomogeneities in both commercially pure and zone refined vanadium irradiated to 3.6×10^{22} n/cm^{-2} at 450-600°C. These inhomogeneities were much larger than any detected effect of sample purity on void formation.

In more recent studies by Bressers and Cambini[89] and Bressers and van Witzenburg[90] significant increases in void concentrations with increasing oxygen content have been noted. These samples were irradiated at 450°C to fluences of 3×10^{20} n/cm^3. Unfortunately, the details of this study are not yet available. It should be noted, however, that the

oxygen doped samples irradiated by Bressers and van Witzenburg contained only 850 appm O, and the pure samples contained only 30 appm O. It is, therefore, difficult to compare this study to previous studies where the "pure" material often contained as much as 1000 appm interstitial impurities.

Although a number of experimenters have attempted to study the effect of interstitial impurities on void formation in vanadium, no clear trend has been established. This conclusion is illustrated in Figure IV-1 where void density has been plotted as a function of irradiation temperature for a range of experiments in vanadium. (No data from the experiments by Bressers and Cambini or Bressers and van Witzenburg is included.) The samples labeled "pure V" were all reported to have interstitial impurity contents less than 1000 appm, while those labeled "impure V" were either reported as being commercial purity or having interstitial impurity contents in excess of 3000 appm. Any effect of the interstitial impurities falls well inside the experimentally observed variance. This variance is accentuated by the inhomogeneous void distributions reported in several studies.

IV-A-2. Vanadium Alloys

The irradiation response of the V-Ti binary system has been studied by several investigators. Elen[82,83] first observed in 1970 that the addition of 2.8 to 5.5 at% Ti suppressed void formation in vanadium. Wiffen[81] also observed that void formation was suppressed in a V-20 at% Ti alloy. A number of V-Ti binary and V-Ti-Cr ternary alloys were then surveyed by Carlander et al.[79] The only Ti bearing alloy in which voids were observed was V-1%Ti. Although voids were observed in

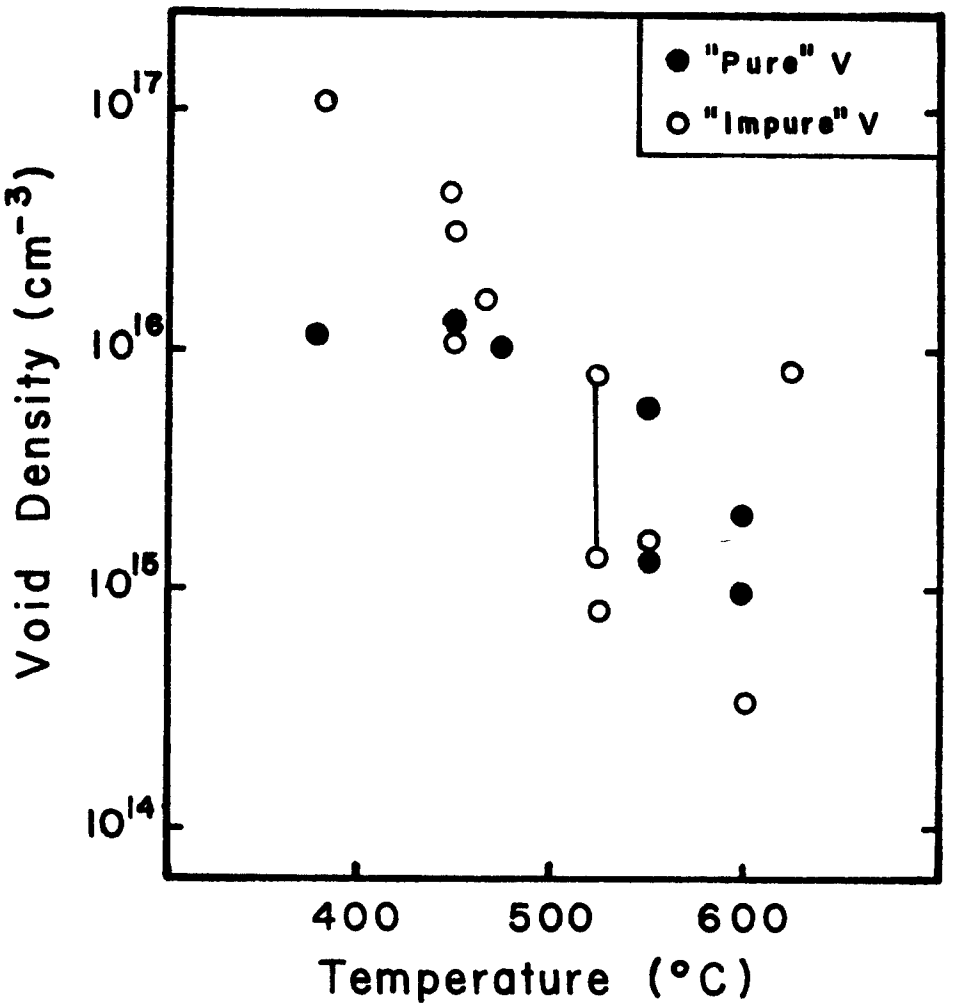

Figure IV-1. Summary of results from neutron irradiations of vanadium. Solid circles represent samples of "high purity" vanadium containing less than 1000 appm interstitial impurities. The open circles represent samples having interstitial impurity concentrations in excess of 3000 appm. The two impure vanadium data points connected by a solid line were taken in a single sample with an inhomogeneous void distribution. There is no evidence of an effect of interstitial impurities on void nucleation in these studies.

the V-1%Ti alloy, the swelling values only became comparable to the unalloyed vanadium when 1.75 at% O was added to the solution. The suppression of void swelling in V by Ti additions has also been observed by Bartlett et al.[88] and Bentley and Wiffen.[91]

A very few irradiations of V-Cr binary alloys have been performed. Carlander et al.[87] report seeing a high density of extremely small voids in V-10Cr and V-15Cr alloys irradiated to 1 x 10^{22} n/cm^2 (E 0.1 MeV) at 525^{o}C. The resultant swelling values in these V-Cr alloys were extremely low, and the void parameters were not reported. Bentley and Wiffen[91] also irradiated a V-10%Cr alloy and obtained similar results in samples irradiated at 500^{o}C and 580^{o}C. In extending these irradiations to 700^{o}C and 800^{o}C, Bentley and Wiffen found that significant swelling levels were achieved through the formation of a low density ($\sim$5 x 10^{12} cm^{-3}) of extremely large voids (> 1500 Å diameter).

IV-B. Heavy Ion Irradiations

The use of heavy ion simulation techniques has provided more data on void formation at higher dpa levels. A summary of heavy ion studies in vanadium is given in Table IV-2. These studies span the range from 1 to 60 dpa and dose rates vary from 10^{-4} to 10^{-2} dpa/sec. Dose rates in steady state fast fission reactors are typically of the order of 10^{-6} dpa/sec.

The first heavy ion irradiations of vanadium were performed with 7.5 MeV Ta ions by Kulcinski and Brimhall.[92] They found voids in samples irradiated to 80 dpa at 800^{o}C. Plate-like precipitation was noted in the samples irradiated at 700^{o}C. The effect of helium on void nucleation

TABLE IV-2 Void Formation in Vanadium and Vanadium Alloys--Heavy Ion Studies

Material	Interstitial Impurities (appm)	Helium (appm)	Ion	dpa rate (sec^{-1})	dpa	Temperature (°C)	N_v (cm^{-3}) x 10^{15}	d (Å)	Swelling (%)	Precipitation Reported	Reference
V	600	0	7.5 MeV Ta	8×10^{-3}	30	700	0.27	-	2.3	Yes	92
V	600	0	7.5 MeV Ta	8×10^{-3}	22	800	0.1	-	2.9	No	92
V	600	0	7.5 MeV Ta	8×10^{-3}	22	900	-	-	-	No	92
V	600	0	7.5 MeV Ta	8×10^{-3}	83	900	-	-	-	No	92
V	550	10	3.3 MeV Ni	4×10^{-3}	60	650	0.97	120	0.21	Yes	95
V	550	100	3.3 MeV Ni	4×10^{-3}	60	650	1.60	115	0.29	Yes	95
V	550	100	3.3 MeV Ni	4×10^{-3}	60	650	1.50	100	0.21	Yes	95
V	4500	10	3.3 MeV Ni	4×10^{-3}	60	650	18.0	52	0.22	Yes	95
V	4500	100	3.3 MeV Ni	4×10^{-3}	60	650	19.0	45	0.13	Yes	95

TABLE IV-2 (continued)

Material	Interstitial Impurities (appm)	Helium (appm)	Ion	dpa rate (sec^{-1})	dpa	Temperature (°C)	N_v (cm^{-3}) x 10^{15}	d_o (Å)	Swelling (%)	Precipitation Reported	Reference
V	550	10	3.3 MeV Ni	4×10^{-3}	60	750	1.9	206	2.17	Yes	95
V	550	100	3.3 MeV Ni	4×10^{-3}	60	750	1.7	141	0.61	Yes	95
V	4500	10	3.3 MeV Ni	4×10^{-3}	60	750	1.8	212	2.12	Yes	95
V	4500	10	3.3 MeV Ni	4×10^{-3}	60	750	2.1	238	3.45	Yes	95
V	4500	100	3.3 MeV Ni	4×10^{-3}	60	750	2.3	113	0.47	Yes	95
V	4500	100	3.3 MeV Ni	4×10^{-3}	60	750	2.5	100	0.34	Yes	95
V	550	10	3.3 MeV Ni	4×10^{-3}	60	700	0.94	302	2.99	Yes	96
V	550	10	3.3 MeV Ni	4×10^{-3}	60	700	1.0	285	2.86	Yes	96
V	550	10	3.3 MeV Ni	4×10^{-3}	60	700	1.0	279	2.68	Yes	96

TABLE IV-2 (continued)

Material	Interstitial Impurities (appm)	Helium (appm)	Ion	dpa rate (sec^{-1})	dpa	Temperature (oC)	N_v (cm^{-3}) x 10^{15}	d (Å)	Swelling (%)	Precipitation Reported	Reference
V	4500	100	3.3 MeV Ni	4×10^{-3}	60	700	16.3	58	0.25	Yes	96
V	4500	100	3.3 MeV Ni	4×10^{-3}	60	700	15.6	61	0.29	Yes	96
V[a]	550	10	3.3 MeV Ni	4×10^{-3}	60	850	0.22	407	1.83	Yes	96
V[b]	550	10	3.3 MeV Ni	4×10^{-3}	60	850	0.035	414	0.38	Yes	96
V	4500	10	3.3 MeV Ni	4×10^{-3}	60	850	1.2	186	0.99	Yes	96
V	4500	10	3.3 MeV Ni	4×10^{-3}	60	850	1.0	184	0.79	Yes	96
V	C.P.	0	46 MeV Ni	8×10^{-4}	16	750	-	-	0	No	93
V	C.P.	3	46 MeV Ni	1.2×10^{-4}	2.4	750	0.01	640	0.27	No	93
V	C.P.	3	46 MeV Ni	4.5×10^{-4}	9	750	0.2	300	0.54	No	93

TABLE IV-2 (continued)

Material	Interstitial Impurities (appm)	Helium (appm)	Ion	dpa rate (sec^{-1})	dpa	Temperature (°C)	N_v (cm^{-3}) x 10^{15}	d o (A)	Swelling (%)	Precipitation Reported	Reference
V	C.P.	3	46 MeV Ni	8×10^{-4}	16	750	0.17	350	0.73	No	93
V	C.P.	0	7.5 MeV Ta	10^{-2}	15	700	0.25	330	0.6	No	93
V	C.P.	0	7.5 MeV Ta	10^{-2}	16	800	0.005-0.05	550-900	0.7	No	93
V	C.P.	0	7.5 MeV Ta	10^{-2}	15	900	-	-	0	No	93
V	C.P.	100-300[c]	5 MeV Ni	1.2×10^{-2}	50-60	750	3-5	120-142	0.66-0.83	No	94
V	C.P.	0	5 MeV Ni	1.2×10^{-2}	50-60	750	5-10	116-140	0.92-1.15	No	94
V	550	0	3 MeV V	5.5×10^{-3}	2.4	700	6	70	0.2	No	97
V	550	0	3 MeV V	5.5×10^{-3}	4.3	700	1.8	100	0.2	No	97
V	550	0	3 MeV V	5.5×10^{-3}	22	700	0.15-0.34	350	1.2	No	97

TABLE IV-2 (continued)

Material	Interstitial Impurities (appm)	Helium (appm)	Ion	dpa rate (sec^{-1})	dpa	Temperature (^oC)	N_v (cm^{-3}) x 10^{15}	d o (A)	Swelling (%)	Precipitation Reported	Reference
V	550	0	3 MeV V	5.5×10^{-3}	34	700	0.2-0.4	375	1.2	No	97
V	550	0	3 MeV V	5×10^{-3}	1	650	5.5	70	0.12	No	98
V	550	0	3 MeV V	5×10^{-3}	4	650	2.0	110	0.18	No	98
V	550	0	3 MeV V	5×10^{-3}	13.4	650	1.7	150	0.38	Yes	98
V	550	0	3 MeV V	5×10^{-3}	23.5	650	3.0	70	0.072	Yes	98
V	550	0	3 MeV V	5×10^{-3}	42	650	2.8	60	0.05	Yes	98
V	550	0	3 MeV V	5×10^{-3}	54.3	650	1.0	60	0.03	Yes	98
V	625	0	19 MeV Cu	3×10^{-4}	1	600	0.25	140	0.1	Yes	103
V	625	0	19 MeV Cu	3×10^{-4}	1.5	600	0.07	270	0.15	Yes	103

TABLE IV-2 (continued)

Material	Interstitial Impurities (appm)	Helium (appm)	Ion	dpa rate (sec^{-1})	dpa	Temperature (°C)	N_v (cm^{-3}) x 10^{15}	d_o (A)	Swelling (%)	Precipitation Reported	Reference
V	625	0	19 MeV Cu	3×10^{-4}	1	650	0.1	370	0.5	Yes	103
V	625	0	19 MeV Cu	3×10^{-4}	2	650	0.015	750	0.5	Yes	103
V	625	0	19 MeV Cu	3×10^{-4}	5	650	0.055	760	2.5	Yes	103
V[d]	625	0	19 MeV Cu	3×10^{-4}	1	650	0.4	160	0.2	Yes	103
V	625	0	19 MeV Cu	3×10^{-4}	1	700	0.045	590	1.0	Yes	103
V	625	0	19 MeV Cu	3×10^{-4}	1	700	0.02	730	1.0	Yes	103
V	625	0	19 MeV Cu	3×10^{-4}	3	700	0.0015	850	0.1	Yes	103
V[d]	625	0	19 MeV Cu	3×10^{-4}	1	700	0.3	410	1.0	Yes	103
V	625	0	19 MeV Cu	3×10^{-4}	1	750	0.0003	980	0.03	Yes	103

TABLE IV-2 (continued)

Material	Interstitial Impurities (appm)	Helium (appm)	Ion	dpa rate (sec^{-1})	dpa	Temperature (°C)	N_v (cm^{-3}) x 10^{15}	d o (A)	Swelling (%)	Precipitation Reported	Reference
V	1000	0	3 MeV V	5.5×10^{-3}	20	650	0.9	120	0.1	Yes	99
V	1000	0	3 MeV V	5.5×10^{-3}	20	720	0.1	700	2.4	No	99
V	1000	0	3 MeV V	5.5×10^{-3}	20	740	0.1	600	1.4	No	99
V	1000	0	3 MeV V	5.5×10^{-3}	20	810	0.02	780	1.0	Yes	99
V	1000	0	3 MeV V	5.5×10^{-3}	20	910	0.007	700	0.2	Yes	99
V	550	0	3 MeV V	5.5×10^{-3}	7	700	0.5-0.9				98
V	550	0	3 MeV V	5.5×10^{-3}	43	700	0.3-0.9				98
V	550	0	3 MeV V	5.5×10^{-3}	54	700	0.3-0.5				98
V-1% Ti	1400	0	3 MeV V	5.5×10^{-3}	2.4-34	700	-	-	0	Yes	97

TABLE IV-2 (continued)

Material	Interstitial Impurities (appm)	Helium (appm)	Ion	dpa rate (sec^{-1})	dpa	Temperature (^{o}C)	N_v (cm^{-3}) x 10^{15}	d_o (A)	Swelling (%)	Precipitation Reported	Reference
V-1% Ti	1400	0	3 MeV V	5.5×10^{-3}	54	700	0.5	70	0.02	Yes	97
V-0.1%C	-	0	3 MeV V	5.5×10^{-3}	20	660	0.5	90	0.2	Yes	99
V-0.1%C	-	0	3 MeV V	5.5×10^{-3}	20	725	0.08	600	0.9	Yes	99
V-0.1%C	-	0	3 MeV V	5.5×10^{-3}	20	780	0.01	1000	1.0	Yes	99
V-0.1%C	-	0	3 MeV V	5.5×10^{-3}	20	790	0.1	500	1.0	Yes	99
V-0.1%C	-	0	3 MeV V	5.5×10^{-3}	20	900	0.005	800	0.1	Yes	99
V-0.4%C	-	0	3 MeV V	5.5×10^{-3}	20	685	1.0	130	0.2	Yes	99
V-0.4%C	-	0	3 MeV V	5.5×10^{-3}	20	700	0.2	440	1.1	Yes	99
V-0.4%C	-	0	3 MeV V	5.5×10^{-3}	20	765	0.1	400	0.5	Yes	99

TABLE IV-2 (continued)

Material	Interstitial Impurities (appm)	Helium (appm)	Ion	dpa rate (sec^{-1})	dpa	Temperature (^oC)	N_v (cm^{-3}) x 10^{15}	d o (A)	Swelling (%)	Precipitation Reported	Reference
V-0.4%C	-	0	3 MeV V	5.5×10^{-3}	20	800	0.01	500	0.4	Yes	99
V-0.4%C	-	0	3 MeV V	5.5×10^{-3}	20	900	0.004	800	0.2	Yes	99
V-1% N	-	0	3 MeV V	5.5×10^{-3}	20	650	0.1	280	0.13	No	99
V-1% N	-	0	3 MeV V	5.5×10^{-3}	20	720	0.04	420	0.3	No	99
V-1% N	-	0	3 MeV V	5.5×10^{-3}	20	765	0.02	470	0.2	No	99
V-1% N	-	0	3 MeV V	5.5×10^{-3}	20	780	0.01	380	0.1	No	99
V-1% N	-	0	3 MeV V	5.5×10^{-3}	20	895	0.006	290	0.05	No	99
V-1% O	-	0	3 MeV V	5.5×10^{-3}	20	660	6.5	110	0.9	Yes	99
V-1% O	-	0	3 MeV V	5.5×10^{-3}	20	710	0.06	590	0.8	No	99

TABLE IV-2 (continued)

Material	Interstitial Impurities (appm)	Helium (appm)	Ion	dpa rate (sec^{-1})	dpa	Temperature (^oC)	N_v (cm^{-3}) x 10^{15}	d o (A)	Swelling (%)	Precipitation Reported	Reference
V-1% O	-	0	3 MeV V	5.5×10^{-3}	20	760	0.06	420	0.3	No	99
V-1% O	-	0	3 MeV V	5.5×10^{-3}	20	785	0.03	590	0.4	No	99
V-1% O	-	0	3 MeV V	5.5×10^{-3}	20	910	0.003	710	0.1	No	99
V-1% O	-	0	3 MeV V	5.5×10^{-3}	20	550	40	30	0.065	No	102
V-1% O	-	0	3 MeV V	5.5×10^{-3}	20	600	4.0	50	0.03	No	102
V-1% O	-	0	3 MeV V	5.5×10^{-3}	20	700	0.04	510	0.4	No	102
V-1% O	-	0	3 MeV V	5.5×10^{-3}	2	700	0.07	160	0.02	?	102
V-1% O	-	0	3 MeV V	5.5×10^{-3}	15	700	0.02	510	0.2	No	102
V-1%)	-	0	3 MeV V	5.5×10^{-3}	25	700	0.2	470	1.0	No	102

TABLE IV-2 (continued)

Material	Interstitial Impurities (appm)	Helium (appm)	Ion	dpa rate (sec^{-1})	dpa	Temperature (^oC)	N_v (cm^{-3}) x 10^{15}	d o (A)	Swelling (%)	Precipitation Reported	Reference
V-2% O	-	0	3 MeV V	5.5×10^{-3}	3	700	0.06	70	0.001	?	102
V-2% O	-	0	3 MeV V	5.5×10^{-3}	17	700	0.01	400	0.06	?	102
V-2% O	-	0	3 MeV V	5.5×10^{-3}	32	700	0.02	450	0.2	?	102
V-3% O	-	0	3 MeV V	5.5×10^{-3}	22	700	0.004	520	0.03	?	102
V-3% O	-	0	3 MeV V	5.5×10^{-3}	37	700	0.007	490	0.1	?	102
V-4% O	-	0	3 MeV V	5.5×10^{-3}	35	700	0.008	240	0.008	?	102
V-1% Ti	NG	0-150	4 MeV Ni	NG	45-120	600	0	-	0	Yes	100
V-10% Ti	NG	5-150	4 MeV Ni	NG	45-120	600	0	-	0	Yes	100
V-1% Ti	1400	0	3 MeV V	5.5×10^{-3}	2.4-34	700	-	-	0	Yes	97

TABLE IV-2 (continued)

Material	Interstitial Impurities (appm)	Helium (appm)	Ion	dpa rate (sec^{-1})	dpa	Temperature (^oC)	N_v (cm^{-3}) x 10^{15}	d o (A)	Swelling (%)	Precipitation Reported	Reference
V-1% Ti	1400	0	3 MeV V	5.5×10^{-3}	54	700	0.5	70	0.02	Yes	97
V-1% Ti	NG	0	2.7 MeV V	5×10^{-3}	2-60	650	0	-	0	Yes	101

C.P. -- Commercial Purity
N.G. -- Not Given
Z.R. -- Zone Refined

a.) Near grain boundary
b.) In center of grain
c.) Simultaneous injection
d.) 25 μm surface layer removed

was studied by Brimhall and Simonen.[93,94] They found that in order to nucleate voids at 750°C helium was necessary at a dose rate of 8×10^{-4} dpa/sec, while a dose rate of 1×10^{-2} dpa/sec was sufficient to nucleate voids in the absence of helium. The difficulty in nucleating voids in the absence of helium at the lower dose rate could reflect the temperature shift described in Section II-C. At the higher dose rate, no difference between helium pre-doping and simultaneous helium injections was detected. This is the only simultaneous helium ion irradiation of pure vanadium that has been reported.

Other than the two aforementioned studies, all of the heavy ion irradiations of vanadium and vanadium alloys have been performed at Argonne National Laboratory (ANL) or the University of Wisconsin. The University of Wisconsin results will be reviewed in section IV-C. The ANL irradiations described below were performed using the 4 MeV Dynamitron facility. The dpa rate for all of these experiments was approximately 5×10^{-3} dpa/sec.

The initial irradiations performed at ANL in 1973 by Santhanam Taylor and Harkness used 3 MeV Ni ions to study void formation in commercial and high purity vanadium. Swelling was measured as a function of temperature at 60 dpa. The peak swelling temperature shifted from 700°C in the high purity vanadium to 750°C in the commercial purity vanadium. Even though the samples were pre-injected with at least 10 appm of helium, this effect was attributed to impurity enhanced void nucleation, because larger densities of smaller voids were observed in the commercial purity vanadium. Segregation of impurity atoms to voids was observed in both purities of material. At the lower temperature, segre-

gation was observed as strain fields around the voids, while at higher temperatures precipitation was observed on the void faces. In all cases the unirradiated control samples displayed no signs of precipitation. It was postulated[51] that this segregation was caused by the "dragging" of implanted nickel ions to sinks by diffusing point defects.

In 1974 the ANL researchers began using 3 MeV vanadium ions for their irradiations. The first self ion irradiations were performed by Santhanam, Taylor, Kestel and Steves,[47] who studied the dose dependence of swelling in high purity vanadium at 700°C. Although the swelling increased monotonically with dose, the void density actually decreased. When the swelling in the self ion irradiated vanadium was linearly extrapolated to 60 dpa, agreement with the previous nickel ion irradiations was obtained. However, the self ion irradiations cannot be directly compared to the nickel ion irradiations, because all of the nickel ion irradiated specimens were pre-doped with helium, while the self ion irradiated specimens contained no helium. A similar study of the dose dependence of swelling at 650°C in self ion irradiated vanadium was conducted by Agarwal and Taylor.[98] At this lower temperature, swelling did not increase monotonically. A sharp reduction in swelling, associated with a reduction in void size, was noted at doses about 13.4 dpa. This reduction in swelling was attributed to the large number of irradiation induced precipitates which formed at the higher doses. No clear trend can be seen in the evolution of the void density.

The ANL researchers then initiated a study of the temperature dependence of swelling in pure V irradiated to 20 dpa with 3 MeV V ions.[99]

In that study, swelling was observed over the range 650°C to 900°C. The peak in swelling occurred at 720°C.

Irradiations of V-1Ti, V-10Ti and V-10Cr have also been performed at ANL. No voids were detected at 600°C in the V-1Ti alloy or the V-10Cr alloy even when they were pre-doped with as much as 150 appm He and irradiated with Ni ions to doses up to 120 dpa.[100] When irradiated at 700°C with V ions and no helium pre-doping, the V-1Ti alloy was resistant to swelling up to 34 dpa but at 54 dpa small voids began to form.[97] V-10Ti was also shown to be resistant to swelling up to 60 dpa at 650°C.

A series of vanadium specimens doped with carbon (0.1 and 0.4 at%), nitrogen (1 at%) and oxygen (1, 2, 3 and 4 at%) were irradiated using 3 MeV V^+ ions in the temperature range 550°C to 880°C by Agarwal, Potter and Taylor.[99] The samples doped with oxygen and carbon both exhibited precipitates in the form of fine platelets forming on (012) habit planes. In the carbon doped specimens, these precipitates were observed at higher temperatures; and their density increased with increasing carbon content, indicating that they were probably irradiation induced carbides. No precipitation was observed in the nitrogen doped specimens. Of the three alloying additions, nitrogen had the most pronounced effect on swelling. One percent nitrogen, as compared to pure V, reduced the void density in samples irradiated to 20 dpa at all temperatures. The average void diameter was also reduced by nitrogen additions at temperatures above 650°C. The level of interstitial doping in the carbon alloys was lower (0.1 and 0.4 at%), and the overall decrease in swelling was less dramatic.

A more thorough study was made of the vanadium-oxygen system.[102] A series of V-1%O samples were irradiated to 20 dpa at temperatures between 550°C and 900°C. At temperatures below 700°C, oxygen doping increased the void density and did not significantly change the average void size. Above 700°C, the predominant effect of oxygen doping was the reduction of the average void diameter, while the void density was only slightly decreased. The addition of 1 at% oxygen, therefore, increases swelling at temperatures below 700°C and decreases swelling at higher temperatures. The effect of oxygen concentration on swelling rate at 700°C was then studied. Increasing the oxygen content was shown to dramatically decrease the void density. This effect, coupled with an overall decrease in average void size, resulted in an exponential reduction in swelling with increasing oxygen content.

IV-C. University of Wisconsin Irradiations

A previous study of void formation in high purity vanadium using the University of Wisconsin Heavy Ion Irradiation Facility was completed in 1977 by W.J. Weber.[103,104] The same base material was used in Weber's thesis and in this author's irradiations. The irradiation conditions were also similar for both studies. However, improved beam transmission has given a three-fold increase in dpa rate, allowing higher dose levels to be obtained in the present study.

Weber divides his results into two groups.[25] The samples in the first group[103] were all annealed in the heavy ion irradiation facility prior to irradiation. These samples can be characterized by a high density of slab shaped precipitates, which are often associated with voids. The actual density of precipitates is a strong function of

temperature and can be roughly correlated with the void density. The extent of precipitation was decreased by two orders of magnitude in samples which were electropolished to remove a 25 μm layer after the anneal but prior to irradiation. These samples were then outgassed at the maximum irradiation temperature (750°C) to remove hydrogen introduced during electropolishing. These samples with a decreased precipitation also exhibited an increase in void density and a decrease in the average void size. This experiment demonstrated that the precipitation was associated with a surface related contamination which occurred during the high temperature anneal. Although the pressure during the anneal ($<5 \times 10^{-8}$ Torr) seemed too low to explain the observed amounts of contamination, a series of samples was sent to Grumman Aerospace Corporation for analysis of the interstitial impurity content.[25] By using light ion beams and resonances in the charged particle production cross section, a depth dependent determination of the interstitial impurity content was performed. No increase in the carbon, oxygen or nitrogen level was observed in the region of examination. Subsequent energy-dispersive x-ray analysis studies proved that the precipitates were nickel rich. The nickel contamination is presumed to have arisen from stainless steel portions of the heater and the chromel/alumel thermocouples.

The second group[104] of samples were annealed in a separate high vacuum furnace. The problem of nickel contamination was not as great in this furnace, because all of the hot portions of the furnace were constructed of refractory metals. However, the sample temperature was still measured using chromel/alumel (nickel alloy) thermocouples. Some of the samples annealed in the high vacuum furnace were electropolished

to remove 25 μm, and others were irradiated in the as annealed condition.

The swelling obtained at one dpa in the second group of samples is plotted as a function of temperature in Figure IV-2. Voids were observed over the temperature range from 200°C to 700°C. At 150°C only black spot damage was observed; and at temperatures above 750°C, no voids were found. Weber concluded that voids form in heavy ion irradiated, high purity vanadium at temperatures approaching two tenths of the melting point. Prior to this study, no heavy ion irradiations of vanadium had been performed below 550°C. Weber also observed that the temperature dependent swelling curve was double peaked. A broad, low temperature peak occurred between 200°C and 550°C; and a narrow, high temperature peak occurred at 650°C. A minimum at 550°C between the two peaks was attributed to the formation of thin-plate precipitates unlike those observed in the nickel contaminated specimens.

IV-D. Summary of Previous Studies

There is not yet enough systematic data to draw any specific conclusions about void swelling in vanadium, but some general trends can be seen. No direct correlations of neutron and heavy ion studies is possible because there are too many variables, such as dose rate, dose, sample purity, irradiation environment, etc., which are not sufficiently understood. There is, as predicted by theory, a dose rate induced shift in the peak swelling temperature; but the exact temperature dependence has not been quantified. Plate-like radiation induced precipitation has been observed in many of the neutron studies and several of the heavy ion simulation studies. The addition of titanium in all cases enhances

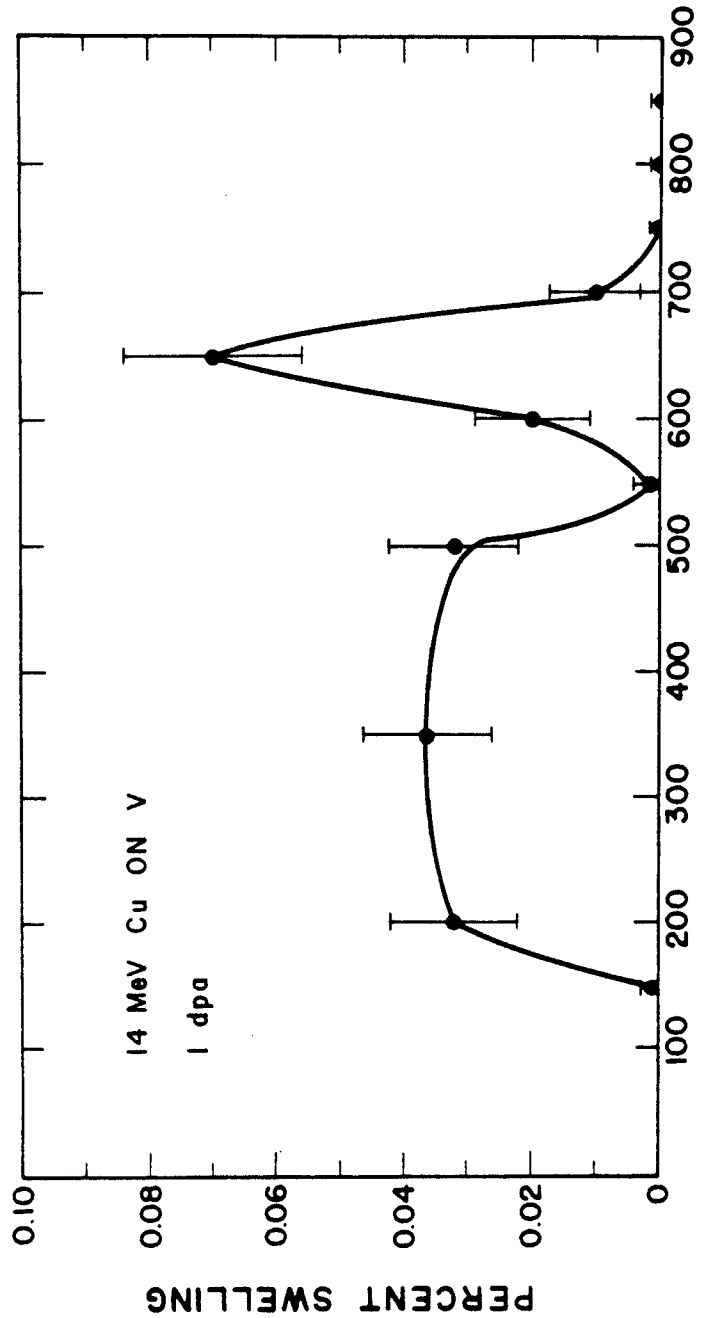

Figure IV-2. Results of previous heavy ion irradiations of pure vanadium at the University of Wisconsin. These samples were irradiated as part of W.J. Weber's thesis program.[25]

precipitation and suppresses swelling. Interstitial impurities seem to play a more significant role in heavy ion irradiations than in neutron irradiations.

Although the results obtained in both neutron and heavy ion irradiations are quite encouraging, caution must be used in extrapolating them to fusion reactor environments, where high helium production rates are to be expected. Results recently obtained by Erlich and Kaletta[105] demonstrate that significant amounts of swelling occur at 600°C due to helium bubble formation in both pure V and V-20Ti doped with 500 appm He.

CHAPTER V EXPERIMENTAL METHODS

V-A. Sample Preparation

Two sources of stock material were used for the irradiations reported in this study. The specimens for the pure vanadium irradiations were taken from extremely high purity stock, containing less than 800 appm interstitial impurities and 10 appm substitutional impurities. The same high purity vanadium stock was used in irradiations performed by W.J. Weber.[25] This high purity vanadium was supplied by Dr. R.E. Reed[106] of Oak Ridge National Laboratory. The specimens of V-lat%N were prepared from the same high purity stock material. The vanadium-lat%Ni stock was provided by Dr. P.R. Okamoto[107] of Argonne National Laboratory. The chemical analysis of the high purity vanadium is given in Table V-1. The low carbon, nitrogen and oxygen contents of the high purity vanadium were confirmed in an independent analysis by investigators at Grumman Aerospace Corporation.[25]

The V-lat%N alloy was prepared from the high purity vanadium stock material. This nitrogen doping was accomplished in a Sieverts apparatus at Argonne National Laboratory under the direction of Dr. D. I. Potter.[108] In this apparatus a strip of high purity vanadium 0.4 cm x 0.02 cm x 20 cm was heated resistively to 1250^{o}C at a base pressure of 5 x 10^{-7} Torr. A known quantity of high purity nitrogen gas was bled into the apparatus and absorbed by the vanadium strip. The samples were then homogenized for 15 minutes at 1250^{o}C and helium quenched. Samples of 1at%N and 0.1at%N were prepared, but only two preliminary irradiations of the 0.1at%N alloy were performed.

TABLE V-1 Chemical Analysis of Vanadium Stock

Impurity	appm (atomic)
C	213
O	153
N	259
H	153
Ta	0.06
W	0.05
Al	0.09
Fe	3
Si	5
Ti	0.1
Co, Cr, Cu, Ni	Not detected

All of the samples were prepared using the same pre-irradiation treatment. Prior to this treatment, the pure V and V-1% Ni stock was in the form of thin sheets, while the V-1%N was already punched into 3 mm discs. First, the samples were mechanically polished with fine emory paper to produce a flat surface and then electropolished to remove the surface damage. The pure V and V-1%Ni were then punched into 3 mm discs. Identification numbers were scratched on the back of all of the specimens and a final electropolish performed to remove any sharp edges or residual scratches. The samples were annealed for one hour at 1050 ^{o}C. The pressure during the anneal was less than 1 x 10^{-8} Torr. The temperature was raised gradually over a three hour period prior to the anneal and furnace cooled after the anneal. After this treatment, all of the specimens exhibited a single phase, well annealed microstructure with a dislocation density $<10^{8}$ cm^{-2}.

It was suggested in Weber's thesis[25] that the chromel/alumel thermocouples used in the high vacuum annealing furnace were a possible source of nickel contamination. This mechanism for nickel contamination was confirmed in this study and the chromel/alumel thermocouples were replaced with W/W-Re thermocouples. These results are reported in Section VI.

It is extremely important to anneal the specimens after electropolishing because significant levels of hydrogen can be introduced during the electropolish. This effect was observed in nickel by Whitley[109] and was suggested to explain Weber's results in vanadium. To demonstrate the effect of hydrogen in vanadium, two samples of V-0.1%N (both well annealed from the nitrogen doping procedure) were irradiated under identical conditions at 650^{o}C to 2 dpa. Both samples were electropolished

to produce a flat surface, but one was outgassed for 1 hour at 1050°C prior to irradiation, and the other was irradiated in the as electropolished condition. The results of these irradiations are reported in Table V-2. The hydrogen introduced during the electropolish produced a higher density of slightly smaller voids in the sample that was not outgassed. These results are consistent with Weber's observations.

V-B. Irradiation Facility

All of the irradiations in this study were performed in the University of Wisconsin Heavy Ion Irradiation Facility.[26] This is a high temperature, high vacuum facility, which was designed specifically for the irradiation of vanadium and other reactive refractory metals.

A schematic of the University of Wisconsin tandem accelerator facility is given in Figure V-1. Negative ions are created in the heavy ion source and accelerated up the negative acceleration tube to the high voltage terminal, which, in these experiments, was operated at a positive potential of 3.5 million volts. At the high voltage terminal, the ion beam passes through a nitrogen gas stripper canal; and the positive ions are then accelerated down the positive acceleration tube. If the terminal voltage is V and the charge of a positive ion exiting at the high energy end of the accelerator is q, then its energy, E, is

$$E = q(1+V). \qquad (5\text{-}1)$$

The mass energy product (30 MeV-amu) of the 90° analyzing magnet located in front of the sample chamber is too low to bend the energetic heavy ion beam. The sample chamber, therefore, is located near the tandem axis, and slight ($\sim 1/4^{\circ}$) magnetic analysis must be used to prevent

TABLE V-2 Vanadium-0.1% Nitrogen Irradiated to 2 dpa at 650°C With 14 MeV Cu^{3+} Ions

Sample	<d>	ρ_V	$\Delta V/V$ (%)
Outgassed	584 Å	3×10^{12} cm^{-3}	0.07
Electroplated	386 Å	6×10^{13} cm^{-3}	0.41

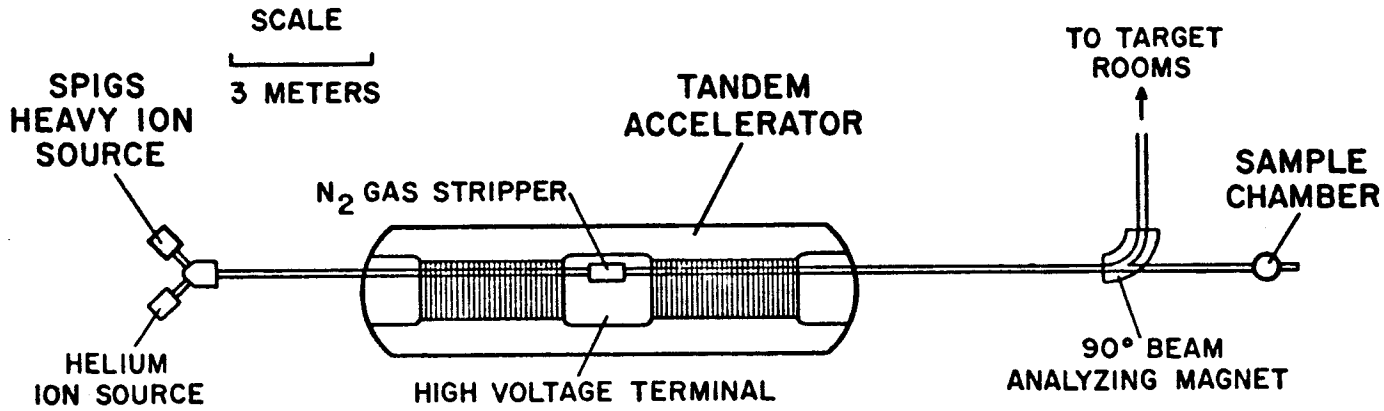

UNIVERSITY OF WISCONSIN HEAVY ION SIMULATION FACILITY

Figure V-1. Schematic of the University of Wisconsin tandem accelerator facility. Negative copper ions are created at the negative ion source and injected into the accelerator. For these irradiations the terminal potential was 3.5 MV, and the primary ion charge state was 3^+. The ions exit the accelerator with 14 MeV of energy and strike the samples located in the radiation damage target chamber.

neutrals and low Z ions from striking the specimen.

The negative ion sources for this system were developed at the University of Wisconsin. A series of Sputter Penning Ion Gauge Sources (SPIGS) developed by Smith and Richards[110] were originally used in this system. In SPIGS, the plasma is maintained by a Penning discharge and the negative metal ions are created through Cs assisted sputtering of the cathode. Currently a new source, SNICS, developed by Billen and Richards,[111] is being used for irradiations. The SNICS source also creates negative metal ions through sputtering of the cathode, but the Cs ions are produced by surface ionization on a hot filament. This new source is simple and reliable and may, in the future, produce beams of refractory metal ions for irradiation.

The radiation damage target chamber was designed to provide the high vacuum environment required to control the contamination of refractory metals such as vanadium with gaseous impurities. The extent and type of contamination is determined by the composition of the vacuum, and a residual gas analyzer is used in this system to perform the partial pressure analysis. The samples are irradiated in a high temperature radiation furnace, which provides a constant, uniform sample temperature. In order to characterize the damage state, provisions for beam measurement and analysis have also been made. This system has been designed to comply with the proposed standard recommended practice for neutron radiation damage simulation.[112]

The section of accelerator beam line immediately preceding the sample chamber operates at a pressure of 5×10^{-6} Torr and a system of two differential pumping stages is used to reduce the pressure to less

than 10^{-8} Torr in the sample chamber region. The ultimate pressure obtained in the sample chamber is limited by the outgassing of its components, rather than the streaming of gas down the beam line. A schematic of the sample chamber vacuum system is given in Figure V-2. A 200 ℓ/sec diffusion pump with a liquid nitrogen trap typically provides a vacuum of 2×10^{-6} Torr in the first pumping stage, and a 400 ℓ/sec orbitron pump provides a vacuum of 1×10^{-7} Torr in the intermediate pumping stage. All of the vacuum seals on the high vacuum side of the valve separating the two pumping stages are made with metal gaskets.

A series of fifteen 6.5 mm diameter Ta apertures separates the sample chamber environment from the intermediate pumping stage. This pumping impedance has a conductance of 0.25 ℓ/sec. When samples are at room temperature, a 1000 ℓ/sec getter-ion pump provides a base pressure of 5×10^{-9} Torr. A pressure of 5×10^{-8} Torr is maintained when the samples are heated to 1100°C. The walls of the sample chamber are externally water cooled.

A Varian VGA-100 quadrapole residual gas analyzer, which can resolve partial pressures as low as 5×10^{-11} Torr is permanently mounted on the system. In Figure V-3, the results of a residual gas analyzer scan taken during the irradiation of a vanadium sample are displayed. The irradiation temperature for this sample was 650°C and the total pressure was 1×10^{-8} Torr. The primary constituents of the vacuum are hydrogen and water vapor.

The sample heater is a 4 cm diameter cylindrical thermal radiation furnace constructed of 0.025 mm Ta sheet and surrounded by a spirally wound heat shield. The hot zone of the furnace is approximately 9 cm

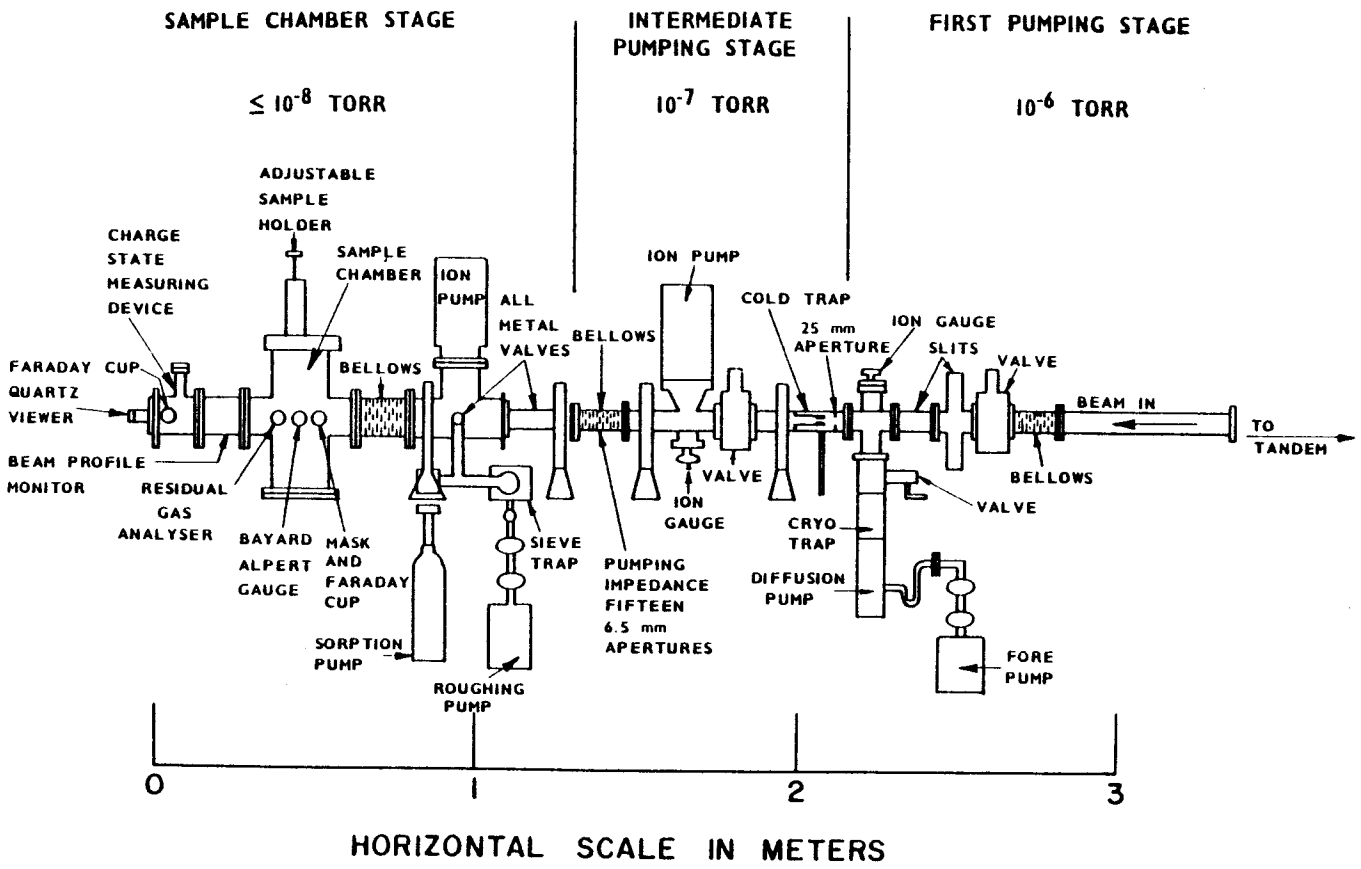

Figure V-2. Schematic of the vacuum system for the heavy ion irradiation facility. The vacuum in the irradiation target chamber is reduced to less than 10^{-8} torr by using an intermediate pumping stage and a series of pumping impedances. The vacuum in the target chamber is monitored with a residual gas analyzer.

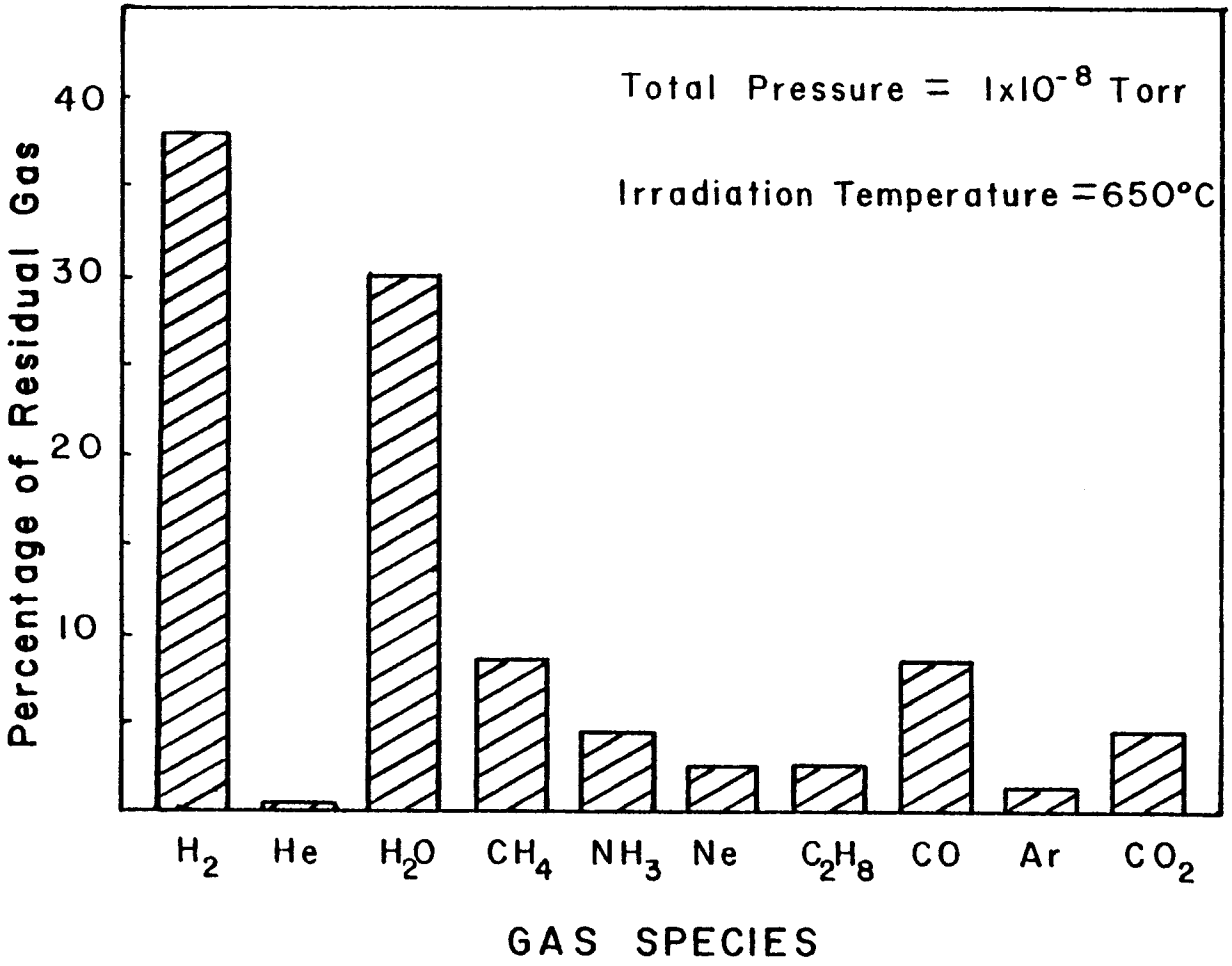

Figure V-3. Analysis of residual gasses in the radiation damage target chamber taken during the irradiation of a specimen at 650°C.

long. A schematic of this system is given in Figure V-4. In order to reach a sample temperature of 1000°C, 200 amperes must be passed through the furnace, resulting in a total power input of 400 watts. One centimeter holes have been cut through the front and back of the heat shield and furnace to allow the beam to pass through.

The samples are suspended in the center of the furnace and heated by thermal radiation. Vertical motion is provided through a bellows mounted on top of the sample chamber. The sample holder, which is shown in Figure V-5, has spaces for eight 3 mm discs, which are clamped between two 1 mm thick plates of tantalum. There are also three holes cut through the sample holder, which are used for beam alignment. The temperature is measured on eight chromel/alumel thermocouples, one mounted behind each sample position.

The heavy ion beam striking the sample is collimated by a 3 mm mask-aperture located 13 cm in front of the samples. The beam current is measured by collecting the total charge deposited on the sample holder, furnace and heat shield. Secondary electrons emitted when the beam strikes the sample are collected by the heater and heat shield, which subtend approximately 90% of the solid angle surrounding the sample. This system also compensates for thermionic emission of electrons from the furnace to the sample holder. The beam current may also be measured by passing the beam through one of the holes in the sample holder and collecting it on the faraday cup mounted behind the furnace.

In order to detemine the energy and particle current of the beam striking the sample, the charge state composition must be known. The energy distribution of the beam is determined by recording, in a solid

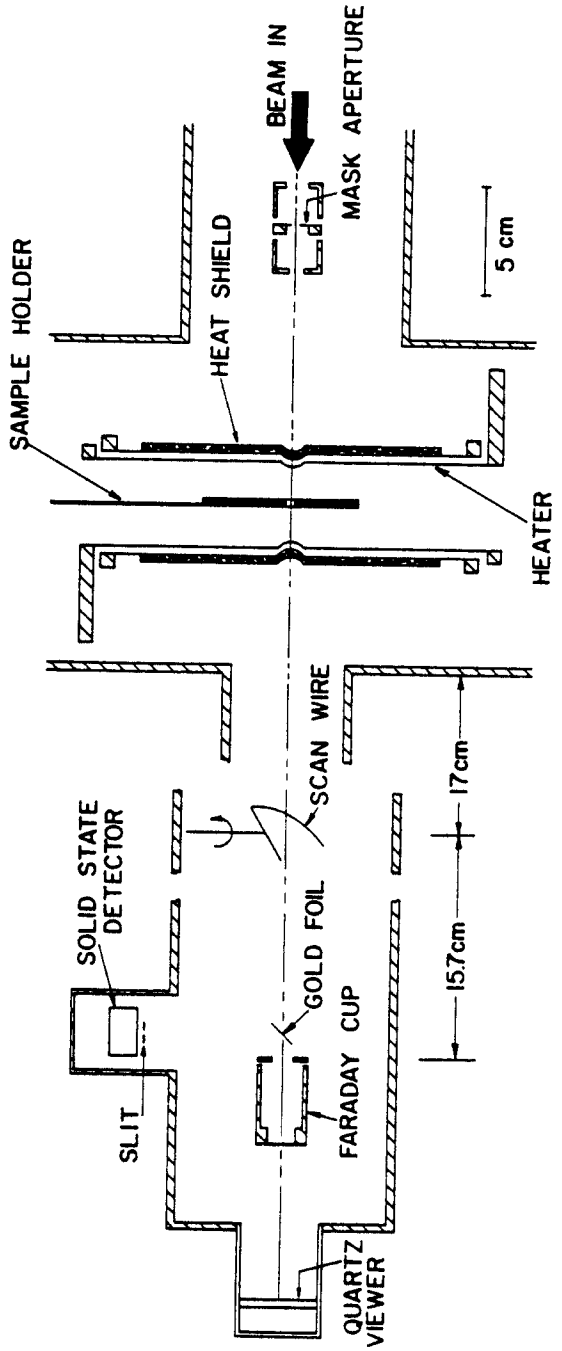

Figure V-4. Sample heater and beam diagnostics system.

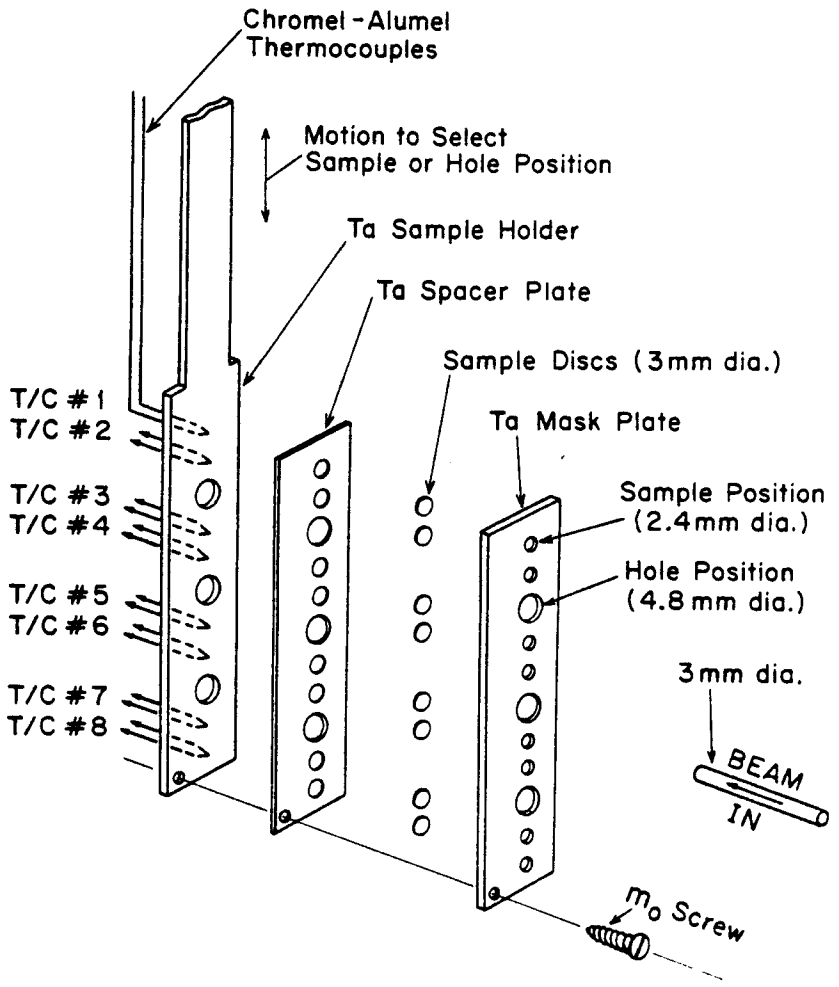

SAMPLE HOLDER (EXPLODED VIEW)

Figure V-5. Sample holder for three millimeter specimens. This assembly is suspended in the center of the cylindrical radiation furnace.

state detector, the beam particles scattered through 90^{o} by a thin gold foil. A schematic of this charge state measuring system, which is similar to the one described in reference 113, is included in Figure V-4. The slight magnetic analysis provided by the 1/4 deflection in the 90^{o} analyzing magnet allows the selection of primarily one charge state. For these irradiations, the Cu^{3+} charge constituted over 99% of the total beam intensity with only a small Cu^{+} peak detected. This system will also detect the presence of impurity species in the ion beam. The most probable impurities are nitrogen ions formed in the N_2 gas stripper and transported to the sample as "satellite" beams. These measurements indicate that the nitrogen beams represent less than 0.2% of the total beam.

Typical beam currents, as measured at the sample,are approximately 35 particle nA, which corresponds to a dpa rate of 6×10^{-4} dpa/sec at a depth of 1 μm in vanadium. The displacement rate is limited by beam transport through the accelerator. Only 1% of the ions injected into the low energy side of the accelerator actually strike the sample.

V-C. Post Irradiation Examination

During irradiation, damage is produced in the 3 μm zone near the irradiated surface. There are two techniques that have been used to prepare transmission electron microscopy foils from irradiated samples. The conventional technique involves removing a small amount of material from the irradiated surface and then backthinning the sample to obtain a foil in a plane parallel to the surface. The less conventional cross-sectioning technique is used to study the variation in damage over the range of

the irradiating ion.

In this study, the samples were prepared by the conventional technique, which is described below. However, an attempt was also made to prepare irradiated vanadium specimens by the cross-sectioning technique. This cross-sectioning work achieved only limited success.

V-C-1. Conventional Technique

After irradiation, specimens were electropolished in a solution of 20% H_2SO_4 in methyl alcohol for 1 minute at -30°C to remove a 1 μm layer from the irradiated surface. The reasons for choosing this depth to examine the samples can be seen by examining Figure II-1 which represents the calculated damage profile for 14 MeV Cu ions in vanadium. At 1 μm, the damage gradient is relatively low, which minimizes the uncertainty in dose level due to difficulties in determining the exact depth. Also, this region is well removed from the deposited copper ions. The amount of material removed from the irradiated surface was determined by painting the edges of the sample with stop-off lacquer prior to the electropolishing and measuring the resultant step height in a light interference microscope. The step height was measured at three different spots on each sample. The uncertainty in this method was primarily associated with variations in the amount of material removed across the three millimeter discs. Each fringe represents approximately 3000 Å, and a tolerance of ± 1 fringe was maintained. This variance in surface removal corresponds to an uncertainty of ± 20% in the dpa level.

The entire irradiated surface was then painted with step-off lacquer, and the samples were backthinned in a commercial jet-polishing unit. The same 20% H_2SO_4 in methyl alcohol solution was used at a

temperature of -27°C.

Approximately 10% of the specimens were lost or deformed during the backthinning process due to hydride formation. This phenomenon, which was observed in unirradiated specimens as well, can be extremely important in the preparation of thin foils. The precipitates were identified by their electron diffraction pattern as the ordered V_2H phase which has a body centered tetragonal structure. This phase forms by a shearing mechanism in a manner similar to a martensitic transformation. The energy required for this transformation is greatly reduced in the transmission electron microscope foils, which are extremely thin. The increase in hydrogen content due to electropolishing is then enough to cause the hydride formation. An optical micrograph of a backthinned sample containing hydrides is presented in Figure V-6. The surface deformation in the grain immediately surrounding the perforation was caused by the shearing of the matrix when the hydrides formed.

Enrichment of the hydrogen concentration in vanadium during electropolishing has been observed in other studies. Evidence for hydrogen enrichment in the pre-irradiation treatment of vanadium specimens was seen in this study as well. Westlake and Gray[114] suggest that during electropolishing hydrogen initially present is concentrated in the ever thinner specimen. This explanation, however, would not account for the hydrogen doping observed in the pre-irradiation electopolish, where only a small fraction of the sample thickness is removed. Attempts to determine the exact conditions which caused the hydride formation were unsuccessful. However, it appears that this phenomenon is associated with the stability of the viscous layer, which may be affected by the pumping speed of the electrolitic jets and the solution purity.

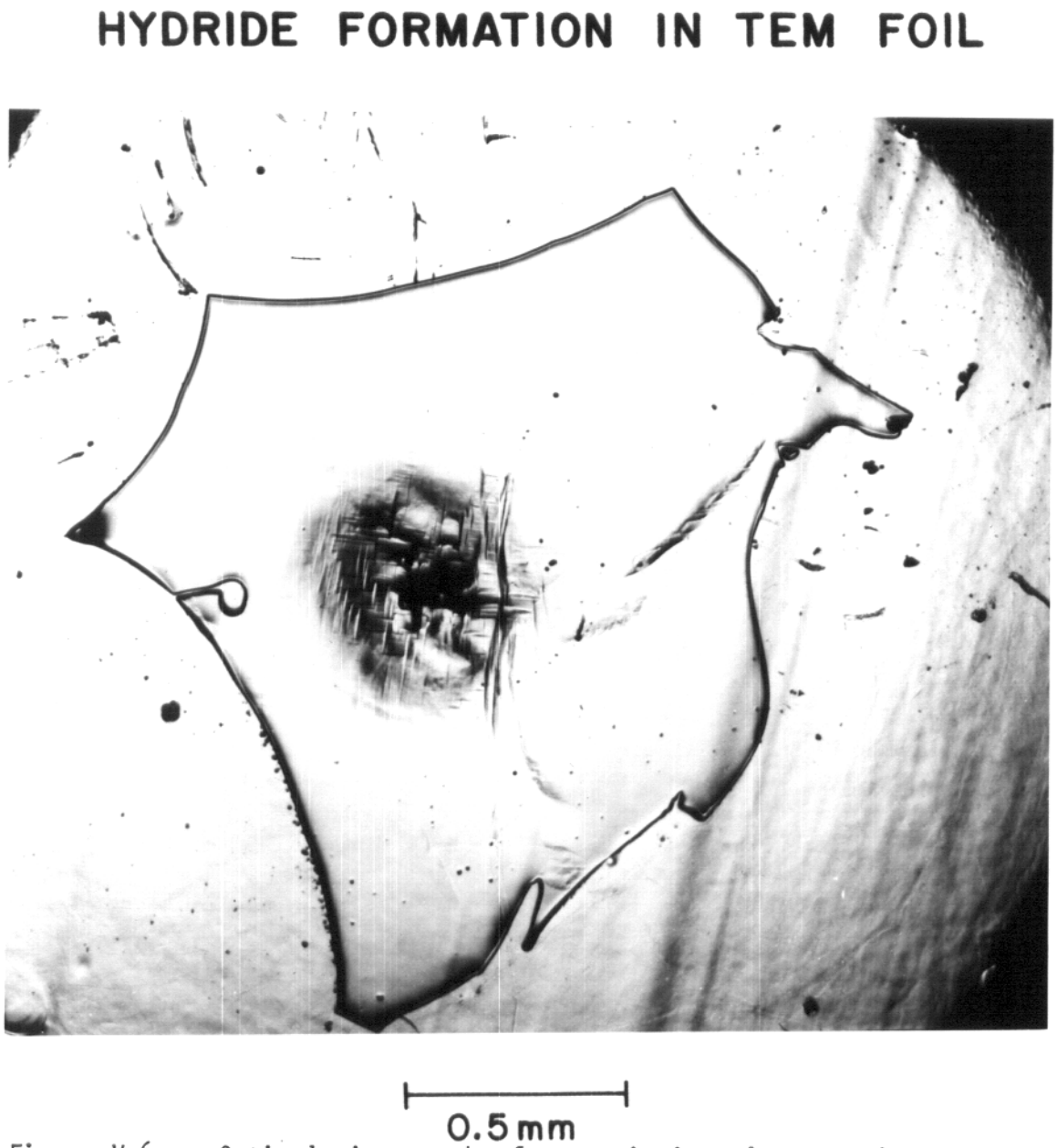

Figure V-6. Optical micrograph of transmission electron microscope specimen containing hydrides. The surface stryations near the center hole were caused by a martensitic-like hydride precipitation phenomenon.

The thinned specimens were examined in a JEM 100 B electron microscope modified to work at 120 KV. Void sizes, void densities, dislocation densities (including loop densities) and precipitate densities were determined using conventional transmission electron microscopy techniques. The nickel content of the specimens was determined with Energy Dispersive X-Ray Analysis (EDXA) using the microscope in the scanning transmission mode. The foil thickness was determined by using the microscope in the scanning transmission mode to focus the electron beam to an extremely small spot ($\sim$50 Å). This beam was used to produce contamination spots on the top and bottom surfaces of the foil. The foil was then tilted through 45° and the thickness determined from the displacement of the contamination spots.

The void size distribution was determined using a Zeiss particle size comparator, which sorts the voids into equally spaced size intervals. Only voids which were completely contained in the foil were counted. To account for differences in the effective foil thickness, the number of voids in each size interval, n_i, was increased by a factor of $\frac{t}{t - d_i}$, where t is the sample thickness and d_i is the average void diameter in the ith interval. The void density, ρ_V, average void diameter, $\langle d \rangle$, and swelling, $\Delta V/V$, were then calculated using the relations

$$\rho_V = \frac{\sum_i n_i}{At} \quad , \tag{5-2}$$

$$\langle d \rangle = \frac{\sum_i n_i d_i}{\sum_i n_i} \tag{5-3}$$

and

$$\Delta V/V = \frac{\alpha}{At} \sum_i n_i d_i^3, \qquad (5\text{-}4)$$

where A is the analyzed area of the sample and α is a geometric factor. For cubic voids, $\alpha = 1$.

The magnitude of the uncertainty in this data was estimated by examining possible sources of error in determining the sample temperature, total dose and swelling. These uncertainties are summarized in Table V-3. The irradiation temperature was measured by thermocouples mounted directly behind the samples, and the maximum variation is $\pm 5^{o}C$. The uncertainty in the total dose was dominated by variations in beam uniformity ($\pm$ 25%) and surface removal ($\pm$ 20%). The total uncertainty in the dose was then $\pm$ 32%. The magnitude of uncertainty in swelling range from 20% to 30% depending on the void density. At large void densities ($>10^{14}$ voids/cm^3), the uncertainty was dominated by errors in determining the sample thickness. While at low void densities ($<10^{13}$ voids/cm^3), the uncertainty was dominated by sampling errors due to statistical variations in the void distribution. No attempt was made to calculate swelling at void densities below 10^{12} voids/cm^3 because the uncertainty became too large.

V-C-2. Cross-Sectioning Technique

The cross-sectioning technique was developed by Spurling and Rhodes[115] for irradiated stainless steel. More recently, Whitley[108] used this technique in a study of heavy ion irradiated nickel at the University of Wisconsin. In both of these studies, nickel was electroplated on the sample surface after irradiation. The samples were then

TABLE V-3 Uncertainties in Void Swelling Measurements

Irradiation Parameters	
Irradiation Temperature	$\pm$ 5°C
Total Dose	
Beam Uniformity	$\pm$ 25%
Surface Removal	$\pm$ 20%
	$\pm$ 32%
Swelling Calculation	
Foil Thickness	$\pm$ 15%
Sampling Error	$\pm$ 5% - $\pm$ 20%
Defect Size	$\pm$ 10 Å
	$\pm$ 20% - $\pm$ 30%

sliced and thinned in a plane normal to the irradiated surface. Because vanadium cannot be electroplated from aqueous solutions, an attempt was made to cross-section vanadium by using a sputter deposition technique.

In a preliminary study, 1 1/2 mm of vanadium was sputter deposited on both sides of a series of unirradiated vanadium discs by Dr. S. Dahlgren at Battelle Northwest Laboratories.[116] During the plating process, which took approximately 100 hours, the sample temperature was estimated to be between 300°C and 400°C. No direct measurement of sample temperature was made. The plated discs were then returned to the University of Wisconsin where they were sliced with a low speed diamond saw and thinned for transmission electron microscopy. A micrograph of one of these unirradiated cross-sectioned specimens is presented in Figure V-7. An excellent bond was achieved between the specimen and the plated material. However, this sample which was plated in the as received, heavily cold worked condition now exhibits a well recovered microstructure. This result indicates that the substrate temperature was higher than previously believed.

A series of six irradiated specimens was then sputter deposited in the same facility. Unfortunately, four of the specimens were nickel contaminated prior to irradiation (see section VI), and void formation was suppressed. Of the remaining two specimens, only one was successfully cross-sectioned. A micrograph of this V-1N specimen, which was irradiated at 550°C to 2 dpa, is presented in Figure V-8. This sample was electropolished and not outgassed prior to irradiation to enhance void formation. Voids were observed in this cross-sectioned specimen in the range 1.5-2.5 μm. The void density in this region was approximately

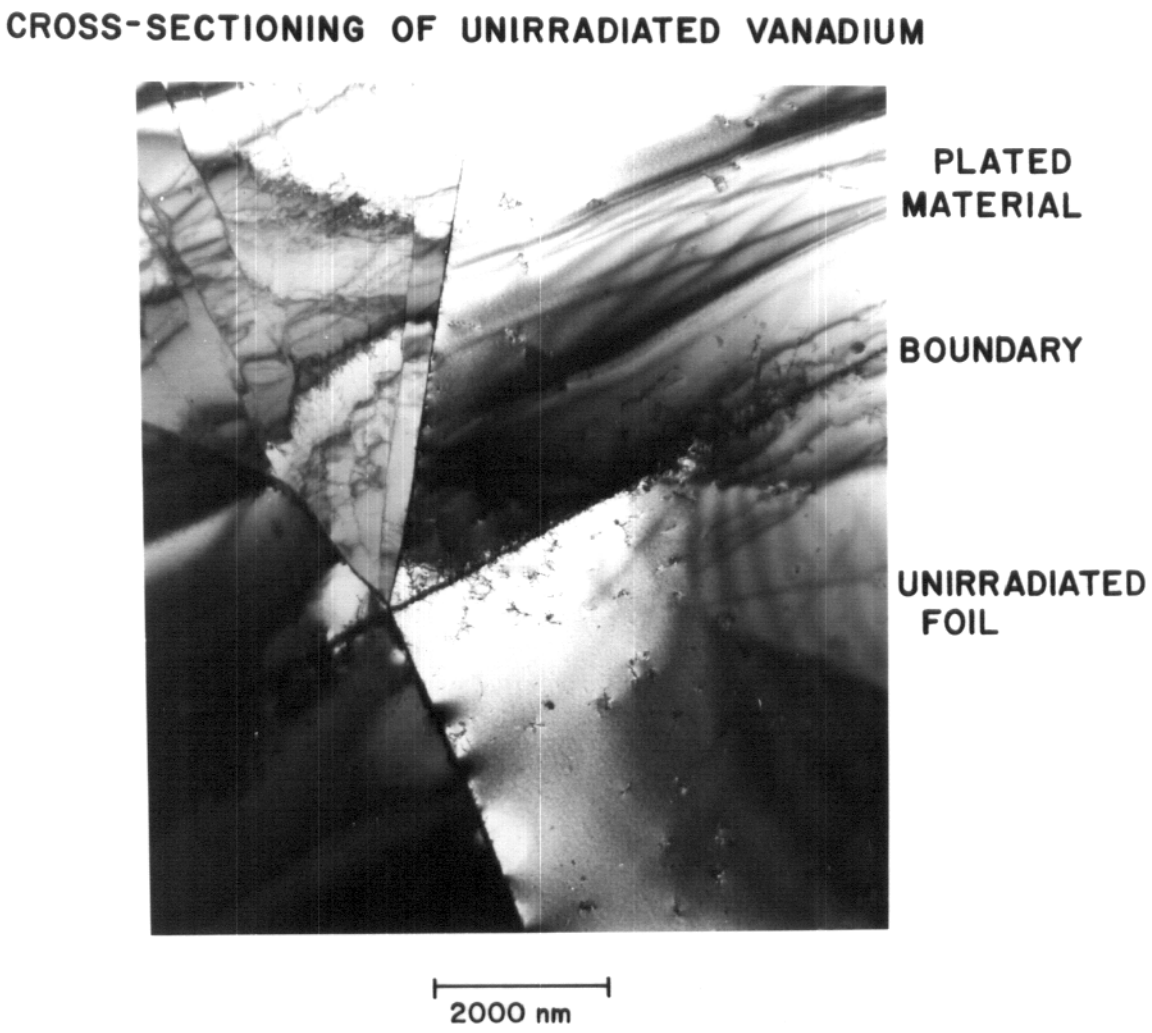

Figure V-7. Boundary between sputter deposited material and unirradiated vanadium specimen.

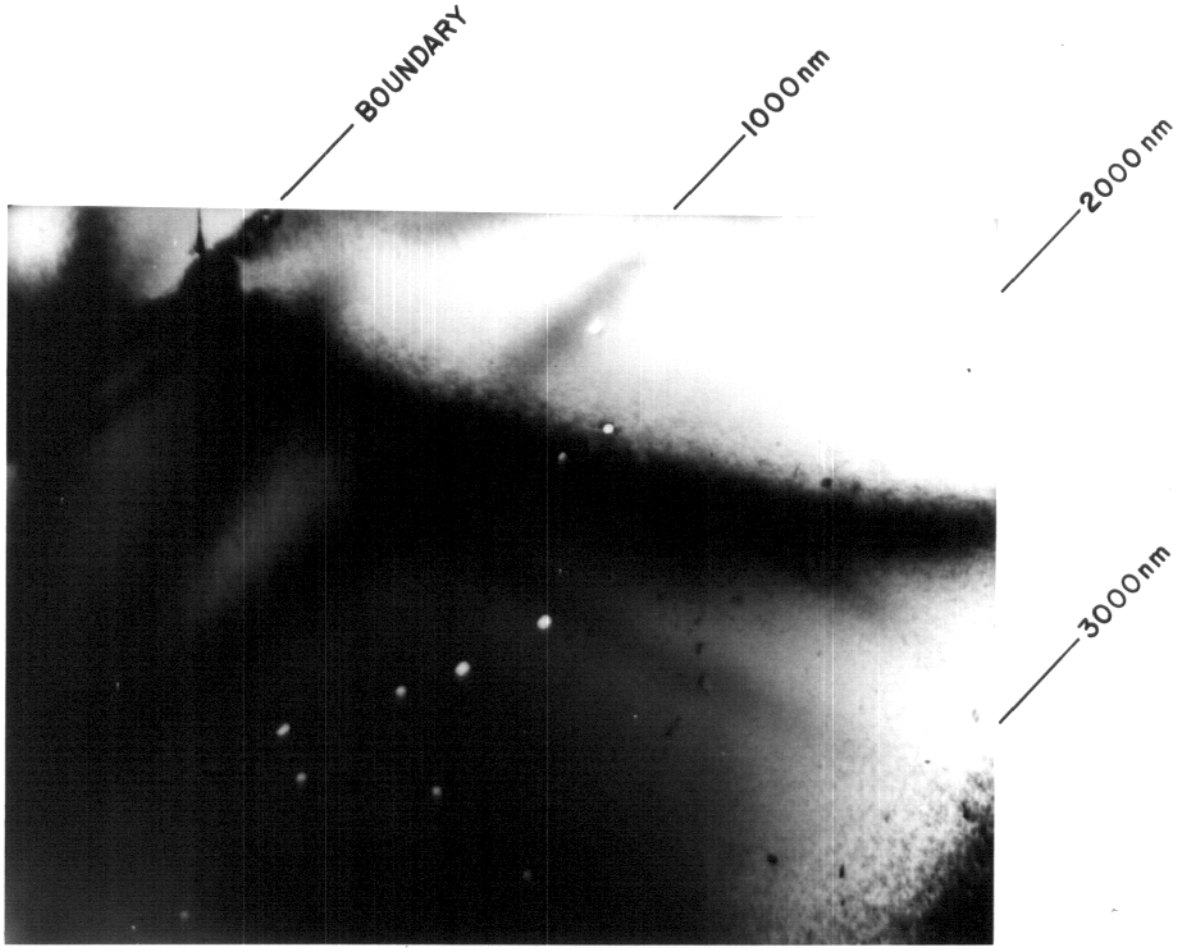

Figure V-8. Voids in cross-sectioned vanadium-1% nitrogen speciment irradiated to 2 dpa at 550°C. This specimen was not outgassed prior to irradiation.

2×10^{13} cm^{-3}. The calculated peak in the damage curve for 14 MeV Cu ions occured at 2.8 μm and the maximum range was 3 μm. This behavior might be explained by the complex temperature and dose dependence of swelling observed in this study (see Chapter VI). It is also possible that the discrepancy in the observed and calculated maximum range was caused by annealing during the sputter deposition process.

Based on this experience, the cross-sectioning technique was abandoned in this study. There were two reasons for this decision: first, it was not possible to assess the effect of post irradiation annealing on the observed void structure; second, the void density in most of these irradiations was not sufficient to provide statistically significant data as a function of depth. Over two thirds of the specimens in this study exhibited void densities at a depth of 1 μm which were lower than the density in the peak swelling region of Figure V-8. This second problem was overcome in Whitley's study of ion irradiated nickel by doping the samples with hydrogen to increase void density.[109]

CHAPTER VI RESULTS OF IRRADIATIONS

Specimens of high purity vanadium and two vanadium alloys, V-1%Ni and V-1%N were irradiated in this study. The irradiation parameters for each of the specimens are listed in Table VI-1. The dpa rates and levels listed in Table VI-1 have been adjusted to account for the variance due to surface removal. For the remainder of this discussion, the dpa levels will be quoted as nominal values of 1, 2.5, 5 and 10 dpa. The void parameters for all of the specimens in this study are listed in Table VI-2.

VI-A. Nickel Contamination

The first attempts to produce specimens of high purity vanadium were frustrated by problems of nickel contamination similar to those described by Weber. In the conclusions to his thesis,[25] Weber suggested that the chromel/alumel thermocouples in the high vacuum annealing furnace were a potential source of nickel contamination. All of Weber's "Group II" samples were annealed using chromel/alumel thermocouples. The first eight pure vanadium specimens irradiated in this study were also annealed using the same thermocouples. However, a minor difference in operating procedures between the two studies accentuated the problem of nickel contamination in this study. The temperature gradient in the furnace produces a 75°C difference between the two thermocouples in the furnace. In Weber's study, the samples to be annealed were grouped around the high temperature thermocouple, while in this study, the samples were grouped around the low temperature thermocouple. Typical annealing conditions were T_{HI} = 1050°C and

TABLE VI-1 Summary of Irradiation Parameters

Sample	Irradiation Temperature (°C)	Fluence (Ions/cm^2)	dpa	Displacement Rate dpa/sec
—PURE VANADIUM—				
00 111	650	6×10^{15}	1.1	3.6×10^{-4}
00 110	650	1.5×10^{16}	2.4	4.5×10^{-4}
00 109	650	3×10^{16}	5.8	4.1×10^{-4}
00 115	550	6×10^{15}	1.1	3.4×10^{-4}
00 123	550	1.5×10^{16}	2.8	3.5×10^{-4}
00 120	550	3×10^{16}	6.3	3.8×10^{-4}
00 112	550	6×10^{16}	11.1	3.6×10^{-4}
00 122	450	6×10^{15}	1.3	3.9×10^{-4}
00 117	450	1.5×10^{16}	2.9	6.1×10^{-4}
00 125	450	1.5×10^{16}	2.9	4.6×10^{-4}
00 126	450	5×10^{16}	8.8	4.5×10^{-4}
00 119	250	1.5×10^{16}	3.5	6.5×10^{-4}
00 127	250	1.5×10^{16}	2.6	4.6×10^{-4}
—VANADIUM-1% NITROGEN—				
N01 11	650	6×10^{15}	0.9	3.2×10^{-4}
N01 10	650	1.5×10^{16}	2.6	4.5×10^{-4}
N01 21	650	1.5×10^{16}	2.8	3.2×10^{-4}
N01 09	650	3×10^{16}	5.8	4.3×10^{-4}
N01 08	650	6×10^{16}	10.5	3.4×10^{-4}

TABLE VI-1 (continued)

Sample	Irradiation Temperature (°C)	Fluence (Ions/cm^2)	dpa	Displacement Rate dpa/sec
—VANADIUM-1% NITROGEN—				
NO1 15	550	6×10^{15}	1.4	4.5×10^{-4}
NO1 14	550	1.5×10^{16}	2.9	4.0×10^{-4}
NO1 22	550	1.5×10^{16}	2.9	4.4×10^{-4}
NO1 13	550	3×10^{16}	6.4	5.2×10^{-4}
NO1 20	550	3×10^{16}	5.3	3.3×10^{-4}
NO1 12	550	6×10^{16}	10.5	3.9×10^{-4}
NO1 18	450	6×10^{15}	1.1	5.6×10^{-4}
NO1 17	450	1.5×10^{16}	2.6	6.0×10^{-4}
NO1 16	450	6×10^{16}	12.7	7.5×10^{-4}
NO1 19	250	1.5×10^{16}	2.6	6.5×10^{-4}
NO1 01 a.)	650	1.2×10^{16}	2	2×10^{-4}
NO1 02 a.)	600	1.2×10^{16}	2	2×10^{-4}
—VANADIUM-1% NICKEL—				
NiO1 02	650	6×10^{15}	1.1	4.6×10^{-4}
NiO1 01	650	3×10^{16}	5.3	4.5×10^{-4}
NiO1 04	550	6×10^{15}	1.1	4.8×10^{-4}
NiO1 05	550	3×10^{16}	7.5	5.7×10^{-4}
NiO1 07	550	3×10^{16}	5.8	4.2×10^{-4}
NiO1 06	450	6×10^{15}	1.1	4.2×10^{-4}
NiO1 08	450	3×10^{16}	5.3	3.6×10^{-4}

TABLE VI-1 (continued)

Sample	Irradiation Temperature (°C)	Fluence, $(Ions/cm^2)$	dpa	Displacement Rate dpa/sec
—NICKEL CONTAMINATED VANADIUM—				
00 100	650	1.2×10^{16}	2	9.0×10^{-4}
00 101 b.)	650	1.2×10^{16}		
00 102	550	1.2×10^{16}	2	8.1×10^{-4}
00 103 b.)	550	1.2×10^{16}		
00 104	450	1.2×10^{16}	2	9.2×10^{-4}
00 105 b.)	450	1.2×10^{16}		
00 106	350	1.2×10^{16}	2	8.8×10^{-4}

a.) Not Outgassed

b.) Cross Sectioned

TABLE VI-2 Summary of Void Parameters

Sample	Temperature	dpa	<d> (Å)	ρ_v (cm^{-3})	$\Delta V/V$ %	Precipitate
			—PURE VANADIUM—			
00 111	650	1	200	2×10^{13}	0.01	slight
00 110	650	2.5	330	4×10^{11}	< 0.001	slight
00 109	650	5	470	9×10^{11}-4×10^{12}	0.005-0.03	slight
00 115	550	1	300	4×10^{13}	0.06	none
00 123	550	2.5	400	3.6×10^{13}	0.28	slight
00 120	550	5	135	3×10^{14}	0.3	slight
00 112	550	10	350	4×10^{12}	0.01	black spot damage
00 122	450	1	210	1×10^{14}	0.13	none
00 117	450	2.5	120	2×10^{14}	0.03	none
00 125	450	2.5	95	8×10^{14}	0.04	none
00 126	450	10	385	3.9×10^{13}	0.26	none
00 119	250	2.5	395	3×10^{13}	0.2	none
00 127	250	2.5	300	8.3×10^{13}	0.31	none

TABLE VI-2 (continued)

Sample	Temperature	dpa	$\langle d \rangle_o$ (A)	ρ_v (cm^{-3})	$\Delta V/V$ %	Precipitate
			—VANADIUM-1% NITROGEN—			
N01 11	650	1	310	1×10^{13}	0.02	none
N01 10	650	2.5	---	0	0	none
N01 21	650	2.5	---	0	0	none
N01 09	650	5	350	1×10^{12}	0.003	slight
N01 08	650	10	730	3×10^{11}	0.005	slight
N01 15	550	1	310	2×10^{12}	0.004	none
N01 14	550	2.5	---	0	0	none
N01 22	550	2.5	---	$< 10^{11}$	< 0.001	none
N01 13	550	5	---	0	0	slight
N01 20	550	5	530	1×10^{11}	0.001	slight
N01 12	550	10	420	8×10^{12}	0.04	slight
N01 18	450	1	---	0	0	none
N01 17	450	2.5	---	0	0	none

TABLE VI-2 (continued)

—VANADIUM-1% NITROGEN (continued)

Sample	Temperature	dpa	$\langle d \rangle$ (Å)	ρ_v (cm^{-3})	$\Delta V/V$ %	Precipitate
N01 16	450	10	---	$< 10^{11}$	~ 0	none
N01 19	250	2.5	---	0	0	none
N01 01 b.)	650	2	510	7×10^{12}	0.12	none
N01 02 b.)	600	2	130	9×10^{13}	0.02	none
—VANADIUM-1% NICKEL—						
Ni01 02	650	1	---	$< 10^{11}$	---	coherent
Ni01 01 a.)	650	5	---	$< 10^{11}$	---	none
Ni01 04	550	1	---	$< 10^{11}$	---	coherent
Ni01 05	550	5	2160	2×10^{12}	2.3	incoherent
Ni01 07	550	5	1360	4×10^{12}	1.2	incoherent
Ni01 06	450	1	970	1×10^{13}	1.0	incoherent
Ni01 08	450	5	1230	3×10^{13}	6.8	incoherent

a.) Samples heavily hydrided during post irradiation preparation.

b.) Samples not outgassed prior to irradiation.

T_{LOW} = 970°C for Weber's study and T_{HI} = 1120°C and T_{LOW} = 1050°C in this study. The difference of 70°C between the two high temperature thermocouples was enough to produce an order of magnitude increase in the vapor pressure of pure nickel. At 1120°C the vapor pressure of pure nickel is 8×10^{-6} Torr.[116]

The eight irradiated specimens which were annealed using chromel/alumel thermocouples were divided into two groups. Each group was exactly the same, consisting of four specimens irradiated to 2 dpa at 350°C, 450°C, 550°C and 650°C. The first group was prepared by the cross sectioning technique, and the second group was prepared by the conventional back-thinning technique. No voids were observed in any of these specimens. The total dislocation density in the 450°C, 550°C and 650°C back-thinned specimens was $3 \times 10^{9}/cm^{2}$. The two high temperature specimens also contained dislocation loops which averaged 300 Å in diameter at a density of $10^{14}/cm^{3}$. Black spot damage, not clearly defineable as dislocation loops, was also observed at 450°C. The formation of a large density of incoherent thin sheet precipitates on (112) planes obscured the radiation induced dislocation density in the 350°C specimen. These precipitates, which are shown in Figure VI-1 resembled the precipitates observed by Weber[25] in the "Group II" specimens at 550°C and 600°C. In Weber's study, low swelling values were observed in samples which exhibited this form of precipitation.

It was the observation of precipitates in the 350°C sample which prompted the use of EDXA to examine the impurity content of these specimens. The results of this analysis are presented in Table VI-3. It is difficult to postulate any mechanism that would have produced

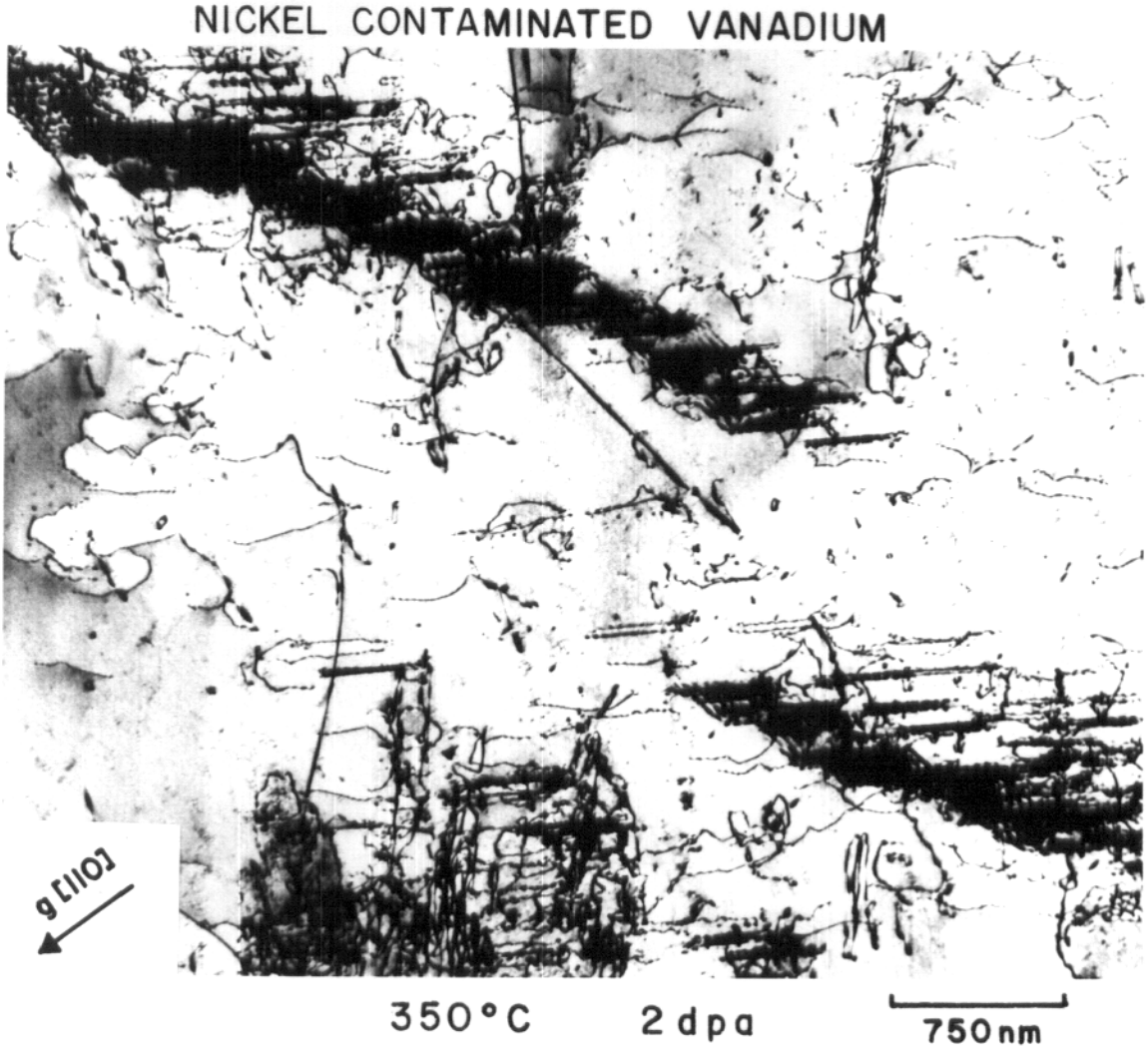

Figure VI-1. Precipitates in nickel contaminated vanadium specimen irradiated to 2 dpa at 350°C. Precipitates lie on (112) planes.

TABLE VI-3 Energy Dispersive X-Ray Analysis Pure Vanadium

Sample	Irradiation Temperature (^{o}C)	dpa	Ni Content	Precipitation
—Annealed with Chromel/Alumel T/C—				
00 100	650	2	0.5%	None
00 102	550	2	2%	None
00 104	450	2	7%	None
00 106	350	2	9%	None
—Annealed with W-W Re T/C—				
00 111	650	1		Yes
matrix			0	
precipitate			0.2%	
00 120	550	5		Yes
matrix			0.1%	
precipitate			1.0%	
00 119	250	2.5	0.6%	None

nickel concentrations as high as the 9% observed in the 350°C specimen and the 7% observed in the 450°C specimen throughout the bulk of the specimen. This result is consistent, however, with the surface related contamination observed by Weber. In this mechanism, it is postulated that nickel was transported from the sample surface into the irradiated region by irradiation enhanced diffusion. The observation of higher nickel content in the low temperature irradiations may indicate that the lower diffusion rates have confined the nickel to a narrow region near the surface. An alternative explanation for these variations would be differences in the sample position with respect to the chromel/alumel thermocouples.

The observed suppression of void swelling by nickel contamination contradicted Weber's observation of heavily precipitated and voided nickel contaminated specimens. To help resolve this contradiction, a series of irradiations of a V-1%Ni alloy were added to the originally planned irradiations of high purity vanadium and vanadium-1%N. All subsequent anneals were performed using W/W-Re thermocouples.

VI-B. Pure Vanadium

Swelling as a function of dose was studied in three series of high purity vanadium samples irradiated at 450°C, 550°C and 650°C. In addition two specimens were irradiated at 250°C to confirm Weber's observation of low temperature void formation.[25] The irradiation parameters and void parameters for these irradiations are listed in Table VI-1 and VI-2. Because of the complicated development of irradiation induced microstructure in these specimens, it is difficult to

draw general conclusions about swelling without understanding how both void density and void size evolve with dose.

Swelling did not increase monotonically with dose for any of the irradiation temperatures surveyed in this study. This behavior is illustrated in Figure VI-2, where swelling has been plotted as a function of dose. Micrographs of the specimens irradiated at 450°C to 1, 2.5 and 10 dpa are presented in Figure VI-3. At this temperature, the maximum swelling was observed at 10 dpa. However, swelling at the intermediate dose level of 2.5 dpa was lower than that observed at 1 dpa. The 2.5 dpa, 450°C irradiation was repeated to verify this result.

In the 550°C series, specimens were irradiated to 1, 2.5, 5 and 10 dpa. Micrographs of these specimens are included in Figure VI-4. The maximum swelling level occurred in the 2.5 dpa and 5 dpa specimens.

The maximum observed swelling in the three specimens irradiated at 650°C was 0.02%. Because of this extremely low level of swelling, no conclusions can be drawn from the development of swelling at this higher temperature.

The void density, which is plotted as a function of dose in Figure VI-5, evolved in a manner similar to the swelling. At 450°C, a void density of $1 \times 10^{14}/cm^3$ had nucleated by 1 dpa and then the density continued to increase more gradually between 1 and 2.5 dpa. There was a slight decrease in void density between 2.5 and 10 dpa.

The same sharp rise and gradual decline in void density with dose was observed in the 550°C specimens. The 550°C, 5 dpa specimen exhibited a distinctly bimodal void size distribution. The swelling

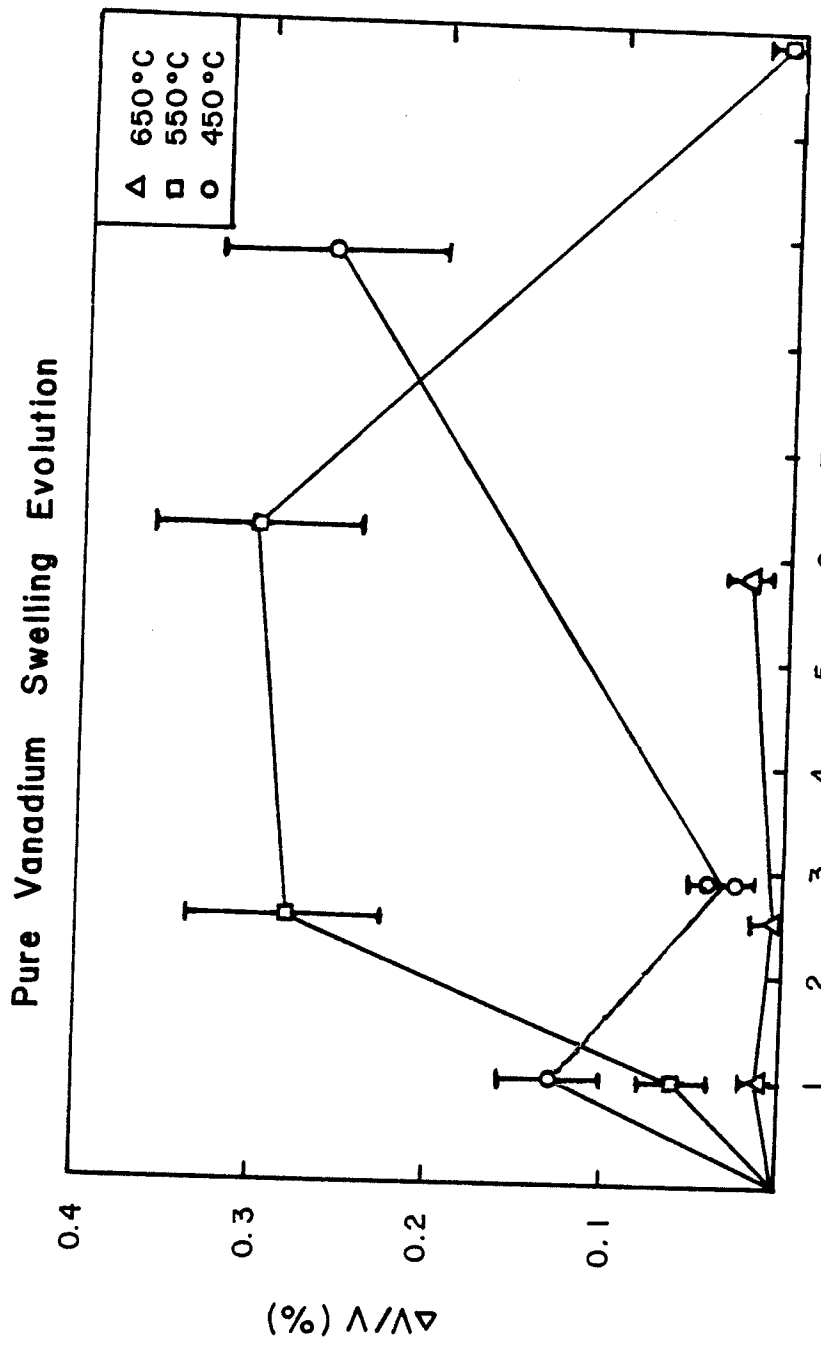

Figure VI-2. Evolution of void swelling with dose in pure vanadium specimens irradiated at 450°C, 550°C and 650°C.

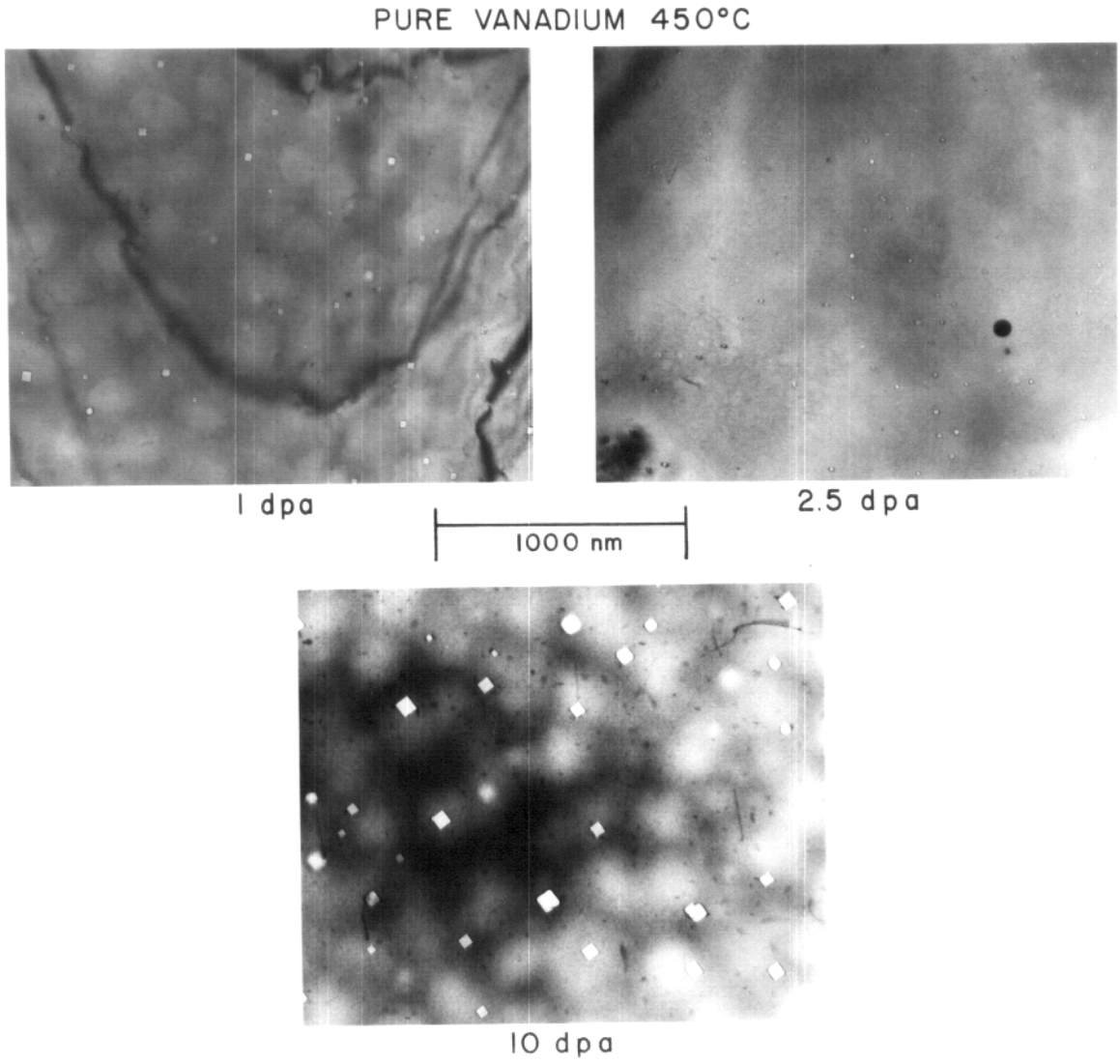

Figure VI-3. Voids in pure vanadium specimens irradiated at 450°C. In all cases, the foil normal is [110].

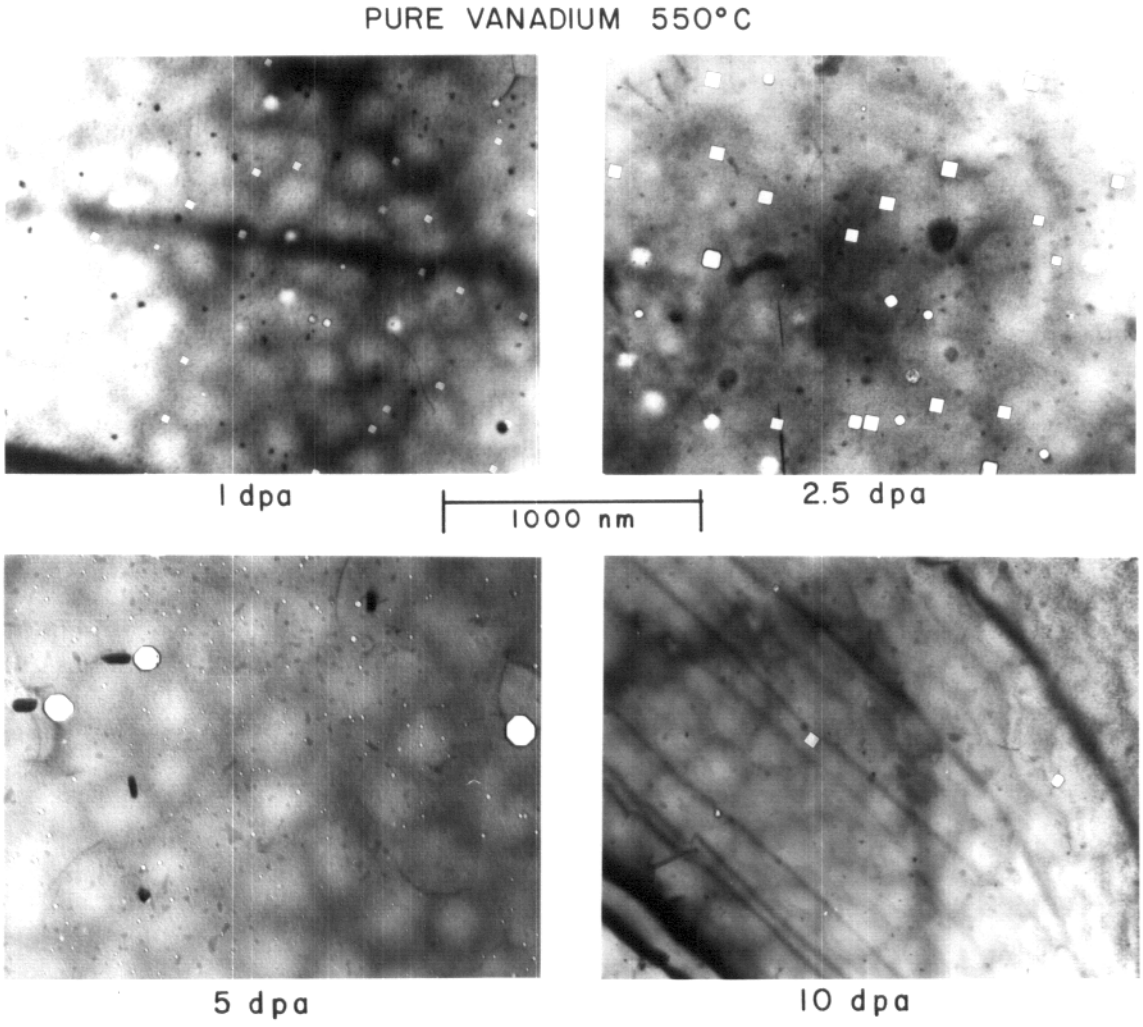

Figure VI-4. Voids in pure vanadium specimens irradiated at 550°C. In all cases, the foil normal is [110].

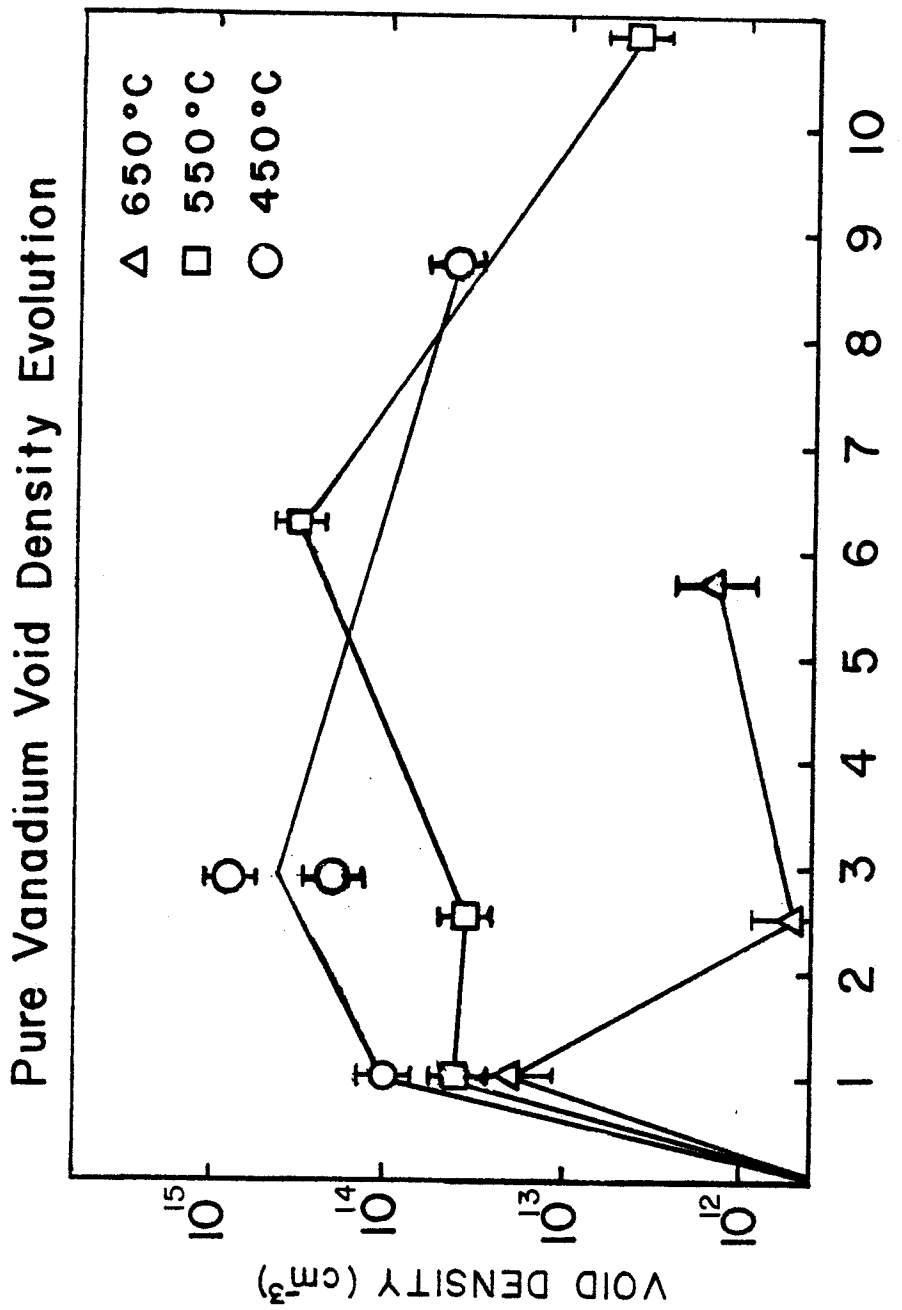

Figure VI-5. Evolution of void density with dose in pure vanadium specimens irradiated at 450°C, 550°C and 650°C.

was dominated by the larger voids (1000 Å diameter), which accounted for less than 2% of the total void density. The smaller voids (120 Å diameter) were homogeneously distributed. The density of large voids was approximately the same as the total void density in the 10 dpa specimen.

In the 650°C specimens, the void density was correlated with precipitate formation. Micrographs of the three specimens irradiated at 650°C to doses of 1, 2.5 and 5 dpa are presented in Figure VI-6. In the 1 dpa specimen, a bimodal size distribution was observed. The larger voids, which averaged 300 Å in diameter, were generally observed in association with small precipitates in rings or sections of arc. This distribution suggests that the larger voids and precipitates had nucleated on pre-existing dislocation loops. The smaller voids were homogeneously distributed throughout the matrix. The void density dropped sharply in the specimen irradiated to 2.5 dpa at 650°C. The voids that were observed at 2.5 were generally associated with precipitates. Precipitation was not observed separate from the voids in the 2.5 dpa sample. At 650°C, 5 dpa, the specimen was more heavily precipitated with precipitates on voids and in the matrix. Approximately one third of the voids were elongated or had irregular shapes. In all cases, the irregularly shaped voids were associated with precipitates. Also in the 650°C, 5 dpa sample, the void distribution was inhomogeneous with variations in void density of a factor of five within the foil. Even the region of maximum void density in the 5 dpa specimen, however, had a lower void density than the sample irradiated to 1 dpa.

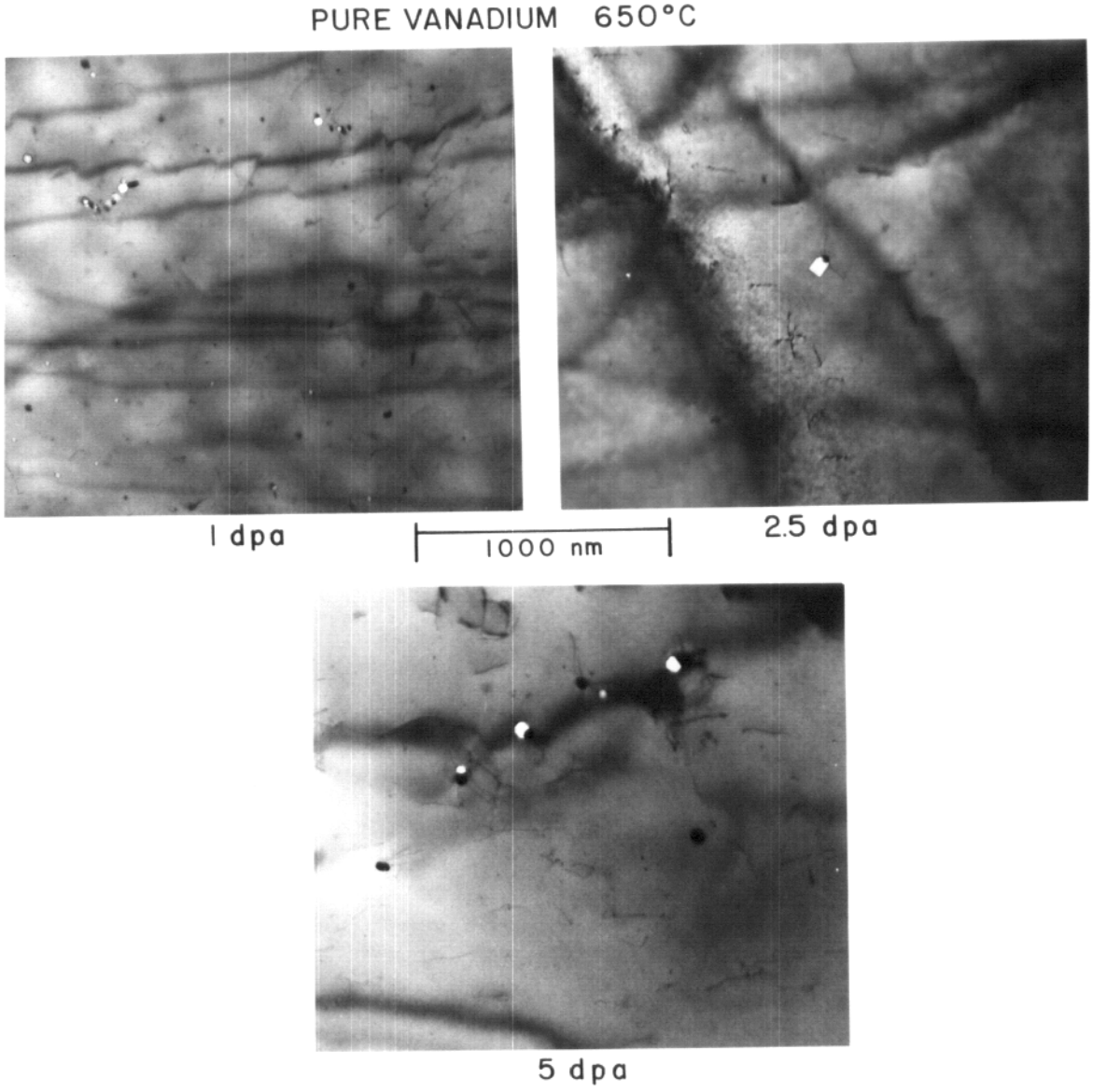

Figure VI-6. Voids in pure vanadium specimens irradiated at 650°C. In all cases, the foil normal is [110].

With the exception of two dose intervals, the void size increased with increasing dose. This behavior is illustrated in Figure VI-7. The two points where a reduction in the average void size was observed were 450°C, 2.5 dpa and 550°C, 5 dpa. These dose levels correspond to the maxima in the void density curves. A second specimen was irradiated to 2.5 dpa at 450°C to verify this result. The average void diameter in the 550°C, 5 dpa specimen was determined by the high density of small voids, while the swelling, which depends on the average value of the cube of the diameter, was determined by the low density of large voids. If it is assumed that it was the large portion of the size distribution which survived in the 10 dpa specimen, then significant void shrinkage must have occurred between 5 dpa and 10 dpa.

This same data on pure vanadium has also been replotted in Figure VI-8 to study swelling as a function of temperature. The most complete set of measurements was taken at 2.5 dpa, where swelling was measured at 250°C, 450°C, 550°C and 650°C. For the other dose levels, irradiations were completed over portions of this temperature range. The peak swelling temperature observed in these samples was a complicated function of the dpa level. At 2.5 dpa, the swelling at 250°C and 550°C appeared to be roughly equivalent, while a much lower value of swelling was observed at 450°C. Alternatively, at 1 dpa and 10 dpa, the maximum observed swelling occurred at 450°C. The maximum swelling observed in the 5 dpa specimen was at 550°C, but irradiations were only performed at 550°C and 650°C.

The void density is plotted as a function of temperature in Figure VI-9. Although the dose dependence of the void density was not

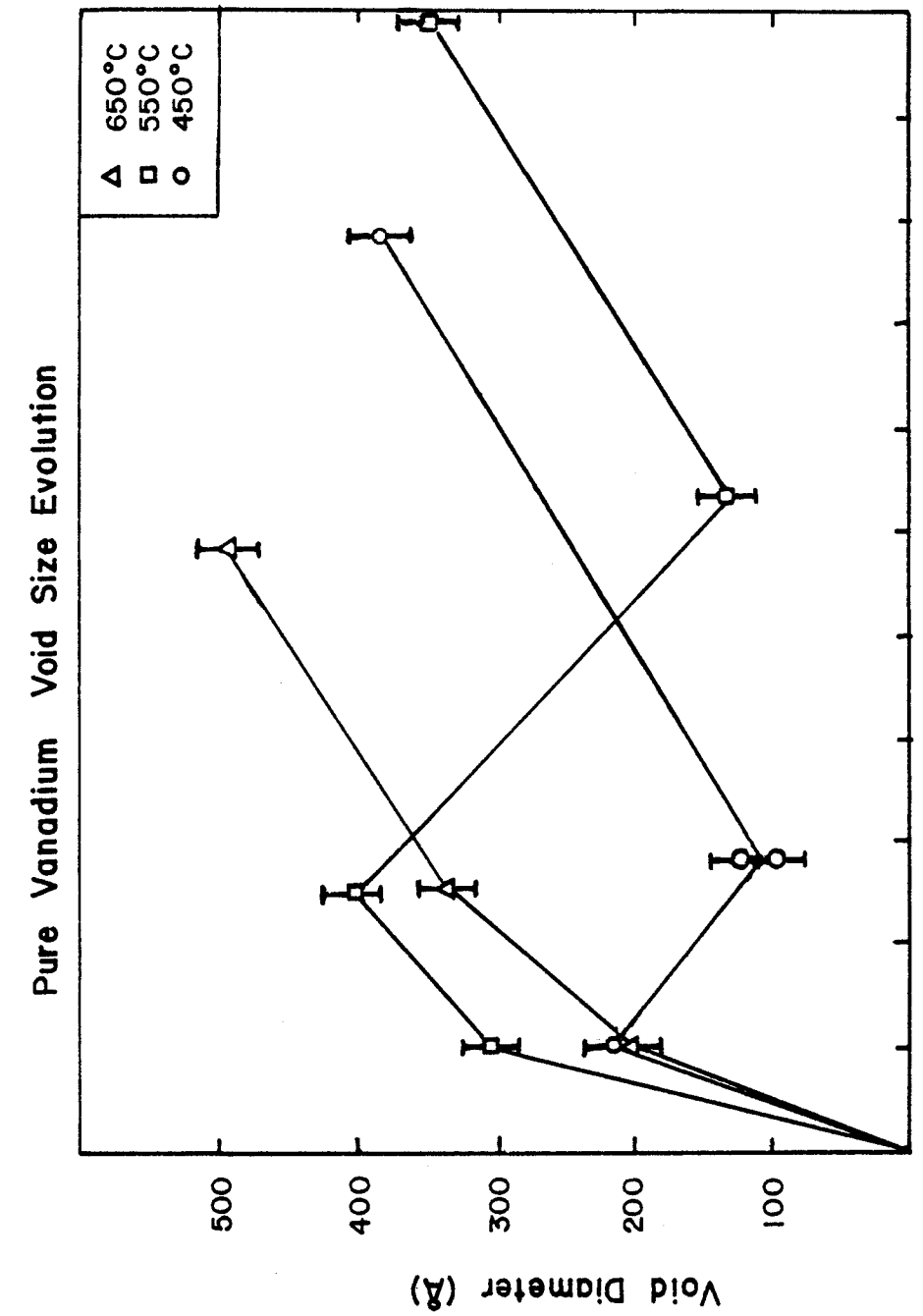

Figure VI-7. Evolution of average void diameter with dose in pure vanadium irradiated at 450°C, 550°C and 650°C.

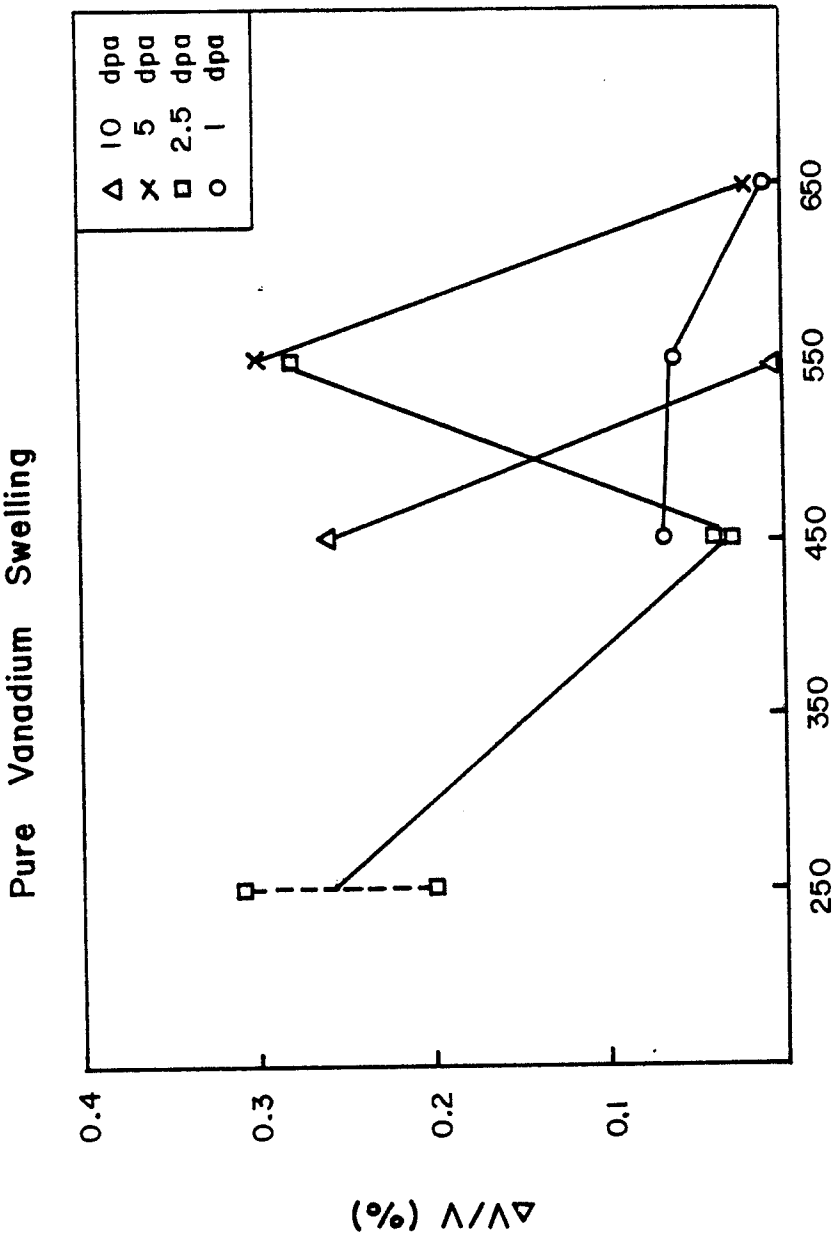

Figure VI-8. Void swelling as a function of temperature for pure vanadium specimens irradiated to doses between 1 dpa and 10 dpa.

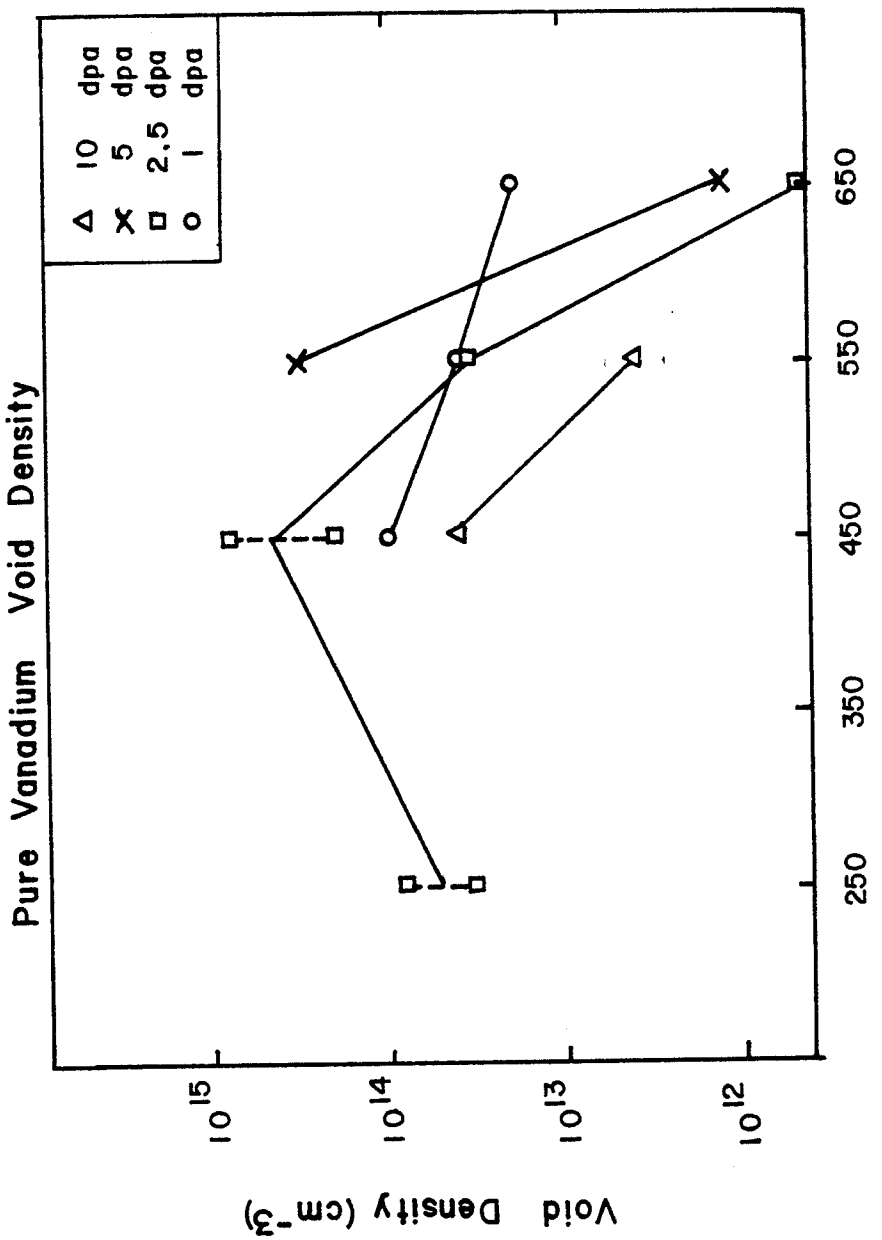

Figure VI-9. Void density as a function of temperature for pure vanadium specimens irradiated to doses between 1 dpa and 10 dpa.

the same at all temperatures, the void density did decrease as expected with increasing temperature at 450°C, 550°C and 650°C. However, the void densities observed in the 250°C, 2.5 dpa specimens were much lower than the 450°C, 2.5 dpa specimens. In addition the average void diameter at 2.5 dpa decreased as the irradiation temperature increased from 250°C to 450°C. This behavior is illustrated in the micrographs of Figure VI-10. Other than the two 450°C, 2.5 dpa specimens and the 550°C, 5 dpa specimen (with the bimodal void size distribution), void size does not appear to be a strong function of temperature.

The dislocation structure in the pure vanadium specimens consisted primarily of network dislocations. A low density of large dislocation loops was also observed in some specimens. All of the dislocation densities measured in the pure vanadium specimens were between 2×10^8 cm^{-2} and 3×10^9 cm^{-2}. In all cases, the dislocation densities were dominated by the network dislocations. The dislocation density is plotted as a function of dose in Figure VI-11. No correlation was found between dislocation density and either dose or irradiation temperature.

Although the sources of impurities responsible for the excessive precipitation observed by Weber have been eliminated, some precipitation was also observed in this study. In all cases the precipitates were too small and too sparse to allow identification by electron diffraction.

Precipitation was most prevelant at the higher temperatures. At 650°C, precipitates were observed at all dpa levels. At 1 and 5 dpa, the precipitate density was approximately twice the void density and

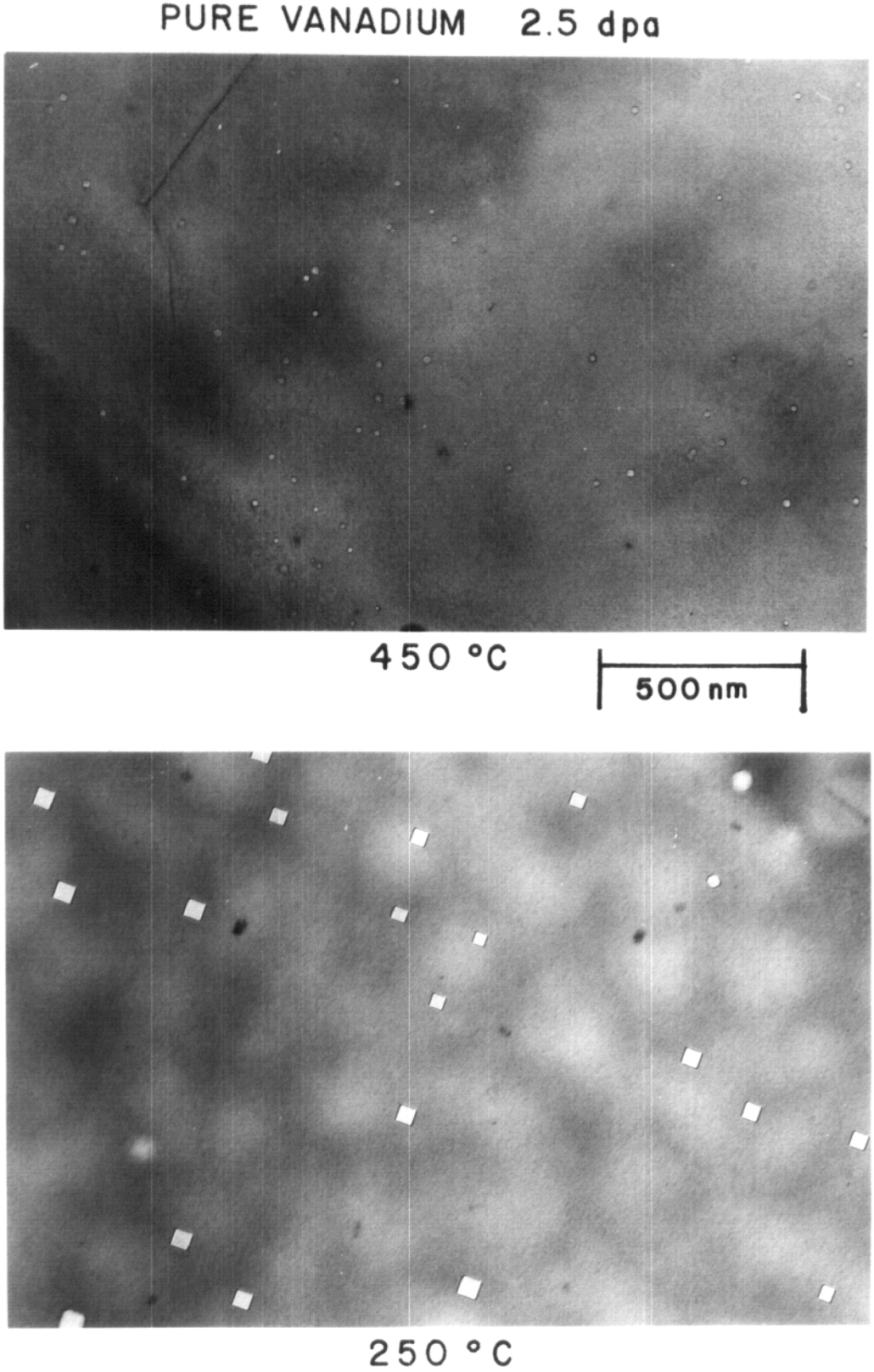

Figure VI-10. Comparison of pure vanadium specimens irradiated at 250°C and 450°C to 2.5 dpa. A higher density of smaller voids was observed in the 450°C specimen. The foil normal for these micrographs is [100].

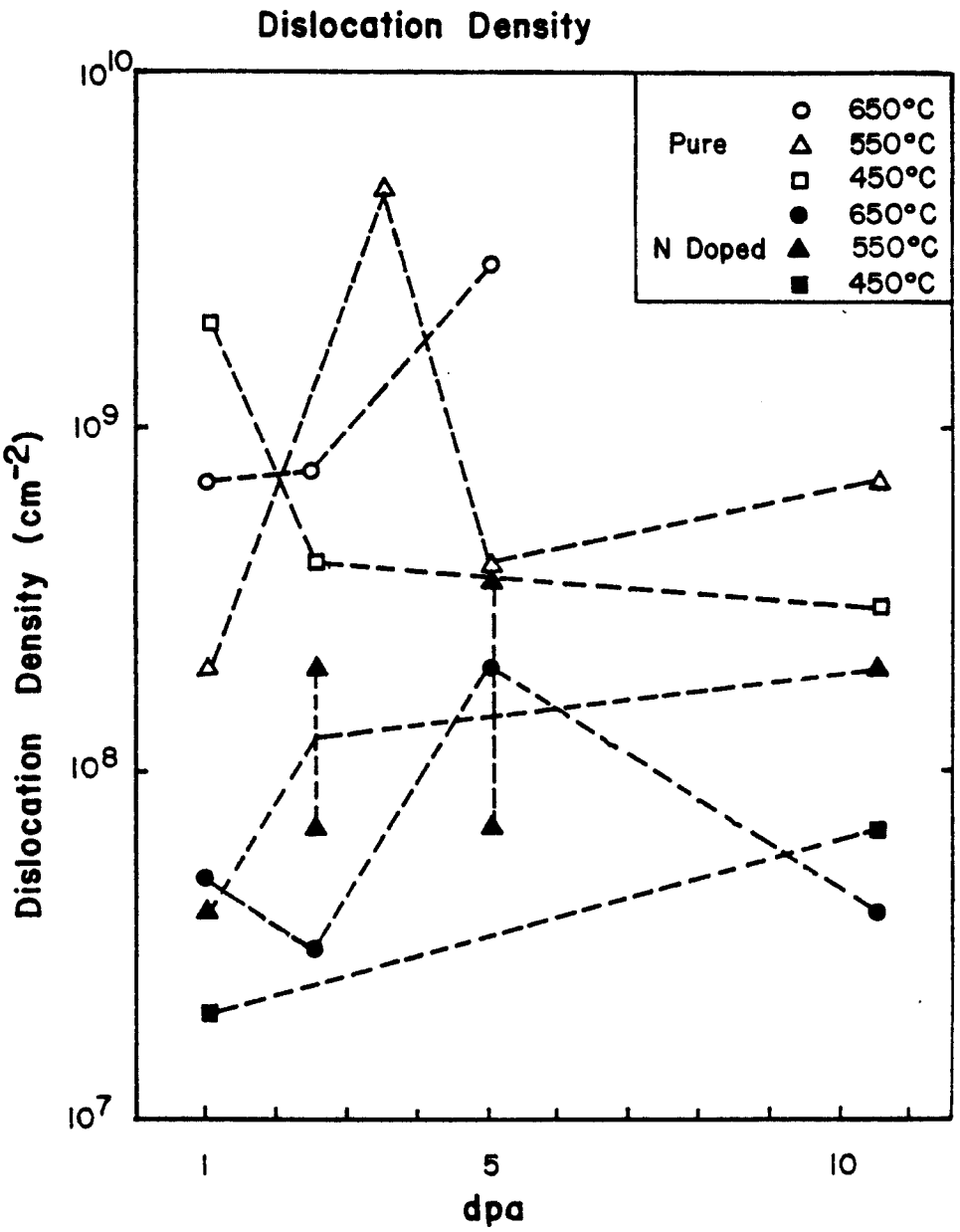

Figure VI-11. Dislocation density for pure vanadium and vanadium-1% nitrogen specimens.

precipitates were frequently observed at void corners. In the 2.5 dpa specimen, the precipitate density was lower and precipitates were only seen in association with voids. Precipitation similar to that observed in the Ni doped specimens was observed in the 550°C, 2.5 dpa specimen. Precipitates also formed on the corners of the large voids in the 5 dpa, 550°C sample. (This sample also had a bimodal void size distribution.) Small black spots, which could not be positively identified as precipitates, were also observed at 550°C, 10 dpa.

Energy Dispersive X-Ray Analysis (EDXA) was used to determine the Ni and Cu contents of all of the pure vanadium samples. In Weber's study and in the preliminary stages of this study, Ni was shown to be an important contaminant in the heavy ion irradiated specimens. It is also possible that copper contamination could have resulted from migration of Cu ions from the end of range region, where they were deposited by the beam, to the region of analysis.

Of the thirteen pure vanadium specimens examined, Ni was detected in three. The analyzed Ni contents for these three specimens are listed in Table VI-3. Nickel contents as low as 0.1% were detected. In the 550°C, 5 dpa specimen and the 650°C, 1 dpa specimen, the nickel concentrations were higher in the region of the precipitate. No nickel was detected in the 650°C, 2.5 dpa and 5 dpa specimens or the 550°C, 2.5 dpa specimen, which were the other specimens where definite precipitation was observed. Nickel was detected in the 550°C, 10 dpa specimen. Although significant Ni contents were detected, no signs of precipitation were observed in the 250°C, 2.5 specimen.

The lower detection limit for Cu in the EDXA system is limited to approximately 1% by the high background peak from Cu containing elements of the microscope column. Individual measurements may be below this limit, but small movements of the position of the sample in the holder will produce large Cu peaks. In some cases, such as the 550°C, 10 dpa specimen, the detected Cu concentration was as low as 0.1 %. An upper limit on the Cu concentration can be calculated by assuming that the deposited Cu ions are distributed uniformly in a 2 μm thick region. In this case, the average Cu concentration in a 10 dpa sample would be 0.5%. These EDXA results indicate that Ni contamination was a more important source of impurities in these irradiations than the Cu beam.

VI-C. Vanadium-Nitrogen

Sixteen specimens of the vanadium-1% nitrogen alloy were irradiated. The irradiation parameters for each of these specimens are listed in Table VI-1. Dose scans over the range 1 to 10 dpa were taken at 450°C, 550°C and 650°C. Most of these irradiations were performed immediately after an irradiation of pure vanadium under identical conditions. In these dose scans the damage rate in the region of examination was 4×10^{-4} dpa/second. One sample was irradiated at 250°C to 2.5 dpa at a dose rate of 7×10^{-4} dpa/second. Two specimens irradiated to 2 dpa at 650°C and 600°C were not outgassed prior to irradiation. The void parameters for these specimens are listed in Table VI-2. In general the outgassed V-1%N specimens exhibited less swelling and lower void densities than the corresponding pure V specimens. However, the two V-1%N specimens which were not outgassed exhibited significant swelling and had relatively high void densities.

Micrographs of the V-1N specimens irradiated at 650°C are presented in Figure VI-12. As can be seen from Figure VI-13, where swelling is plotted as a function of dose, the maximum swelling occurred at 1 dpa. Although the observed swelling at 1 dpa is slightly larger in the nitrogen doped specimen than the corresponding pure V specimen, the swelling levels in both specimens are < 0.02%. At this dose the void density in the nitrogen doped vanadium was one half the density of the pure vanadium, but the voids were slightly larger in the nitrogen doped specimen. The variation of void density with dose is presented in Figure VI-14. In the higher dose specimens, the void densities were very low and the swelling levels were negligible. Even though the swelling levels observed in the pure vanadium at 2.5 and 5 dpa irradiated at 650°C were also low, the void densities in the pure V appeared to be higher than the void densitites in the nitrogen doped specimens.

At 550°C, the suppression of void formation by nitrogen was more dramatic. Micrographs of the nitrogen doped specimens irradiated at 550°C are presented in Figure VI-15. No significant swelling was observed below 10 dpa. Duplicate specimens were irradiated at 2.5 and 5 dpa to confirm this result. At 10 dpa, both the swelling and the void density were a factor of 2 higher in the nitrogen doped sample than in the pure vanadium sample. This is the only nitrogen doped specimen where the void density exceeded that observed in the corresponding pure vanadium specimen and one of the two specimens where swelling was higher. The reason for this discrepancy appears to be the precipitous decrease in swelling with dose in the pure vanadium

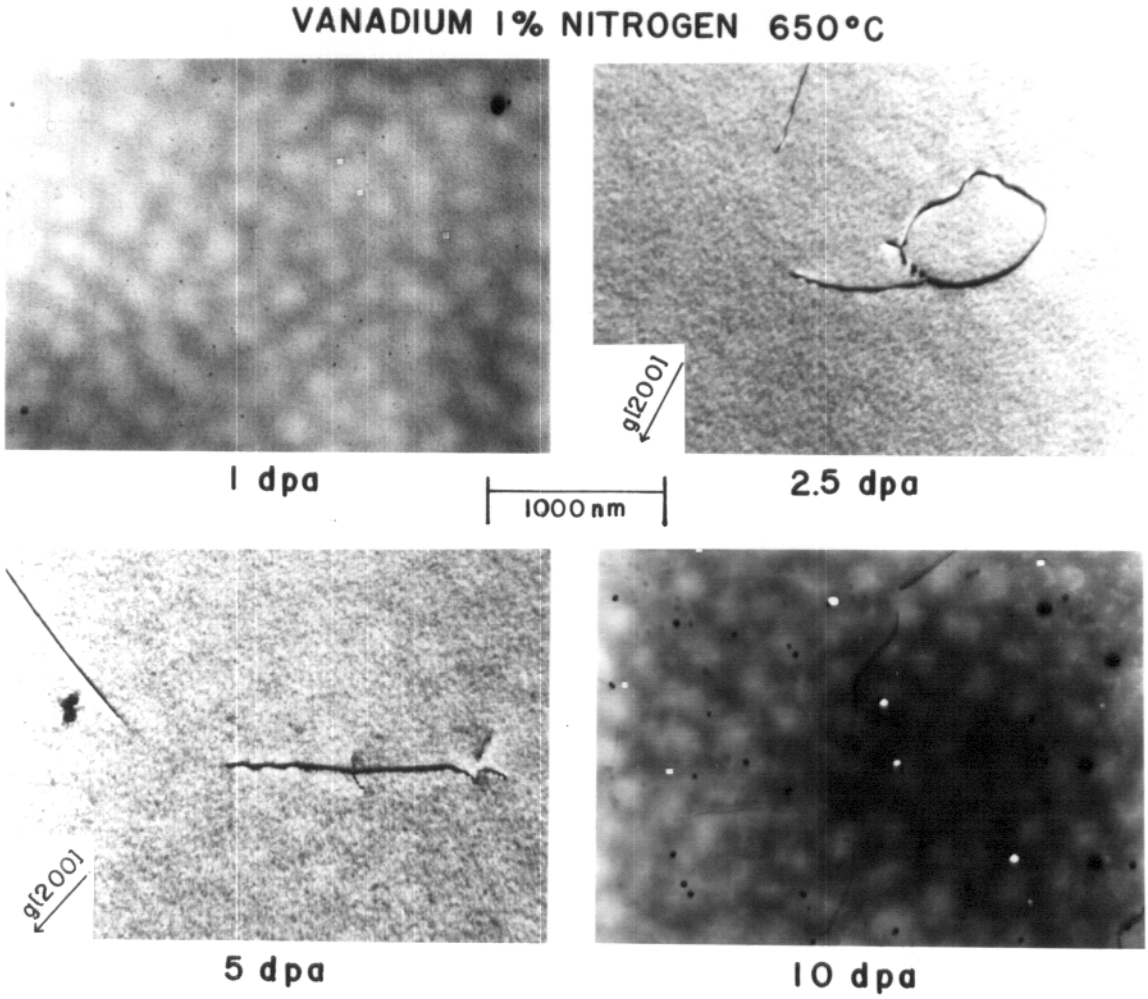

Figure VI-12. Voids and dislocations in vanadium-1% nitrogen irradiated at 650°C. Foil normal is near [100] in all cases.

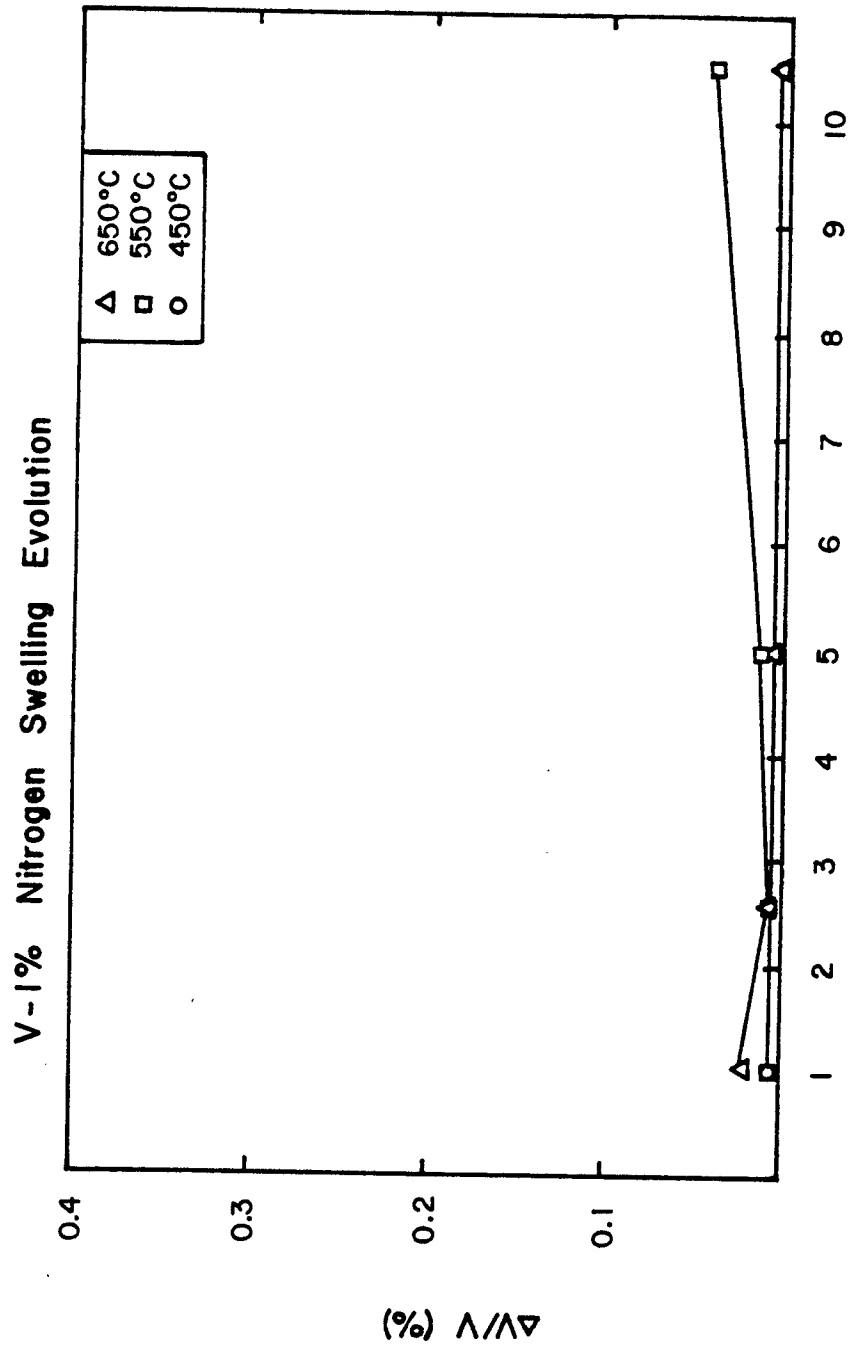

Figure VI-13. Evolution of swelling with dose in vanadium-1% nitrogen specimens irradiated at 450°C, 550°C and 650°C.

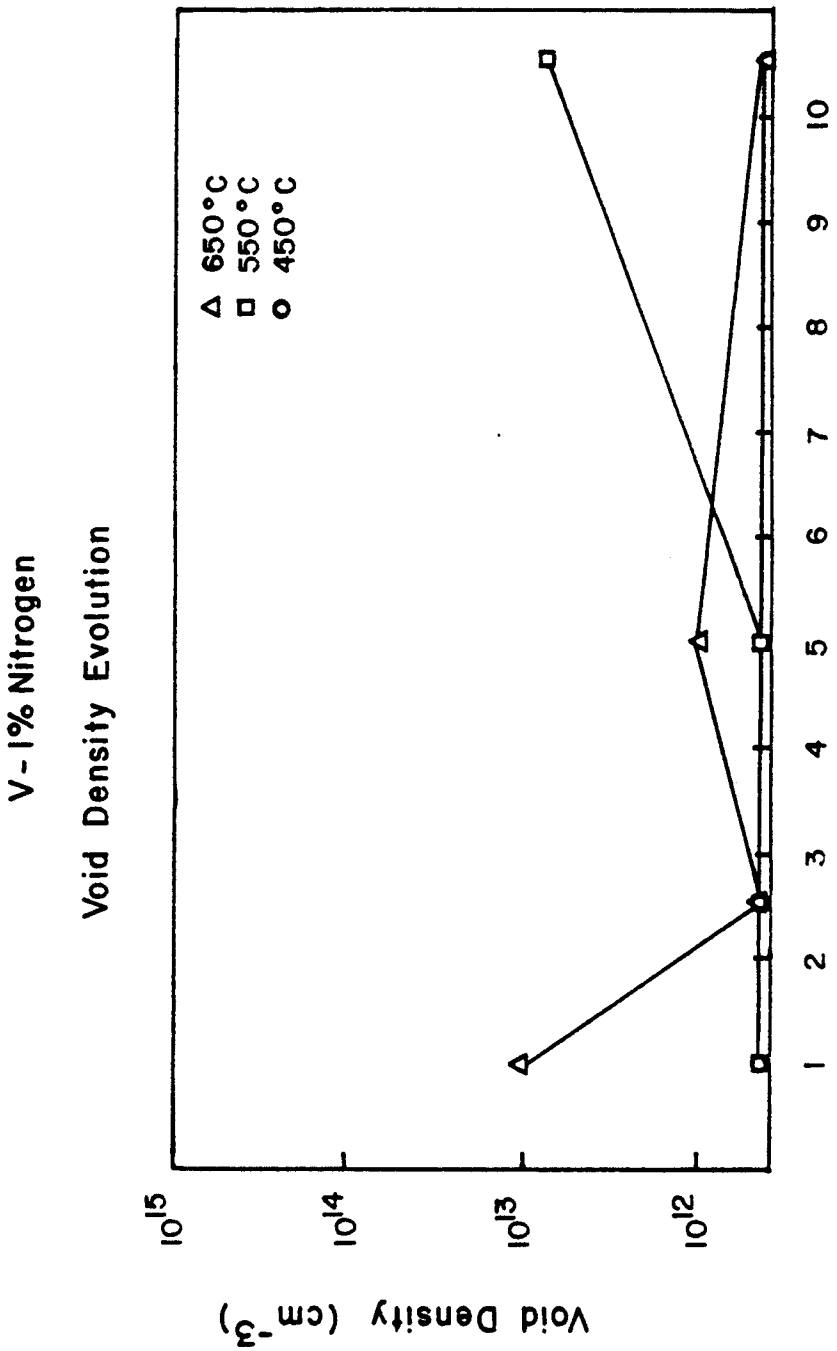

Figure VI-14. Evolution of void density with dose in vanadium-1% nitrogen specimens irradiated at 450°C, 550°C and 650°C.

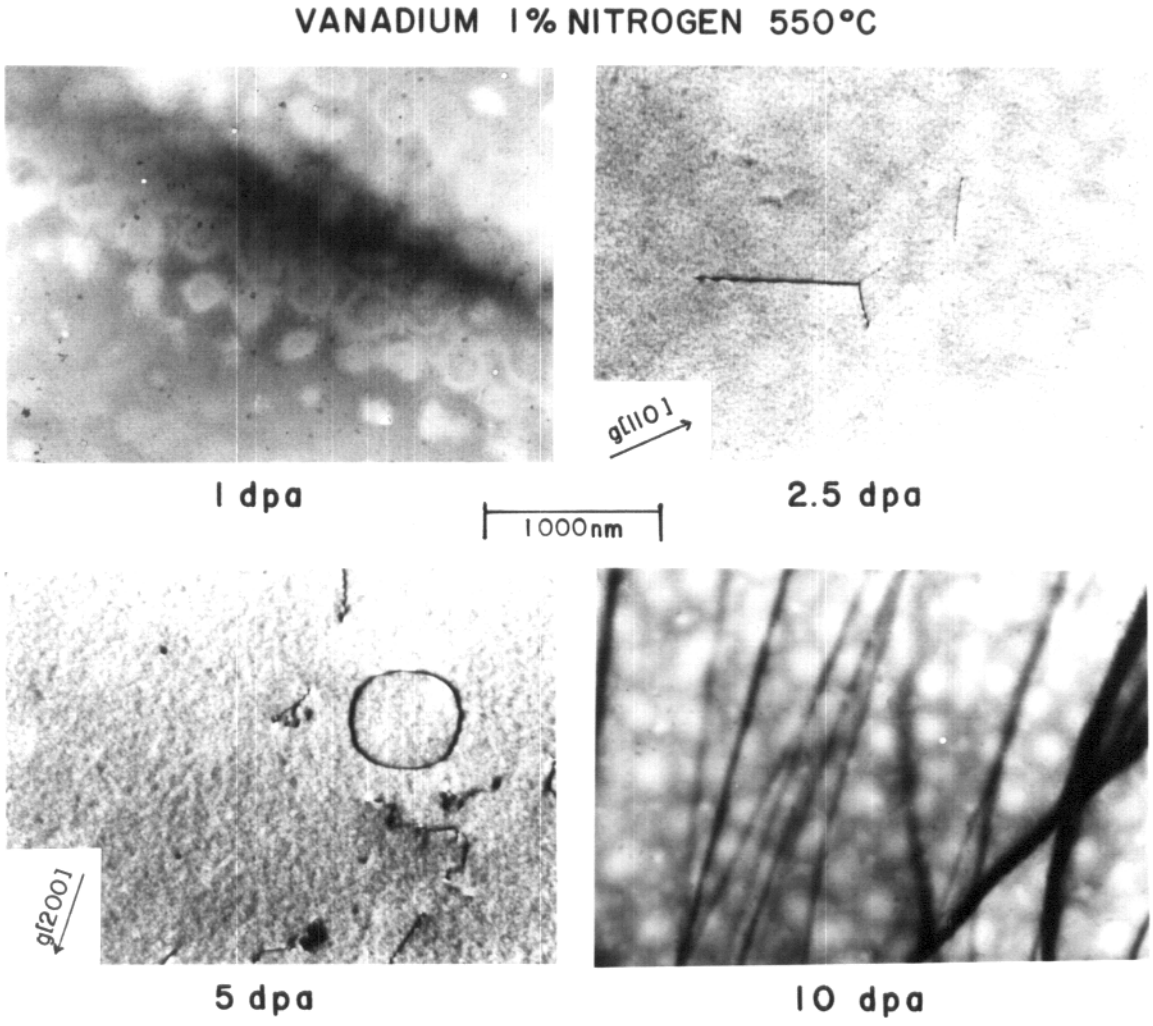

Figure VI-15. Voids and dislocations in vanadium-1% nitrogen irradiated at 550°C. Foil normal near [100] in all cases.

specimen.

The maximum void density observed in the specimens irradiated at 450°C was 1×10^{11} voids/cm^3. In the sample irradiated to 2.5 dpa at 250°C, no voids were observed. Voids were observed in pure vanadium specimens irradiated at these same temperatures and doses.

The vanadium-1% nitrogen specimens displayed lower dislocation densities than the pure vanadium. All of the dislocation densities were within the range 2×10^7 cm^{-2} to 4×10^8 cm^{-2}. This general reduction in dislocation density by nitrogen doping is illustrated in Figure VI-11. As in the pure vanadium case, no correlation was found when the dislocation density was studied as a function of dose and temperature.

Precipitates similar to those observed in the pure vanadium were observed in the nitrogen doped specimens. Precipitation was more prevelant in the higher temperature, higher dose samples. This same tendency was noted in the pure vanadium specimens. The samples that exhibited precipitation were the 650°C, 5 and 10 dpa specimens, the 550°C, 10 dpa specimen and one of the two 550°C, 5 dpa specimens. In each case, precipitates were observed on void corners, and the precipitate density was comparable to the void density.

VI-D. Vanadium-Nickel

Eight specimens of vanadium-1% nickel were irradiated to establish the effect of nickel on void formation. The irradiations of this alloy were performed at 450°C, 550°C and 650°C. The temperature dependence of swelling in specimens irradiated to 1 and 5 dpa is illustrated

in Figure VI-16. In general the low temperature, high-dose specimens contained extremely large voids, while the high temperature specimens did not swell significantly. The samples irradiated at 450°C to 1 and 5 dpa and the two 550°C, 5 dpa samples all exhibited extensive void formation and also contained incoherent V-Ni precipitates. A micrograph of the 450°C, 1 dpa specimen showing both voids and precipitates is presented in Figure VI-17. Both of the 650°C specimens and the 550°C, 1 dpa specimen had void densities which were less than 10^{11} voids/cm^3. Only coherent precipitates were observed in the low swelling specimens. This relationship between incoherent precipitates and voids is consistent with the previously mentioned observations in nickel contaminated vanadium. Weber observed both precipitates and voids in his nickel contaminated specimens, while neither voids nor precipitates were observed in nickel contaminated specimens in this study. The apparent discrepancy between these two studies could have been caused by variations in the level of nickel contamination. Voids may have formed in Weber's specimens because the level of contamination was sufficient to produce incoherent precipitates.

The development of swelling with dose is illustrated in Figure VI-18. At 650°C, very few voids had nucleated and swelling remained at negligible levels at both 1 and 5 dpa. In the 550°C specimens, a sharp transition took place between 1 and 5 dpa. The 550°C, 1 dpa contained only coherent precipitates and an extremely low density of voids, but the two 5 dpa specimens exhibited swelling in excess of 1%. At 450°C, voids formed at both 1 and 5 dpa. As illustrated in Figure VI-19, the void density increased with dose, while the average void size increased

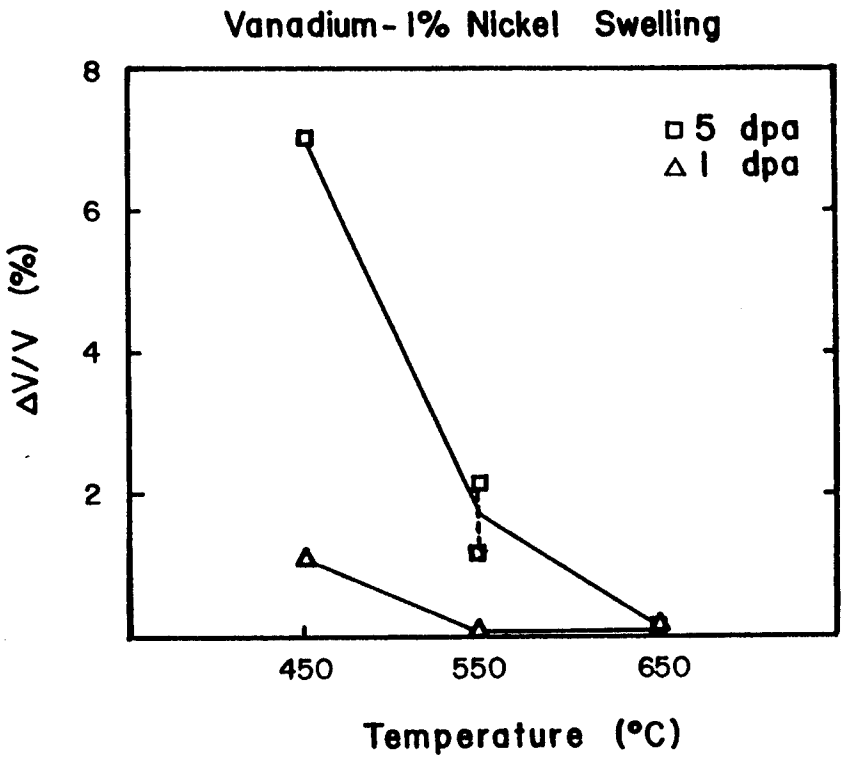

Figure VI-16. Swelling as a function of temperature for vanadium-1% nickel specimens irradiated to 1 dpa and 5 dpa.

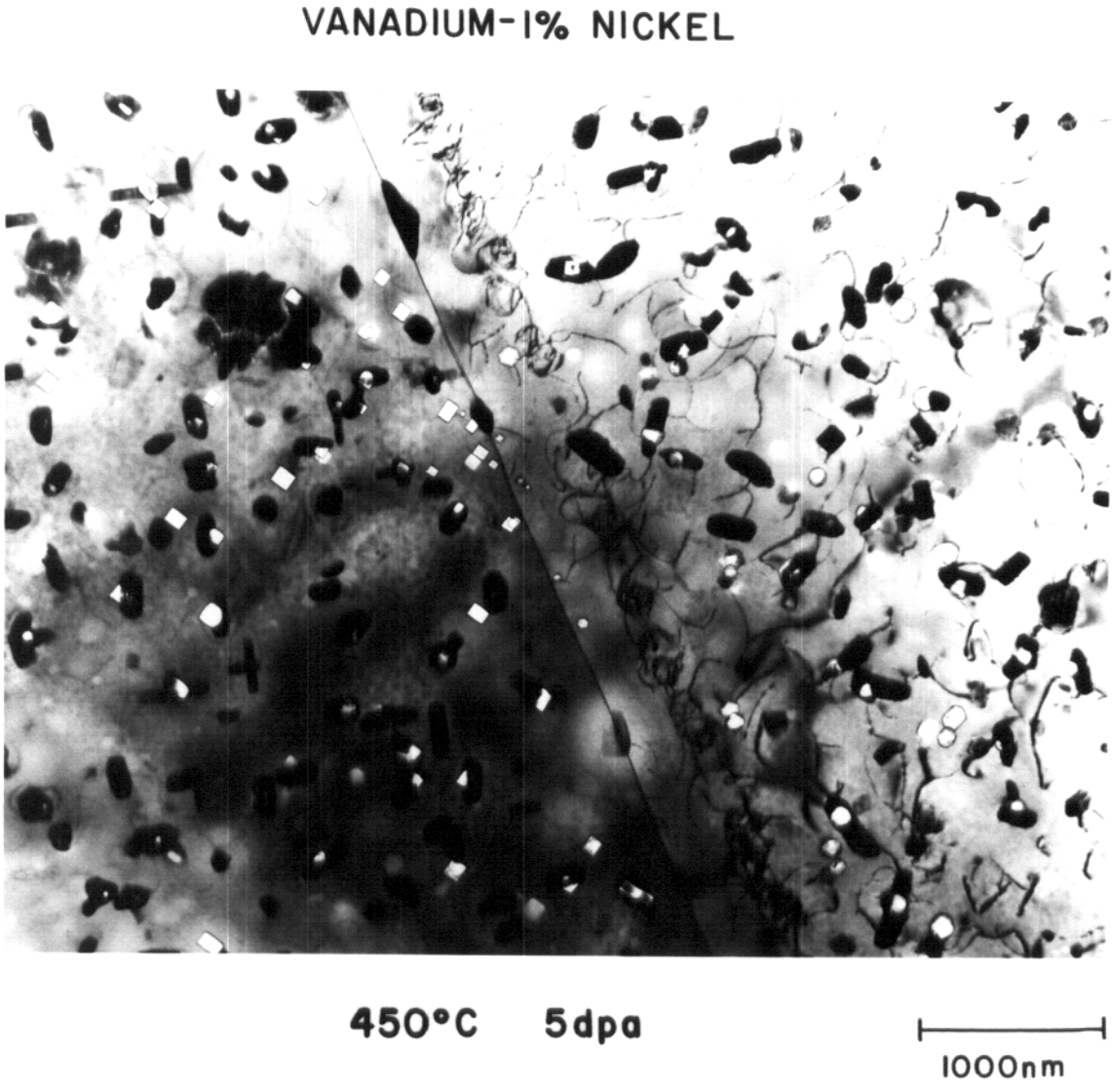

Figure VI-17. Voids and precipitates in a vanadium-1% nickel specimen irradiated to 5 dpa at 450°C.

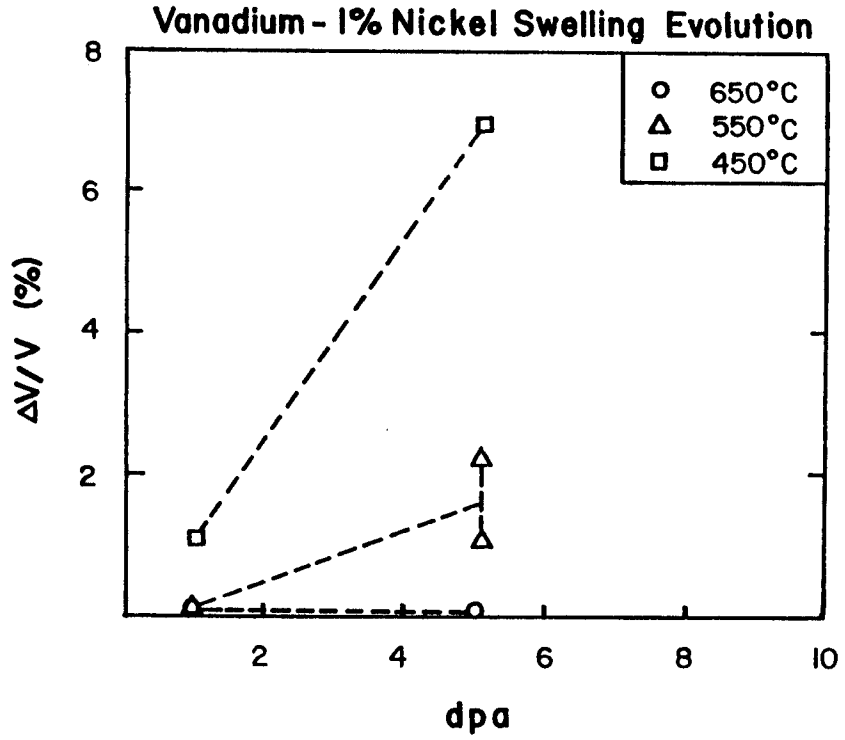

Figure VI-18. Evolution of void swelling as a function of dose in vanadium-1% nickel specimens irradiated at 450°C, 550°C and 650°C. Irradiations in this alloy were limited to dose levels of 1 dpa and 5 dpa.

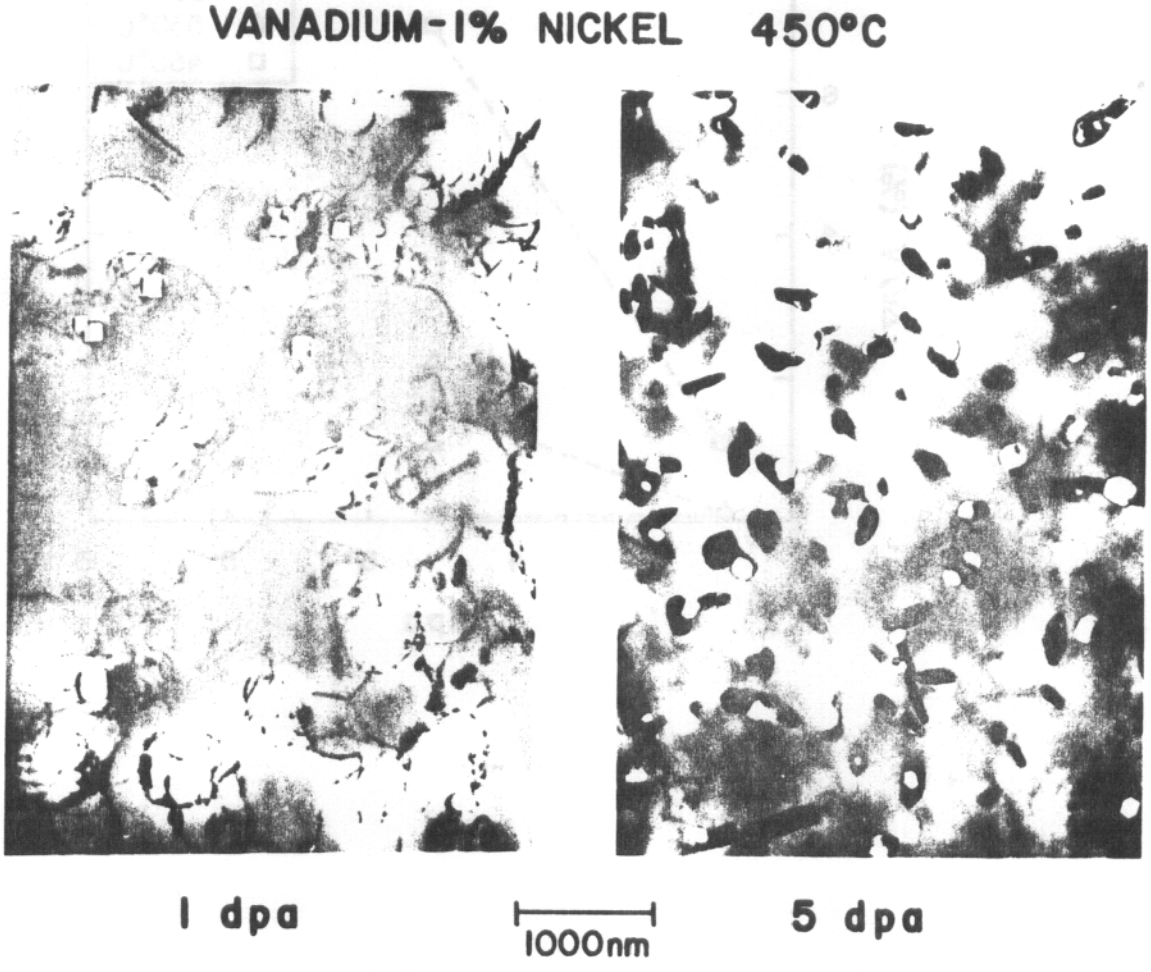

Figure VI-19. Voids and precipitates in vanadium-1% nickel specimens irradiated at 450°C to 1 dpa and 5 dpa.

slightly. This increase in swelling was paralleled by an increase in precipitate density and volume. The 7% swelling observed in the 450°C, 5 dpa vanadium-1% nickel specimen was the highest swelling level recorded in this study.

These results strongly suggest the existence of a temperature dependent incubation dose for void nucleation in the vanadium-nickel alloy. Although specimens were only irradiated to two dose levels at each temperature, a rough estimate of this incubation dose may be derived by examining Figure VI-20, where void density is plotted as a function of dose. At 450°C, the incubation dose is less than 1 dpa, while at 550°C it is between 1 and 5 dpa. The transition from low swelling to high swelling at 550°C is illustrated in the micrographs of Figure VI-21. As voids were not observed at 650°C, it must be assumed that the incubation dose is greater than 5 dpa. In all cases, the incubation dose corresponds to the dose at which coherent precipitates began to form.

Due to differences in the average void size, the swelling in the two 550°C specimens irradiated to a nominal dose of 5 dpa under identical conditions varied by a factor of two. These two samples are compared in Figure VI-22. This variance may be explained by the difference in actual dose level (see Table VI-1). The high swelling sample was examined at a deeper depth, corresponding to a slightly higher dpa level. This difference in dpa level was accentuated by the incubation dose. Also, approximately one-third of the voids in the high swelling sample were smaller, elongated voids indicating some further differences in the nucleation process at the deeper depth.

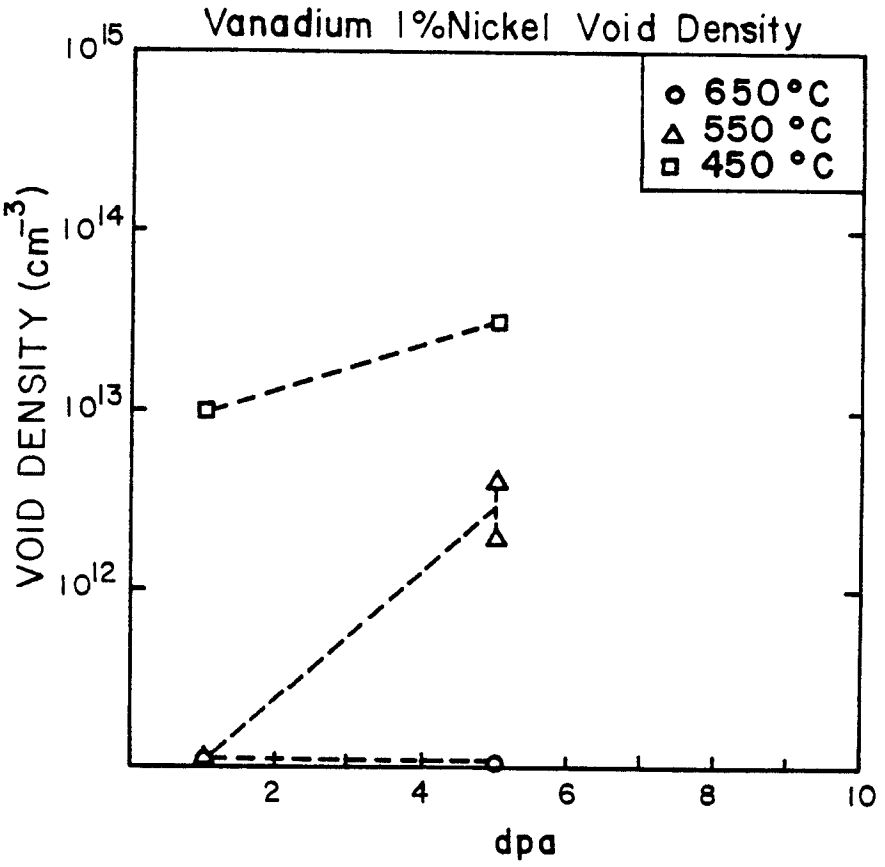

Figure VI-20. Evolution of void density with dose in vanadium-1% nickel specimens irradiated at 450°C, 550°C and 650°C. Irradiations in this alloy were limited to dose levels of 1 dpa and 5 dpa.

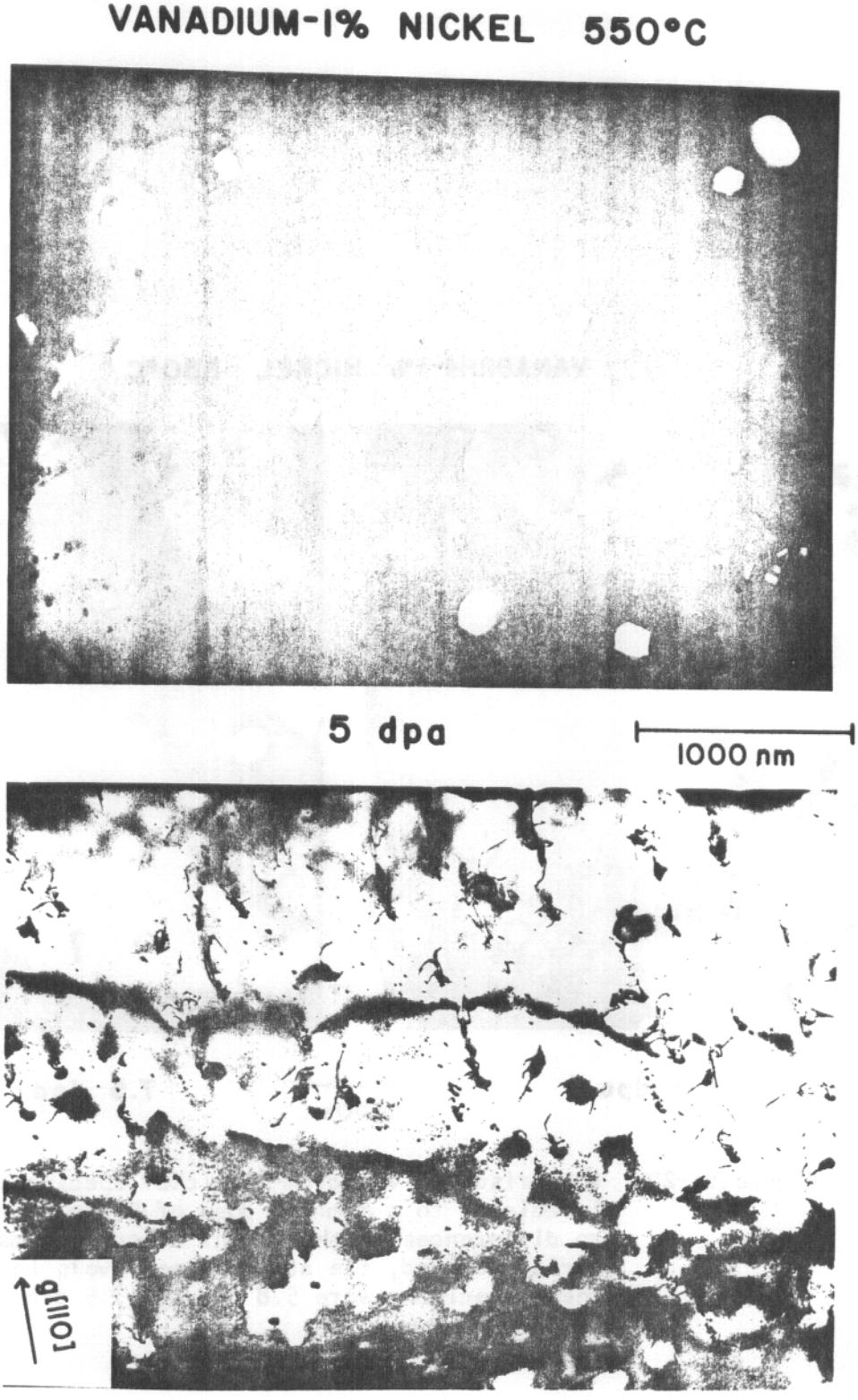

Figure VI-21. Vanadium-1% nickel specimens irradiated at 550°C to 1 dpa and 5 dpa. Incoherent precipitates and voids developed in the 5 dpa specimen.

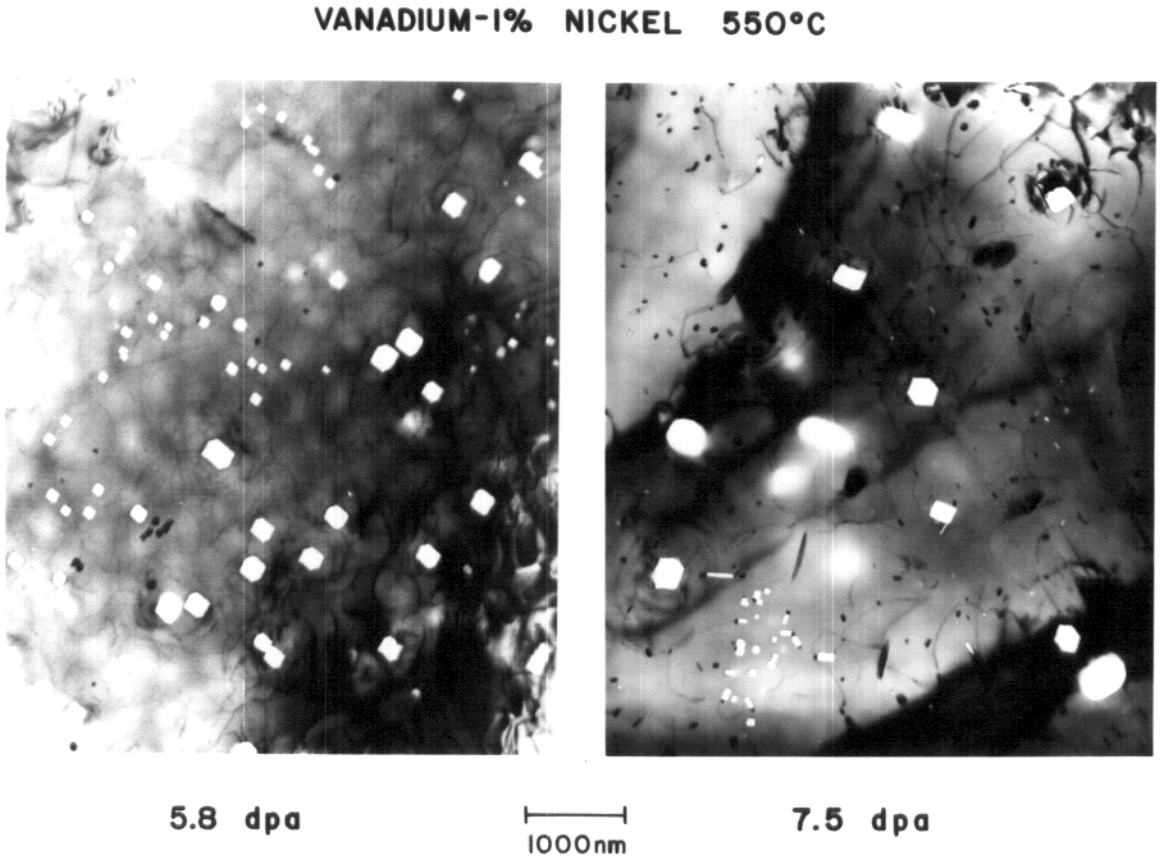

Figure VI-22. Comparison of vanadium-1% nickel specimens irradiated to a nominal dose of 5 dpa. Due to differences in the amount of surface material removed, the actual dose levels in these specimens were 5.8 dpa and 7.5 dpa.

The precipitation process in the V-1%Ni specimens involved the transformation from incoherent to coherent precipitates. This process was most clearly evident at 550°C. The evolution of precipitates in the 550°C specimens is illustrated in the micrographs of Figure VI-23. In the 1 dpa specimen, coherent precipitates were observed as large regions of strain contrast, often associated with dislocations. Large planar precipitates formed at 5 dpa. In addition, the initial stages of incoherency were observed in the 5 dpa specimen as clusters of dislocations around the precipitates. Although only early stages of incoherency were observed, the voids were large in the 550°C, 5 dpa specimen, indicating a high void growth rate. The most extensive precipitation and the most complete development of the precipitation process was observed in the 450°C, 5 dpa specimen (see Figure VI-19). The precipitates developed more rapidly at the lower temperatures. At 450°C, incoherent precipitates had already formed in the 1 dpa specimen, while the transition described above was still in the initial stages in the 650°C, 5 dpa specimen.

The irradiation induced incoherent precipitates observed in the V-1%Ni alloy are identical to the precipitates observed by Weber in nickel contaminated vanadium. Interplanar spacings of 6.24 Å, 4.79 Å and 2.15 Å were measured for this precipitate. These interplanar spacings are too large to correspond to any previously observed V-Ni phase. The structure of this precipitate has not been determined.

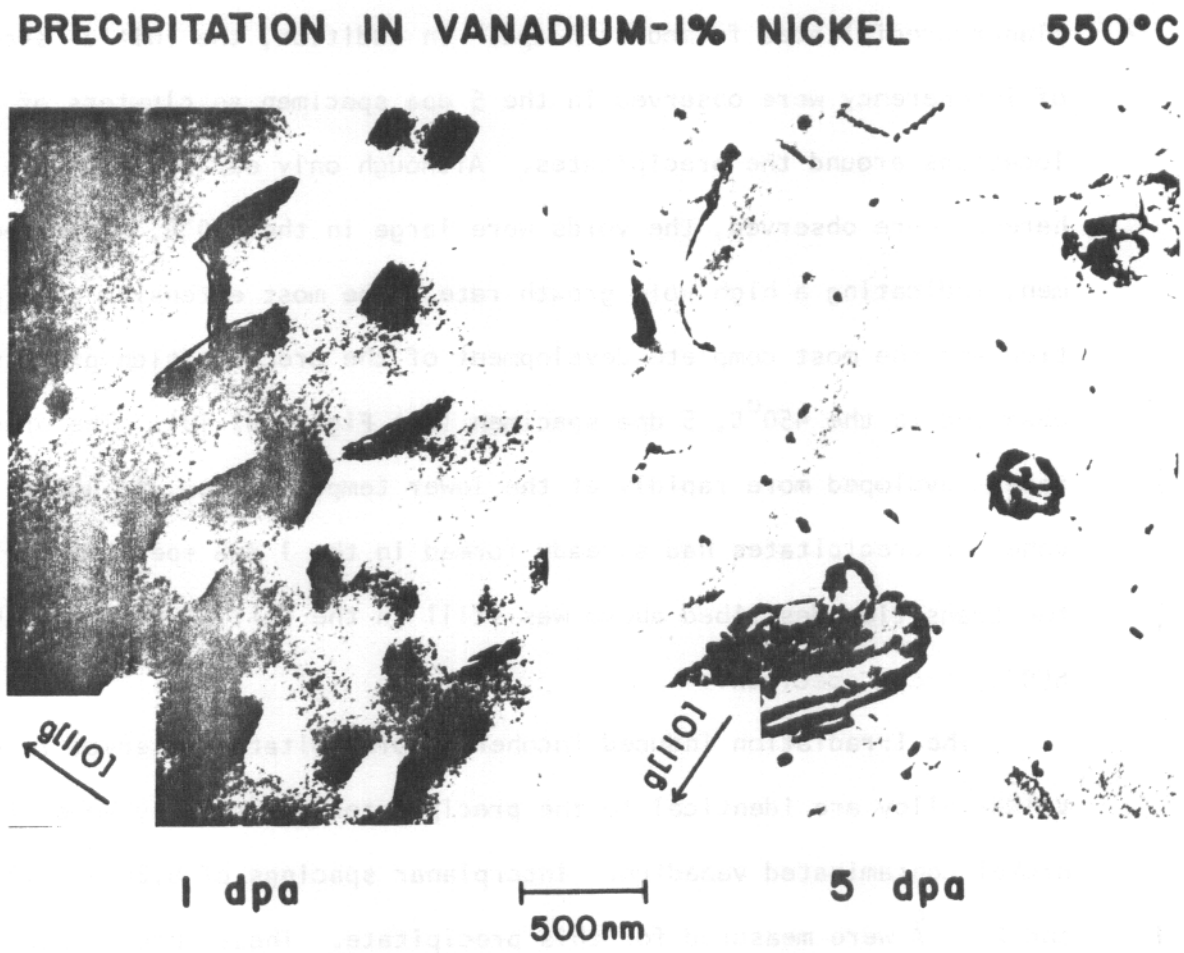

Figure VI-23. Evolution of precipitates in vanadium-1% nickel specimens irradiated to 1 dpa.

CHAPTER VII DISCUSSION

Void formation in pure vanadium was observed at 250°, 450°C, 550°C and 650°C in this study. At 450°C and 550°C, swelling decreased at high doses due to void shrinkage. The void density also decreased in these specimens at the higher doses as a result of the annihilation of the smaller voids. In a series of specimens all irradiated to 2.5 dpa at temperatures ranging from 250°C to 650°C, a low temperature decrease in the void density was observed. These results are compared to previous heavy ion irradiations of pure vanadium at the University of Wisconsin and at Argonne Naitonal Laboratory in Section VII-A. The precipitation phenomenon described in Chapter VI is discussed in Section VII-B.

Homogeneous void nucleation was suppressed in the V-1% N alloy and the V-1% Ni alloy. When void nucleation was assisted, either by high hydrogen contents in the case of the V-1% N alloy or by the formation of incoherent precipitates in the case of the V-1% Ni alloy, no barrier to void growth was apparent. This observation contradicts many qualitative descriptions of void nucleation, which assume that an interstitial impurity, such as nitrogen, would act as an insoluble gas and promote void nucleation. These experiments, however, demonstrate that both nitrogen atoms and nickel atoms in solid solution suppress void nucleation.

Using the theoretical models described in Sections II-B and II-C, the void growth rate and void nucleation rate in vanadium were

calculated in this study. The purpose of these calculations, which are described in Sections VII-C and VII-D, is to provide a qualitative basis for the comparison of the results described in Chapter VI to the present understanding of the theory of void formation. No attempt was made to make quantitative predictions based on these models.

VII-A. Comparison With Previous Studies

One objective of this study was to extend the irradiations performed in Weber's thesis[25] to higher doses. Most of the previous conclusions were based on a series of samples irradiated to 1 dpa at temperatures between 150°C and 750°C. In the present study, samples were irradiated at several different dose levels at temperatures between 250°C and 650°C and voids were observed over this entire temperature range. The swelling levels in the present study are compared to data from Weber's study in Figure VII-1. In general, the swelling observed in this study was higher than the swelling observed in the earlier study. This difference can be attributed to a combination of the higher dose levels in this study and the effect of nickel contamination in the previous work.

Although both studies were performed using the same irradiation facility, there were two important differences between them. First, the displacement rate in Weber's study ranged between 1×10^{-4} dpa/sec and 2×10^{-4} dpa/sec, while the displacement rate in this study was in the range from 3.5×10^{-4} dpa/sec to 7×10^{-4} dpa/sec. Second, the pre-irradiation treatments used in the two studies were different. All of the samples in the previous work were annealed using

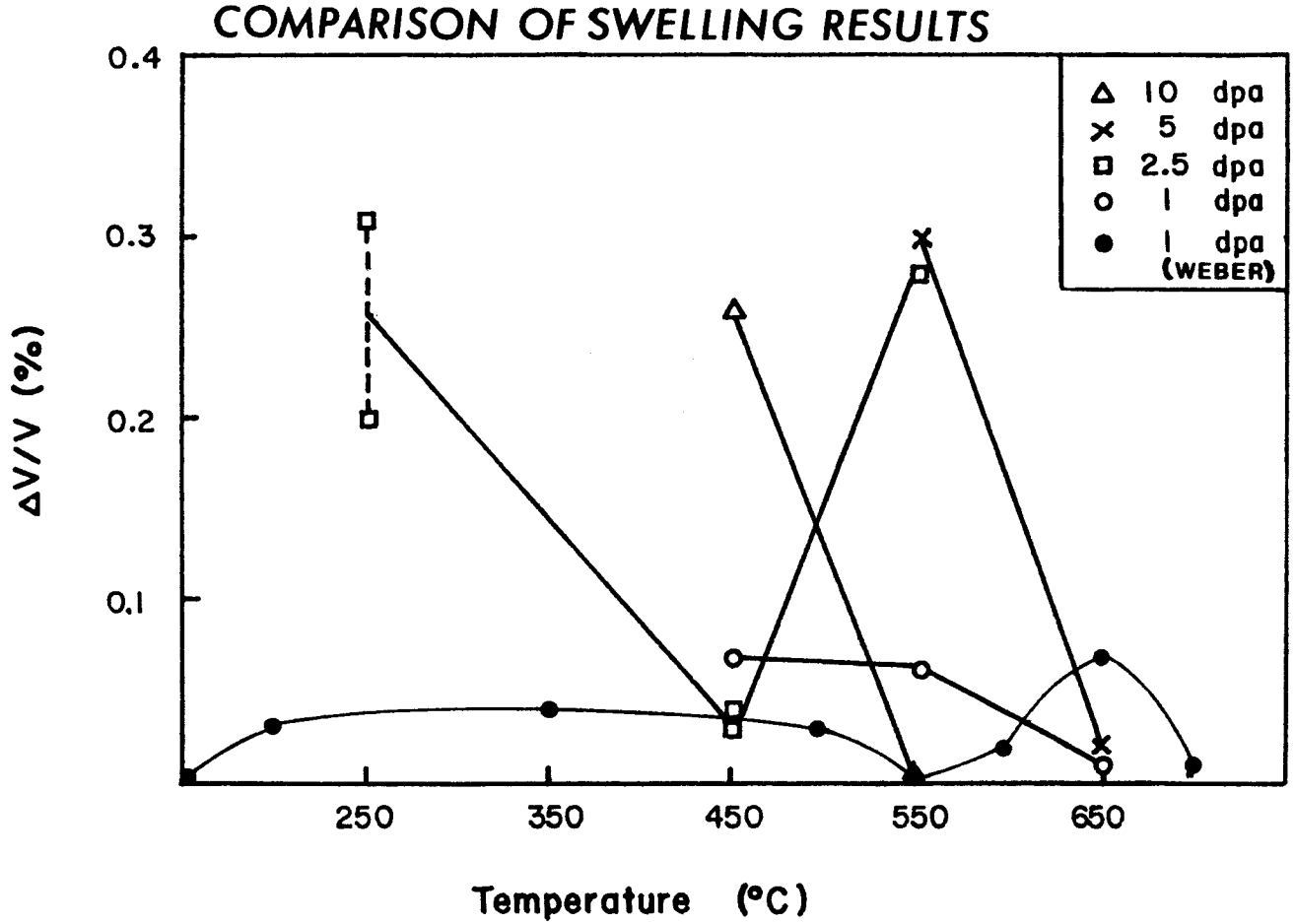

Figure VII-1. Comparison of swelling results from Weber's study[25] and this study. Both studies were performed in the University of Wisconsin Heavy Ion Facility with 14 MeV Cu ions. The dose rate in Weber's study was 1×10^{-4} dpa/sec, while the dose rate for this was 5×10^{-4} dpa/sec.

chromel/alumel thermocouples. Half of the specimens from Weber's study presented in Figure VII-1 were electropolished after the anneal to remove any surface contamination and then outgassed at 805°C in the irradiation chamber. The other half of these specimens were irradiated in the as annealed condition. These differences in the preirradiation treatment introduce uncertainties in the degree of outgassing and nickel contamination in these samples.

The reduction in swelling observed previously at 550°C was not observed in this study. It is possible that this dip was not observed because of the temperature shift due to the higher displacement rates in this study. However, plate-like precipitation was also observed by Weber in the 550°C specimen. This precipitation was similar to the precipitates observed at 350°C in a nickel contaminated specimen (00-106) in this study. This indicates that the reduction in swelling observed at 550°C in the previous study was caused by nickel contamination.

Weber observed a peak swelling at 650°C, which was higher than any observations of sweling at 650°C in this study. It should be noted, however, that sweling at 650°C in both studies was less than 0.1%, which implies that the uncertainties were relatively large. There was, in addition, nickel contamination observed at 650°C in this study, which could have reduced the swelling.

Above 450°C, the temperature dependence of void density was similar in both studies (see Figure VII-2). The void density observed at 550°C by Weber was anomalously low for reasons discussed above. The low temperature decrease in void swelling observed at 250°C in this study was not observed previously. There are two pos-

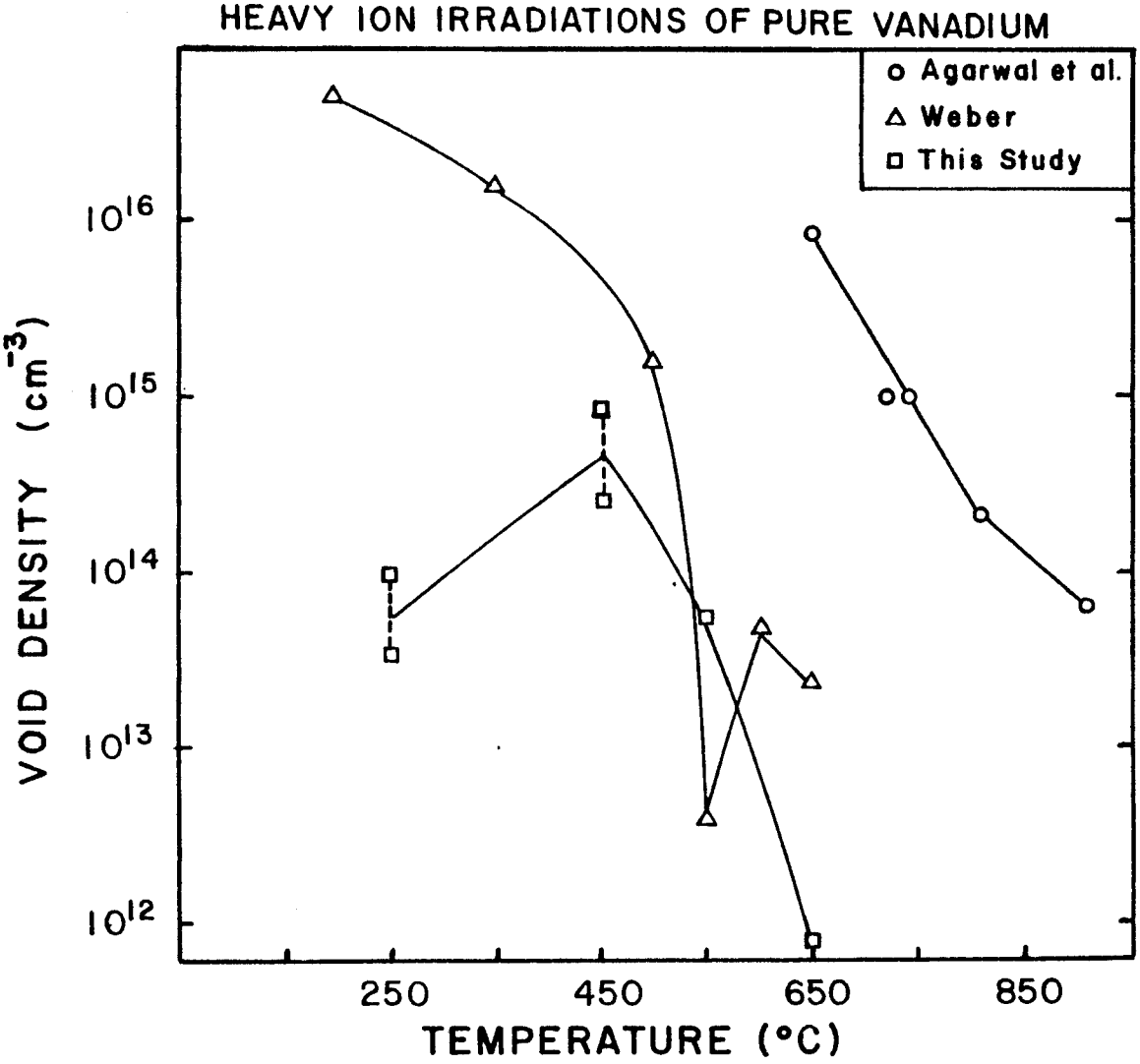

Figure VII-2. Comparison of void density measurements for heavy ion irradiations of pure vanadium. The dose rates for Agarwal et al.'s study,[99] Weber's study,[25] and this study were 5×10^{-3} dpa/sec, 2×10^{-4} dpa/sec and 5×10^{-4} dpa/sec respectively.

sible reasons for this discrepancy. First, the lower dpa rate in Weber's study may have shifted this effect to a lower temperature. Because this decrease in void density occurred so near the threshold temperature for void swelling, it may occur only in an extremely narrow temperature range at the lower dpa rate. The explanation for this low temperature decrease will be discussed in more detail in Section VII-C. The alternative explanation for this discrepancy is based on differences in the pre-irradiation treatment. The 200°C sample irradiated in Weber's study was outgassed at 850°C prior to irradiation. This relatively low outgassing temperature may have increased the void density through hydrogen assisted void nucleation.

Researchers at ANL studied void swelling at 20 dpa over the range 650°C to 875°C[99]. The void densities observed in this ANL study are compared to the University of Wisconsin studies in Figure VII-2. Although the void densities were higher in the ANL study, the temperature dependence was similar to the University of Wisconsin study. The higher void density can be attributed to the higher total dpa level and the higher dpa rate.

The observation of decreasing void density with increasing dose is not limited to this study. As illustrated in Figure VII-3, Agarwal et al.[98] have also observed a reduction in the void density in vanadium irradiated with vanadium ions up to 13 dpa. Between 13 and 24 dpa, a sudden increase in void density occurred, which coincided with the formation of precipitates. Even though the void density decreased up to 13 dpa, the swelling increased steadily with dose due to increases in the average void diameter.

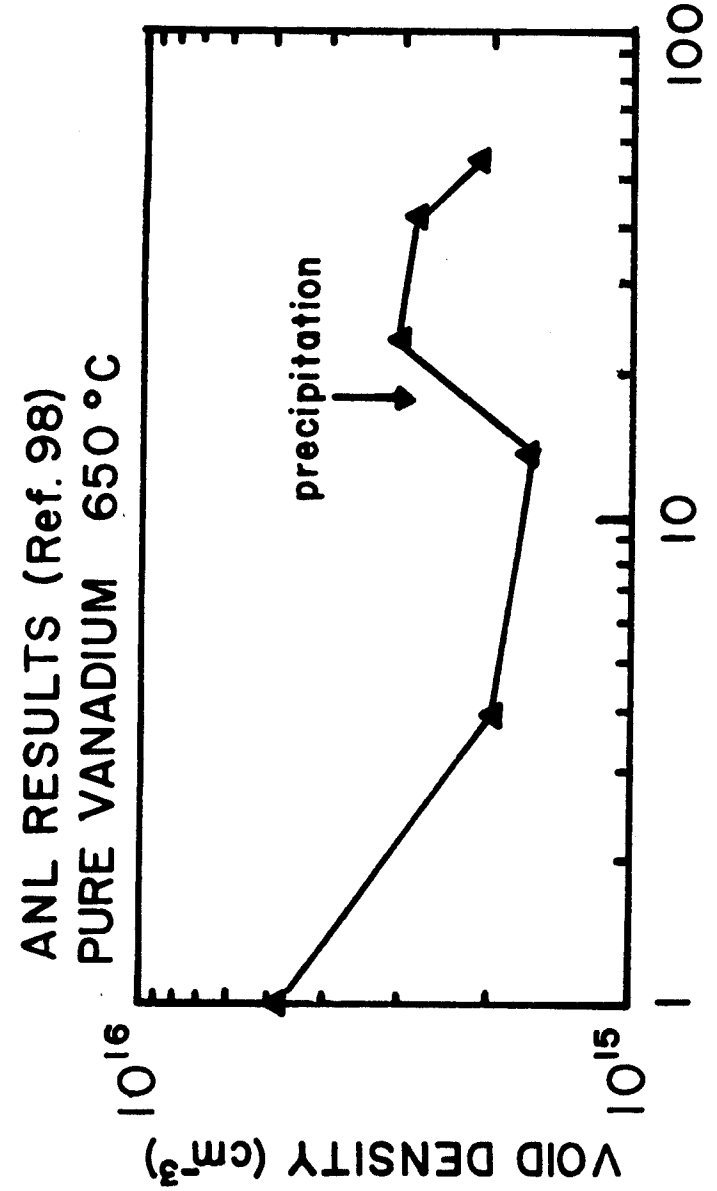

Figure VII-3. Decrease in void density with increasing dose observed by Agarwal, Potter and Taylor.[98] Samples were irradiated at 700°C with 3 MeV vanadium ions.

In a study of molybdenum and TZM (Mo, 0.5% Ti, 0.1% Zr), Evans[119] has also observed a reduction in void density, which produced a decrease in total swelling. In Evans' work, it was shown that this decrease occurred when the larger voids continued to grow and small voids shrank. This process must be more complicated than a simple coarsening phenomenon because it results in a significant decrease in the total void volume of the system. Evans attributed this phenomenon to the segregation of impurities to the voids, causing an effective preference of the voids for interstitials. This mechanism, which was originally proposed by Brailsford[57], is discussed in more detail in Section VII-C.

VII-B. Radiation Enhanced Precipitation

The formation of precipitates and the detection of nickel using the EDXA system indicate that low level nickel contamination is a continuing problem in the pure vanadium and vanadium 1% Ni specimens. The original observations of solute segregation were made in the V-Ni system, and it is not surprising that precipitation was seen at extremely low Ni concentrations. This observation is consistent with the solute drag mechanism originally proposed for this system by Okamoto et al.[51].

Two types of nickel precipitates were observed on (012) planes in the nickel contaminated specimen irradiated at 350°C. This specimen exhibited a similar morphology to the precipitates observed at 550°C and 600°C by Weber. These (012) precipitates did not assist the void nucleation process.

In the V-1% Ni samples, a coherent precipitate was formed prior to the development of the second incoherent phase. The observation of abnormally large strain fields around dislocations in the early stages of precipitation indicates that solute drag to point defect sinks assisted in the precipitation process. Although this precipitate has not been previously observed, it should not be assumed that it is a non-equilibrium precipitate since no data exists on phase equilibria in this temperature range for the V-1% Ni alloy. It is possible for irradiation enhanced diffusion to produce precipitates which would require extremely long times to form thermally.

VII-C. Void Growth Effects

The void growth rates for vanadium were calculated using the rate theory of void swelling[46]. Equation 2-38 can be rewritten to give the rate of change of void radius, r_v:

$$\frac{dr_v}{dt} = (D_v C_v - D_i C_i - D_v \bar{C}_v) \frac{1}{r_v} \qquad (7\text{-}1)$$

The vacancy and interstitial concentrations were determined from equation 2-30 and 2-31. Unfortunately, none of the point defect parameters necessary for this calculation have been measured in vanadium.

The most important parameters in determining the temperature dependence of swelling are the vacancy migration energy, E_m^v, and vacancy formation energy, E_f^v. The self diffusion energy for vanadium is 3.2 eV as measured by Peart[120] and Pelleg[121]. This energy should be equal to the sum of the vacancy formation energy and the

the vacancy migration energy. Schultz[122] has calculated the vacancy migration energy to be 0.6 eV. This value was used by Agarwal, Potter and Taylor[102] to calculate swelling rates with reasonable success. For these calculations, the vacancy formation energy and vacancy migration energy were assumed to be 2.6 eV and 0.6 eV respectively. The estimates which were made for the other point defect parameters are listed in Table VII-1.

Void growth rates were calculated for displacements rates typical of Weber's irradiations (1×10^{-4} dpa/sec), the ANL irradiations (5×10^{-3} dpa/sec) and this study's irradiations (5×10^{-4} dpa/sec). The 20% bias factor used in these calculations is required for the particular form of void nucleation theory used in Section VII-D. This relatively high bias factor was used in the void growth rate calculations for consistency. The dislocation sink density used for all of these calculations was $1 \times 10^{9}/cm^{2}$. This sink density was typical of the two University of Wisconsin studies but an order of magnitude lower than the sink density used by Aragwal, Potter and Taylor.[102] In order to compare these results on a common basis, the void growth rates plotted in Figure VII-4 have been expressed in units of Å/dpa for a 20 Å void radius.

The void growth rates calculated by this method are too high to be physically reasonable and this discrepancy is too large to be attributed to the high interstitial bias factor used for the calculations. This problem could also be resolved by incorporating into the calculations the effects of direct recombination in the displacement cascade and the effects of sub-microscopic point defect clus-

Table VII-1 Parameters for Void Growth Calculations

MATERIAL PARAMETERS		
Vacancy migration energy	E_m^v	= 0.6 eV
Vacancy diffusion pre-exponential	D_v^0	= 0.5 cm^2/sec
Vacancy formation energy	E_f^v	= 2.6 eV
Interstitial migration energy	E_m^i	= 0.1 eV
Interstitial diffusion pre-exponential	D_i^0	= 0.1 cm^2/sec
Surface energy	γ	= 1600 $ergs/cm^2$
IRRADIATION PARAMETERS		
Recombination coefficient	α	= $10^{17}/D_i$
Dislocation sink strength	k_l^2	= $10^9/cm^2$
Dislocation bias	Z	= 20%

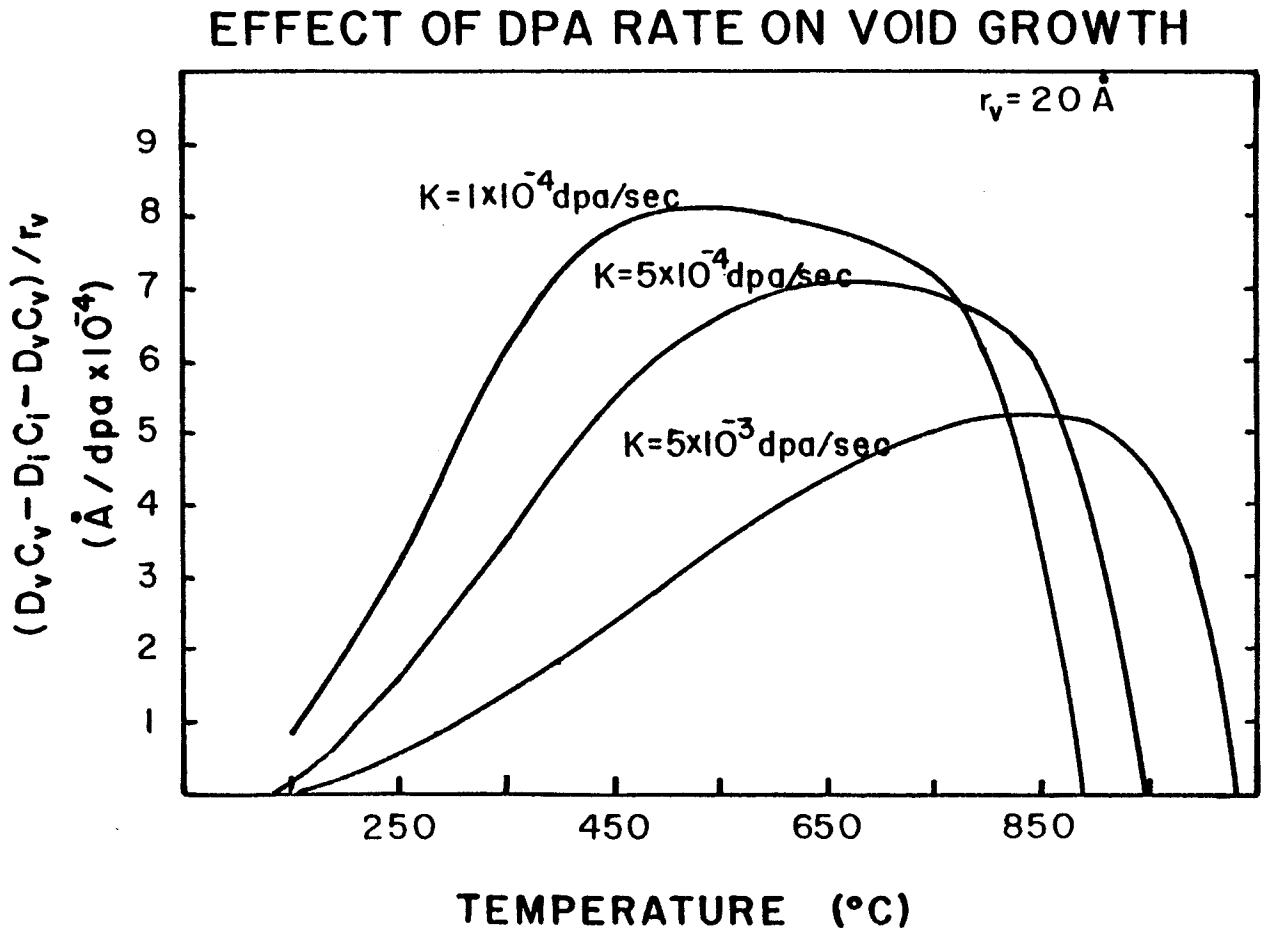

Figure VII-4. Calculated void growth rates for displacement rates typical of the ANL studies (5×10^{-3} dpa/sec), Weber's study (1×10^{-4} dpa/sec) and this study (5×10^{-4}dpa/sec). The low temperature swelling limit observed in Weber's study[25] and this study is predicted by this calculation. Parameters used in this calculation are listed in Table VII-1.

ters, which can act as recombination centers. Any truly quantitative calculation would have to include these effects. However, for the purposes of this discussion, it will be sufficient to compare the relative magnitude and temperature dependence of the curves in Figure VII-4.

This void growth model predicts a low temperature cut off in swelling between 100°C and 250°C, depending on the displacement rate. There is also a temperature shift of swelling to higher temperatures with higher displacement rates as predicted by Brailsford and Bullough[46]. The broad temperature range of swelling is determined by the low vacancy migration energy, which extends the curves to relatively low temperatures, and the high vacancy formation energy, which extends the high temperature swelling limit.

These calculations correctly predict the low temperature swelling observed in this study and in Weber's study. For the ANL studies, which were conducted at a higher dpa rate, the low temperature threshold should have occurred near 250°C. However, no irradiations were performed by the ANL researchers in this temperature range.

The high temperature limit determined from these calculations exceeds the temperatures where voids were observed in any of these three studies. In the void growth model, the high temperature limit is determined by the vacancy evaporation rate from the void, which is a strong function of void size. It would be expected that the upper temperature limit would be determined by the void nucleation rate, which is extremely sensitive to vacancy evaporation from small void nuclei. That this is the case is demonstrated in Section VII-D.

The reduction in void density caused by void shrinkage requires the reversal of the void growth rate. All of the studies where this reversal has been observed were conducted at temperatures where the vacancy evaporation rates were negligible. Therefore, there must be a mechanism which causes the interstitial arrival rate at a void to be higher than the vacancy arrival rate. This mechanism must not operate in the early stages of swelling, where positive void growth rates were observed, but must become predominant at higher doses. This would be the case if a new generation of point defect sinks, which has a net bias for vacancies, developed during the irradiation. However, no sink of this form has been previously postulated, and no new types of point defect sinks were observed in any of these studies.

Void shrinkage may also occur when a coating forms on a void. If the coating were established by solute drag to the void, it could develop through the course of the irradiation. The process of void growth will be reversed if the void coating serves as a barrier to vacancy diffusion into the void and if this barrier is sufficiently large to override the bias of the system. The effect of void coatings as described by Brailsford[57] is discussed in Section II-D. For a coated void, the void growth rate is governed by Equation 2-43, which may be rewritten in terms of the void radius r_v to give

$$\frac{dr_v}{dt} = (W_v D_v C_V - W_i D_i C_i - D_v \bar{C}_V) \frac{1}{r_v} \qquad (7\text{-}2)$$

The terms W_v and W_i, which are defined in Equation 2-44, describe the efficiency of the barrier in inhibiting vacancy and interstitial dif-

fusion into the void. Void shrinkage will occur when the ratio W_i/W_v is greater than the system bias.

Brailsford[57] describes the vacancy barrier in terms of the vacancy diffusion coefficient in the void coating, D_v^c. Using the void growth model described above, the effect of a 10 Å thick void coating, which provides no barrier to interstitial diffusion ($W_i = 1$) but increases the vacancy migration energy by 0.1 eV, was evaluated. The results of these calculations are compared to the bare void growth rates in Figure VII-5. This model predicts that the void coating will cause the smaller voids to shrink, while the larger voids will grow at a reduced rate. This result is consistent with Evans'[119] observation of shrinkage in the lower portion of the void size distribution. In the present study extremely large voids (>500 Å radius) exhibited negative void growth rates. To explain this shrinkage in large voids, the vacancy migration energy must be increased by 0.17 eV.

The trapping of vacancies by impurities affects both void growth and void nucleation. To assess these effects, a computer program was written to calculate vacancy and interstitial concentrations in a material containing vacancy traps. The theoretical basis of this program is explained in Section II-D. The results of this program were then used to calculate void growth rates and void nucleation rates. Void nucleation is discussed in Section VII-D. The results of a void growth calculation including vacancy trapping are presented in Figure VII-6. For this study, a vacancy trap con-

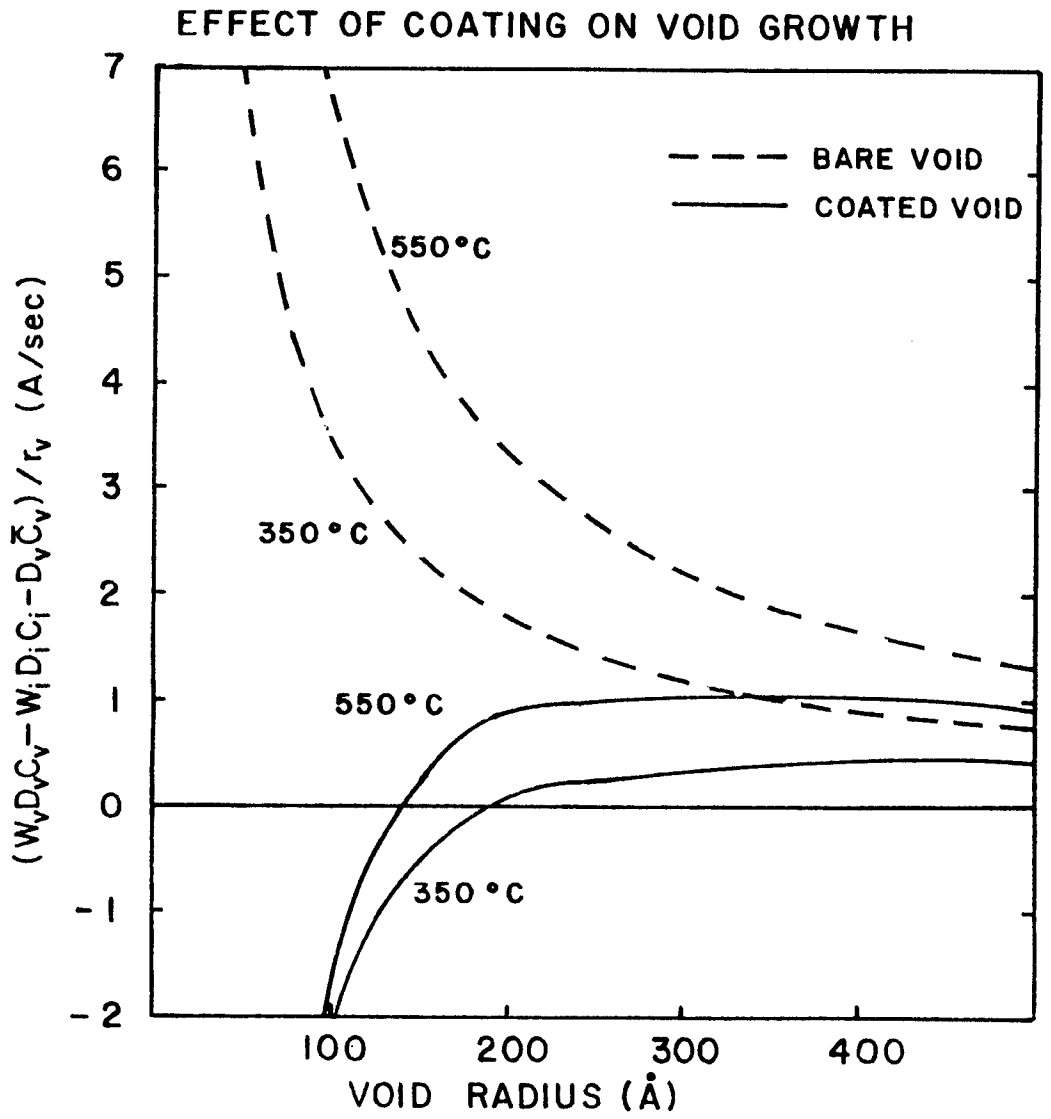

Figure VII-5. Effect of void coating on calculated void growth rate. Calculation based on Brailsford's model[57] (eq. 7-2). The void coating can cause shrinkage of small voids and a reduced void growth rate for large voids. The barrier to vacancy diffusion in the void coating was 0.1 eV for this calculation.

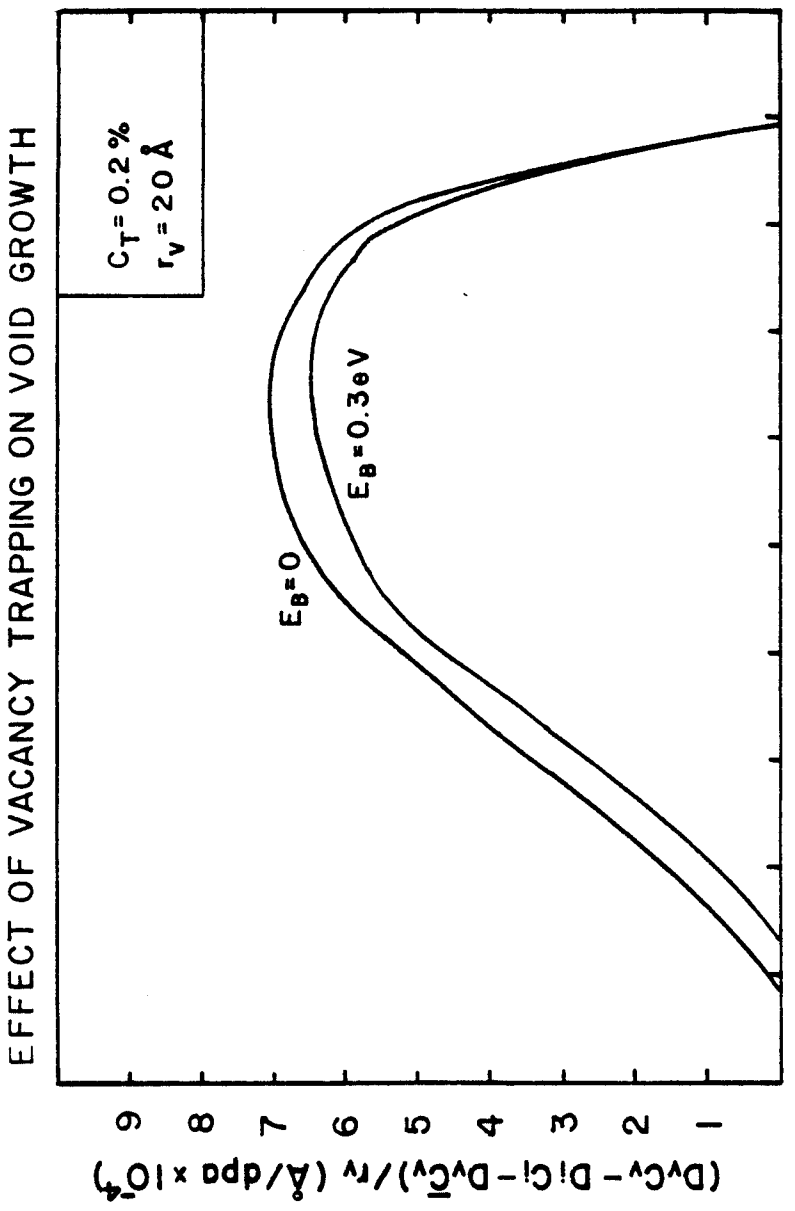

Figure VII-6. Effect of vacancy trapping on calculated void growth rate. A low density (0.2 at%) of strong (E_B = 0.3 eV) vancancy traps was used for this calculation. The other trap parameters are listed in Table VII-2.

centration of 0.2% and a vacancy binding energy of 0.3 eV were assumed. The vacancy trap parameters used in this calculation are listed in Table VII-2. Even at this relatively high vacancy trapping energy, the reduction in void growth is not significant. The greatest effects of vacancy trapping occur at the lower temperatures, where the void growth rate is already low.

VII-D. Void Nucleation Effects

The theory of homogeneous void nucleation in the absence of impurities is described in Section II-B. Two important versions of this theory have been developed. The first version, developed by Katz and Wiedersich[36] and Russell[37] (KWR) calculates the vacancy and interstitial arrival rates at a void using Equation 2-15, which is based on a surface reaction limited model. By assuming a diffusion limited model, Wolfer and Yoo[41] have developed an alternative theory, which uses Equation 2-16 to calculate the vacancy and interstitial arrival rates. These two theories then calculate the void nucleation rate using the logic outlined by Equations 2-12 and 2-14.

A computer program to calculate void nucleation rates, which will use either formulation of the point defect arrival rates, has been developed for this study. This calculation is totally consistent with the vacancy and interstitial concentrations calculated in the void growth model of Section VII-C. The void nucleation rate is extremely sensitive to the value of the surface energy used to calculate the formation enthalpy of small void nuclei. The value of 1600 ergs/cm^2 used in this study was chosen because it extrapo-

Table VII-2 Parameters for Vacancy Trapping Calculations

Trap concentration.	$C_T = 0.002$
Trap binding energy	$E_B = 0.3$ eV
Vacancy-empty trap combination coefficient.	$A_1 = 10^{17}/D_v$
Interstitial-empty trap combination coefficient . .	$A_2 = 2 \times 10^{17}/D_i$
Detrapping attempt rate	$F\nu = 10^{15}$/sec

lates to reasonable values of the divacancy binding energy. The KWR model requires no additional parameters.

The calculation of the void bias factors used in Wolfer's model requires additional point defect parameters and elastic constants for the material. The shear modulus and the Poisson's ratio have been measured for pure vanadium[123]. However, the point defect parameters have not been measured. For this calculation, the point defect parameters used by Wolfer and Yoo[41] for calculations in pure nickel were adjusted in a manner consistent with the more open BCC structure of the vanadium lattice. The material parameters used for the void nucleation calculation are listed in Table VII-3.

The bias factors for the void coating were adjusted to give reasonable values for the nucleation rate. Because of the definition of the void coating bias factor, large negative (<-1) values of the exponential terms E_I^* and E_V^* mean that there is no barrier in the void coating. A positive value for these exponential terms corresponds to a very large bias factor. For these calculations, it has been assumed that the void coating provides a barrier to interstitial accumulation (E_I^* = -0.075 eV) but no barrier to vacancy accumulation (E_V^* = -1.0). Without this void coating, the normal bias factors would prohibit void nucleation. This void coating has exactly the opposite effect as the void coating postulated to explain void shrinkage in Section VII-C.

The results of the calculations using the two different void nculeation models are compared in Figure VII-7. At high temperatures, the two models give similar results, predicting a high temperature limit of 650°C for homogeneous nucleation at a displacement rate of

Table VII-3 Parameters for Void Nucleation Calculations

Surface energy	$\gamma = 1600$ ergs/cm^2
Sheer modulus	$G = 4.7 \times 10^{11}$ dynes/cm^2
Poisson's ratio	$\nu = 0.35$
Vacancy relation volume	$(\frac{V}{\Omega})_v = -0.3$
Interstitial relaxation volume	$(\frac{V}{\Omega})_i = 1.1$
Vacancy polarizability	$\alpha_v = -7$
Interstitial polarizability	$\alpha_i = -70$
Void coating	$E_i^* = -0.075$ eV
	$E_v^* = -1.0$ eV

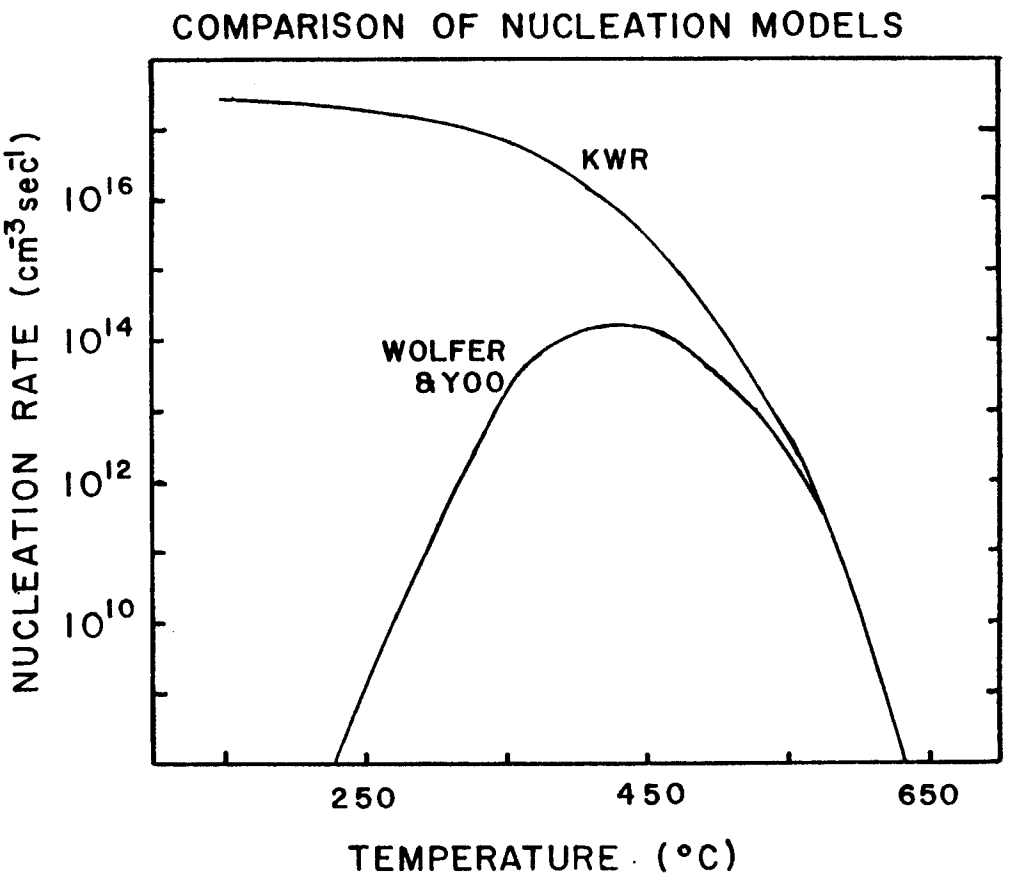

Figure VII-7. Comparison of nucleation models developed by Katz and Wiedersich[36] and Russell[37] and Wolfer and Yoo.[41] The parameters used for these calculations are listed in Table VII-3.

5×10^{-4} dpa/sec. This is important because the void growth calculations predicted much higher temperature limits to void swelling. The similarity between the two models in the high temperature region occurs because the high temperature cut off is determined by the vacancy evaporation rate from the void nuclei. However, at low temperatures, the KWR model predicts extremely high nucleation rates, while Wolfer and Yoo's model predicts a decrease in the void nucleation rate. In the KWR model, the critical void nucleus approaches the monovacancy at low temperatures and the low temperature swelling is limited by the void growth rate, which becomes prohibitively slow. The low temperature void nucleation limit in Wolfer and Yoo's model is a consequence of the temperature dependence of the void bias factors. At low temperatures, the void bias for interstitials becomes large enough to prohibit swelling.

In this study, a low temperature decrease in void density at 2.5 dpa was observed. At 250°C, the void density was lower and the average void size was larger than the corresponding sample at 450°C. This behavior is not predicted by the KWR model of void swelling. The model developed by Wolfer does predict a low temperature decrease in the void nucleation rate. The void nucleation rate decreases sharply in the low temperature region, while the void growth rate decreases more gradually. This combination of high void growth rate and decreased void nucleation rate is consistent with the observations at 250°C, 2.5 dpa. Although no conclusions can be drawn about the exact formulation of the void bias factor, this result in-

dicates that a void bias for interstitials, which increases at lower temperatures, does exist.

The temperature shift in swelling with increasing dose rates is also predicted by void nucleation theory. In Figure VII-8, calculations of the void nucleation rates at 5×10^{-4} dpa/sec and 5×10^{-3} dpa/sec are compared. Although the high temperature limit is slightly low, the temperature range of void nucleation at 5×10^{-4} dpa/sec matches the temperature range of swelling observed in this study. The voids observed at 650°C in this study were generally associated with precipitates, suggesting that they had nucleated heterogeneously. The temperature shift predicted from the calculated nucleation rates is not large enough to explain the observation of voids at temperatures in excess of 750°C in the ANL study[99]. Precipitation on void surfaces was reported in the sample irradiated at 880°C, again indicating that hetergeneous void nucleation may be important at higher temperatures in vanadium.

A number of mechanisms have been suggested to explain the suppression of homogeneous void nucleation by nitrogen and nickel solutes in vanadium. Five different mechanisms, which are described in Section II-D, have been incorporated into the void nucleation model. Calculations were made to evaluate the potential of each mechanism for the suppression of void nucleation in vanadium. These five mechanisms are: (1) the trapping of vacancies by solute atom clusters; (2) a decrease in the bias of the system for interstitials; (3) an increase in the shear modulus of the bulk material; (4) a decrease in the barrier to interstitial diffusion in the void coating,

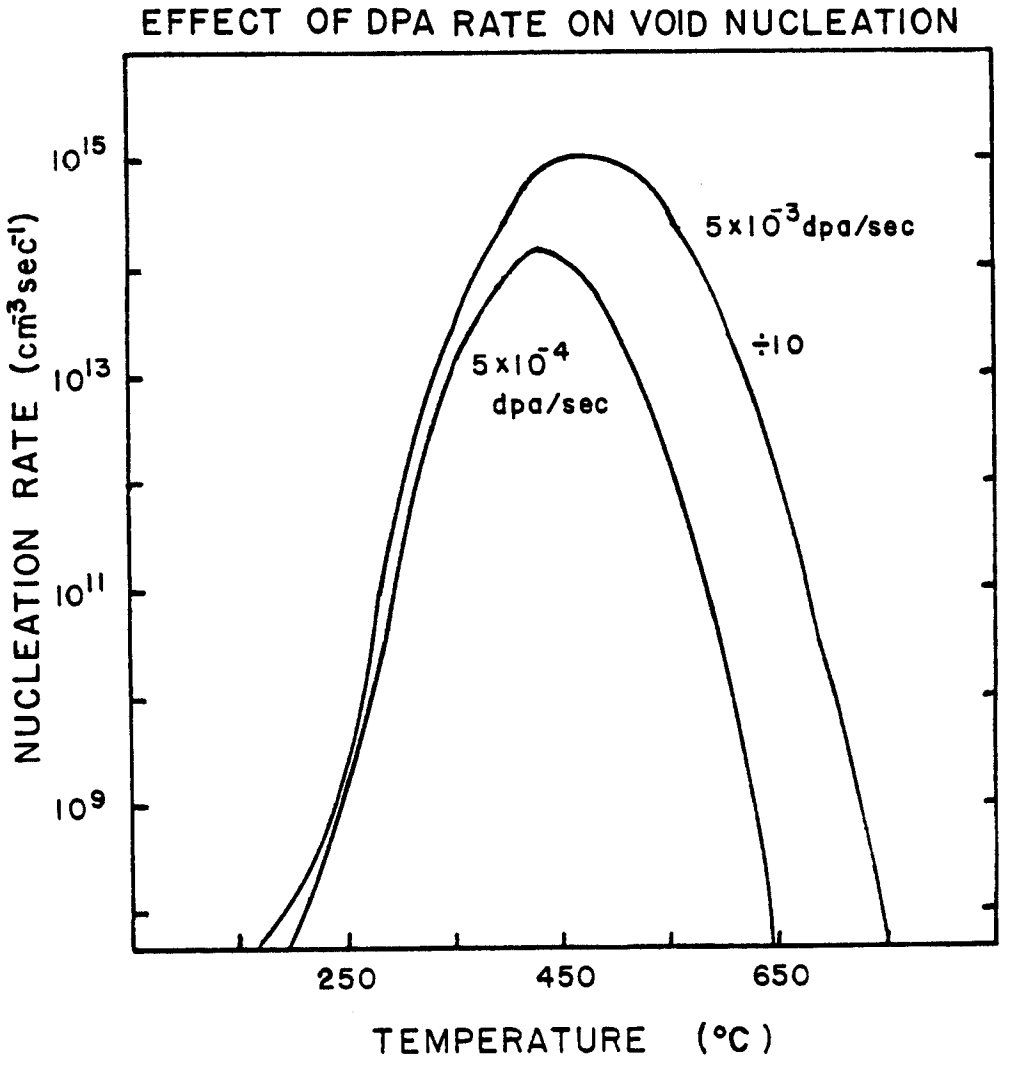

Figure VII-8. Effect of displacement rate on calculated void nucleation rate as predicted by model of Wolfer and Yoo.[41] This calculation predicts the observed high temperature limit for void swelling.

and; (5) an increase in the void surface energy. The results of each of these calculations are presented in Figure VII-9.

The observed suppression of void nucleation in vanadium containing nitrogen and nickel solutes cannot be explained by vacancy trapping or an increase in the shear modulus. Although a reduction in the system bias may explain this suppression of void nucleation, a relatively large reduction is required. On the other hand, relatively small changes in the void coatings or the void surface energy are sufficient to explain the observed phenomenon. It is interesting to note that these latter two mechanisms may be related as both arise from the segregation of solute atoms to the void surface.

VII-E. Conclusions

In vanadium irradiated by copper ions at 450°C and 550°C, voids formed easily and grew rapidly at doses below 2.5 dpa. At higher doses, a reduction in void density, as a result of void shrinkage, was observed. This is not an isolated observation. Reductions in void density with increasing dose have been observed in both heavy ion irradiated vanadium[98] and neutron irradiated molybdenum[119]. A mechanism which produces an effective void bias for interstitials is required to explain these observations. The only mechanism proposed in the literature of radiation damage which could produce this effect is the formation of a void coating by solute segregation. A coating which inhibits vacancy diffusion to the void can reverse void growth. Void coatings and solute segregation to voids were ob-

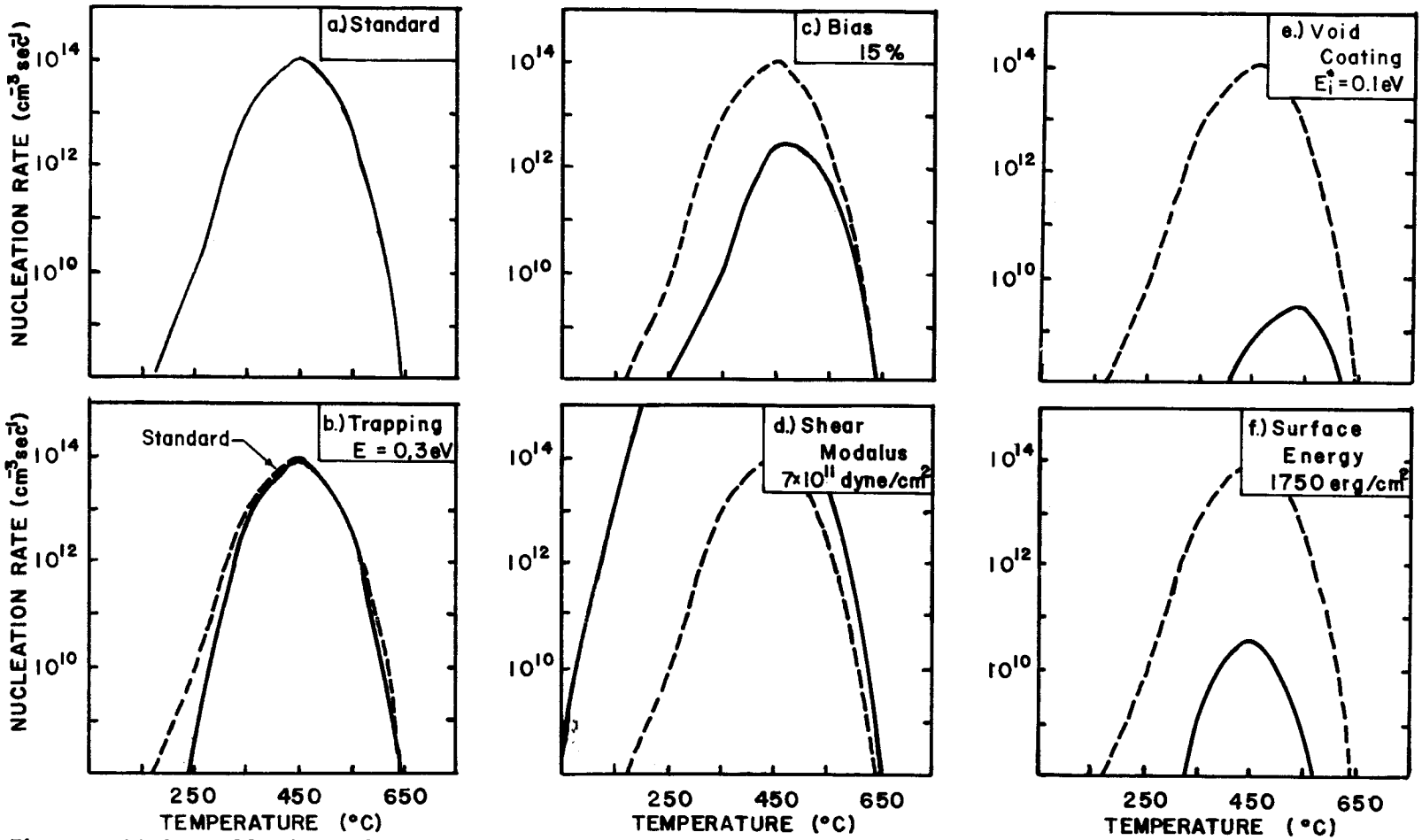

Figure VII-9. Alloying effects on calculated void nucleation rates. The different cases considered are: (a) Standard based on parameters in Table VII-3, (b) Vacancy trapping based on parameters listed in Table VII-2, (c) Reduced bias of sinks for interstitials, (d) Increase in shear modulus, (e) Void coating producing a decreased barrier for interstitial migration to void, and (f) Increase in void surface energy.

served in this study and in studies at Argonne National Laboratory[51]. Based on the theory developed by Brailsford[57], it is demonstrated in this thesis that only a small barrier to vacancy diffusion in a relatively thin void coating is required to explain void shrinkage in vanadium.

Two models for homogeneous void nucleation have been proposed. Although it is not possible to make any conclusive statements about the relative merits of these two models, some insight may be gained by comparing them on the basis of these irradiations. The first model, proposed by Katz and Wiederisch[36] and Russell[37] (KWR), assumes that voids are unbiased sinks. The second model, proposed by Wolfer and Yoo[41], is based on calculations of bias factors of small voids for interstitials. Either of these models may be used to satisfactorily explain the high temperature limit to void swelling. In this study, a low temperature decrease in void nucleation was observed at 250°C, 2.5 dpa. This observation can be explained on the basis of Wolfer's model, but not on the basis of the KWR model as it is presently developed. If Wolfer's calculation of the void bias factors are used, the formation of a void coating which inhibits interstitial diffusion to the void must be postulated. The effect of this void coating is the exact opposite of the effect of the void coating required to explain void shrinkage. This would indicate that either the void bias factors calculated by Wolfer's theory are too large or that more than one type of void coating can form during the course of an irradiation.

Both Ni and N were observed to suppress homogeneous void nucleation in vanadium. Wolfer's model of homogeneous void nucleation was used to evaluate the potential of several different mechanisms for suppressing void nucleation. An increase in the shear modulus increases void nucleation, and vacancy trapping does not produce a significant reduction. A factor of two reduction in the dislocation bias could explain the suppression of void nucleation. The segregation of solutes to the dislocations might produce this reduced bias. However, the homogeneous void nucleation rate is extremely sensitive to changes in the void surface energy or the bias produced by the void coating. A slight increase in either of these parameters is sufficient to completely suppress void nucleation. Although the void surface energy and the void coating enter the equations in different ways, they both have a drastic effect on the void nucleation rate and they both arise from solute segregation.

The correlation in the V-1% Ni alloy between the formation of coherent precipitates and the increase in void density is attributed to heterogeneous void nucleation. The incubation dose for void nucleation observed in the V-1% Ni alloy is determined by the dose required to form incoherent precipitates. In the pure vanadium irradiations, voids were often associated with small precipitates at the higher temperatures, where homogeneous nucleation theory predicts extremely low nucleation rates. This suggests that heterogeneous nucleation can also be important in pure vanadium.

Precipitation in the V-1% Ni alloy was observed to follow a sequence, leading from coherent precipitates to incoherent precipitates.

In the early stages of precipitation, extremely large strain fields around dislocations were observed. This segregation led to the formation of large thin discs of precipitate resembling faulted dislocation loops. At higher doses and lower temperatures, incoherent precipitates were observed. These incoherent precipitates were identical to those observed by Weber in Ni contaminated vanadium. These precipitates have never been reported in unirradiated vanadium. Because the initial stages of precipitation are related to solute segregation to dislocations, it is believed that this precipitation phenomenon is assisted by solute drag.

It is clear that the solute segregation phenomenon is extremely important in interpreting the results of void formation studies in vanadium. Phenomena arising from solute segregation effects have been suggested to explain void shrinkage in pure vanadium, the suppression of void nucleation in V-1% N and V-1% Ni and radiation enhanced precipitation in V-1% Ni. In addition, the homogeneous nucleation model proposed by Wolfer and Yoo[41] requires the segregation of solutes to small void nuclei. In this study, some evidence for solute segregation to voids was observed. Solute segregation under irradiation was also observed in the V-Ni system at Argonne National laboratory[51]. These results may be attributed to a solute drag mechanism. This thesis indicates that solute segregation should be included in any model that is used to describe void formation in vanadium or vanadium alloys.

CHAPTER VIII SUMMARY

The primary objectives outlined for this study were:

(1) to evaluate previous results obtained in heavy ion irradiations of pure vanadium and extend them to higher doses;

(2) to study the effect of the addition of 1% nitrogen on void swelling in vanadium;

(3) to determine how a vanadium 1% nickel alloy behaves under irradiation.

These irradiations were performed using the University of Wisconsin Heavy Ion Irradiation Facility, which was designed and constructed as a part of this thesis project. The following observations were made as a result of these irradiations.

(1) The void density in pure vanadium irradiated at 450°C and 550°C decreases at doses above 5 dpa as a result of void shrinkage.

(2) At 250°C, a low temperature decrease in void density occurs in pure vanadium. The low temperature limit for swelling in vanadium at 5×10^{-4} dpa/sec is approximately 200°C.

(3) The addition of 1 at% nitrogen suppresses void nucleation in vanadium.

(4) Irradiation induced precipitation occurs in the vanadium-1 at% nickel alloy. The initial stages of precipitation produce regions of large strain contrast around dislocations. These coherent precipitates evolve into incoherent precipitates at higher doses. This process proceeds more rapidly

at lower temperatures.

(5) Void nucleation in vanadium 1 at% nickel occurs concurrently with the formation of incoherent precipitates. The time required for the formation of the incoherent precipitates corresponds to the incubation dose for void nucleation. The incubation dose for void nucleation in pure vanadium is less than 1 dpa.

These results were then compared to the predictions of calculations based on the rate theory of void growth and homogeneous void nucleation theory. The conclusions drawn from this comparison were as follows.

(1) Void shrinkage can result from the formation of a coating which inbibits vacancy diffusion to the void.

(2) The high temperature limit for void swelling in vanadium is determined by the void nucleation rate.

(3) The reduction in void nucleation rate at low temperatures can be explained by a temperature dependent void bias term.

(4) Nickel and nitrogen suppress homogeneous void nucleation in vanadium by segregating to the void surface. This segregation phenomenon may result in either an increase in the void surface energy or an increase in the effective bias of small voids for interstitials.

(5) Precipitates form on dislocations and other point defect sinks in the V-1% Ni alloy as a result of solute drag.

(6) Heterogeneous nucleation on incoherent precipitates in the V-1% Ni alloy produces high swelling at intermediate

dose levels.

(7) Any study of radiation damage in vanadium should include a consideration of the effects of solute segregation.

REFERENCES

1. G.A. Whitlow, R.A. Nadler and R.C. Svedberg, WARD 3791-47 (1970).

2. D.L. Harrod and R.E. Gold, Technical Information Center, Oak Ridge, TN, C00-45401-1 (1978).

3. T.F. Kassner and D.L. Smith, RDT Review Meeting on Vanadium Alloy Development, Washington D.C., April 1970.

4. D.L. Smith and K. Natesan, Nucl. Technol., 22, 392 (1974).

5. W.F. Vogelsang, G.L. Kulcinski, R.G. Lott and T.Y. Sung, Nucl. Technol., 22, 379 (1974).

6. R.C. Svedberg, J. Vac. Sci. Technol., 8, VM41 (1971).

7. R.S. Nelson and D.J. Mazey, Ref. 14, p. 157.

8. D.J. Mazey, J. Nucl. Mat., 35, 60 (1970).

9. D.W. Keefer, H.H. Neely, J.C. Robinson, A.G. Pard and D. Kramer, Ref. 17, p. 332.

10. G.L. Kulcinski, J.J. Laidler and D.G. Doran, Rad. Eff., 7, 195 (1971).

11. J. Lindhard, V. Nielsen and M. Scharff, Mat. Fys. Medd. Dan. Vid. Selsk., 37, No. 14 (1968).

12. J. Lindhard, M. Scharff and H.E. Schiott, Mat. Fys. Medd Dan. Vid. Selsk., 33, No. 14 (1963).

13. J. Lindhard, V. Nielsen, M. Scharff and P.V. Thomsen, Mat. Fys. Medd. Dan. Vid. Selsk., 33, No. 10 (1963).

14. Radiation Damage in Reactor Materials, II, IAEA Symposium Proceedings, Vienna, June 1969, STI-PUB-230 (1969).

15. Proceedings of BNES European Conf. on Voids Formed by Irradiation of Reactor Materials, ed. S.F. Pugh, N.H. Loretto and D.I.R. Norris, Reading U.K., March 1971.

16. Proceedings of the Int. Conf. on Radiation-Induced Voids in Metals, ed. J.W. Corbett and L.C. Ianniello, Albany, N.Y., June 1971, AEC Symposium Series, CONF-710601 (1972).

17. Proceedings of ASTM Conf. on Irradiation Effects on Structural Alloys for Nuclear Reactor Applications, Niagara Falls, N.Y., June 1970, ASTM-STP-484 (1971).

18. Proceedings of ASTM Conf. on Effects of Radiation on Substructural and Mechanical Properties of Metals and Alloys, Los Angeles, CA, June 1972, ASTM-STP-529 (1973).

19. Proceedings of Eighth Int. ASTM Symp. on The Effects of Radiation on Structural Materials, St. Louis, MO, May 1976.

20. Proceedings of 1973 Int. Conf. on Defects and Defect Clusters in BCC Metals and Their Alloys, ed. R.J. Arsenault, Gaithersburg, MD (1973).

21. Consultant Symposium on The Physics of Irradiation Produced Voids, ed. R.S. Nelson, Harwell, Oxfordshire, U.K., Sept. 1974, AERE-R7934 (1975).

22. Proceedings of Int. Conf. on Radiation Effects and Tritium Technology for Fusion Reactors, Gatlinburg, TN, Oct. 1975.

23. Proceedings of Int. Conf. on Radiation Effects in Breeder Reactor Structural Materials, AIME, Scottsdale, AZ, June 1977.

24. Proceedings of First Topical Meeting on Fusion Reactor Materials, Miami Beach, FL, January 1979. (To be published in J. Nucl. Mat.)

25. W.J. Weber, Ph.D. Thesis, University of Wisconsin-Madison (1977).

26. H.V. Smith Jr. and R.G. Lott, Nucl. Instr. and Meth., 143, 125 (1977).

27. R.G. Lott, G.L. Kulcinski, P. Wilkes and H.V. Smith Jr., Ref. 24.

28. G.H. Kinchen and R.S. Pease, Reports on Progress in Physics, 18, 1 (1975).

29. I.M. Torrens and M.T. Robinson, Interatomic Potentials and Simulation of Lattice Defects, ed. P.C. Gehlen, J.R. Beeler,Jr. and R.I. Jaffee, (Plenum Press, N.Y. 1972) p. 423.

30. C.Erginsoy, G.H. Vineyard and S. Shimizu, Phys. Rev., 139, A118 (1965).

31. J.R. Beeler, Jr., Phys. Rev., 150, 470 (1966).

32. M.G. Miller and R.L. Chaplin, Rad. Eff., 22, 107 (1974).

33. I. Manning and G.P. Mueller, Comp. Phys. Comm., 7, 85 (1974).

34. D.K. Brice, SAND 75-0622, Sandia Laboratories, Albuquerque, NM (1977).

35. H.I. Aaronson and J.K. Lee, Lectures on the Theory of Phase Transformations, ed. H.I. Aaronson, (The Metallurgical Society of AIME, NY, 1975) p. 83.

36. J.L. Katz and H. Wiedersich, J. Nucl. Mat., 46, 41 (1973).

37. K.C. Russell, Acta Met., 19, 753 (1971).

38. K.C. Russell and D.H. Hall, Ref. 20, p. 545.

39. U.L. Katz and H. Wiedersich, J. Chem. Phys., 55, 1414 (1971).

40. H. Wiedersich and J.L. Katz, Ref. 20, p. 530.

41. W.G. Wolfer and M.H. Yoo, Ref. 22, p. 11-458.

42. R. Bullough and R.C. Perrin, Ref. 15, p. 79.

43. R. Bullough and R.C. Perrin, Ref. 16, p. 769.

44. H. Wiedersich, Rad. Eff., 12, 111 (1972).

45. S.D. Harkness and Che-Yu Li, Met. Trans., 2, 1457 (1971).

46. A. D. Brailsford and R. Bullough, J. Nucl. Mat., 44, 121 (1972).

47. R. Bullough and R.C. Perrin, Ref. 17, p. 317.

48. R. Bullough, B.L. Eyre and K. Krishan, Proc. of the BNES Conf. on Irradiation Behavior of Fuel Cladding and Core Component Materials, Karlsruhe, Dec. 1974.

49. N.M. Ghoniem, Ph.D. Thesis, Univ. of Wisconsin-Madison (1977).

50. W.G. Wolfer, L.K. Mansur and J.A. Sprague, Ref. 23, p. 841.

51. P.R. Okamoto, A.T. Santhanam, H. Wiedersich and A. Taylor Nucl. Technol., 22, 45 (1974).

52. P.R. Okamoto and H. Wiedersich, Ref. 21, p. 231.

53. A.D. Brailsford, J. Nucl. Mat., 56, 7 (1975).

54. N.H. March and J.S. Rousseau, Crystal Lattice Defects, 2, 1 (1971).

55. D.I.R. Norris, Ref. 21, p. 134.

56. W.G. Wolfer, University of Wisconsin-Madison, private communication, 1979.

57. A.H. Cottrell and M.A. Jaswon, Proc. Roy. Soc., A199, 104 (1949).

58. D.I.R. Norris, Rad. Eff., 14, 1 (1972).

59. W. Schilling and K. Schroeder, Ref. 21, p. 212.

60. L.K. Mansur, Paper presented at Workshop on Solute Segregation and Phase Stability during Irradiation, Gatlinburg, TN (1978). (To be published J. Nucl. Mat.)

61. R.S. Nelson, J.A. Hudson and D.J. Mazey, J. Nucl. Mat., 44, 318 (1972).

62. P. Wilkes, University of Wisconsin-Madison, private communication, 1979.

63. K.C. Russell, Scripta Met., 3, 313 (1969).

64. P. Wilkes, K.Y. Liou and R.G. Lott, Rad. Eff., 29, 249 (1976).

65. P. Wilkes and K.Y. Liou, University of Wisconsin Fusion Design Memo, UWFDM-292 (1978).

66. E.R. Stevens and O.N. Carlson, Met. Trans., 1, 1267 (1970).

67. W. Rostoker and A. Yamamoto, Trans. ASM, 46, 1136 (1954).

68. A. Maldonado and K. Schubert, Z. Metallk., 55, 619 (1964).

69. S.T. Zegler and J.W. Downey, Trans. AIME, 227, 1407 (1963).

70. R.C. Ruhl, B.C. Giessen, M. Cohen and N.J. Grant, Mater. Sci. Eng., 2, 314 (1967/1968).

71. F.M. Monroe and J.R. Cost, Trans. TMS-AIME, 245, 1079 (1969).

72. J.L. Henry, S.A. O'Hare, R.A. McCune and M.P. Krug, J. Less-Common Metals, 25, 39 (1971).

73. G. Hörz, J. Less-Common Metals, 35, 207 (1974).

74. D.I. Potter, H.D. Epstein and B.M. Goldstein, Met. Trans., 5, 2075 (1974).

75. D.I. Potter, J. Less-Common Metals, 31, 299 (1973).

76. D.I. Potter and C. Altstetter, Mater. Sci. Eng., 9, 43 (1972).

77. D.I. Potter and C. Altstetter, Acta. Met., 20, 313 (1972).

78. G. Brauer and W.D. Schnell, J. Less-Common Metals, 6, 326 (1964).

79. F.W. Wiffen and J.O. Stiegler, J. Metals, 20, 117A (1968).

80. F.W. Wiffen and J.O. Stiegler, USAEC Rpts. ORNL-4330 (1968) p. 195; and ORNL-4420 (1969) p. 151.

81. F.W. Wiffen, Ref. 16, p. 386.

82. J.D. Elen, Microscopic Electronique 1970, Vol. II, Proc. VII Int. Conf. on Electron Microscopy, Grenoble, August 1970, p. 351.

83. J.D. Elen, Ref. 15, p. 51.

84. J.D. Elen, G. Hamburg and A. Mastenbroek, J. Nucl. Mat., 39, 194 (1971).

85. Y. Adda, Ref. 16, p. 31.

86. J.L. Brimhall, H.E. Kissinger and G.L. Kulcinski, Ref. 16, p. 338.

87. R. Carlander, S.D. Harkness and A.T. Santhanam, Ref. 18, p. 399.

88. A.F. Bartlett, J.H. Evans, B.L. Eyre, E.A. Terry and T.M. Williams, Ref. 22, p. I-122.

89. J. Bressers and M. Cambini, J. Nucl. Mat., 68, 250 (1977).

90. J. Bressers and W. van Witzenburg, Ref. 24 (to be published in J. Nucl. Mat.).

91. J. Bentley and F.W. Wiffen, Nucl. Technol., 30, 376 (1976).

92. G.L. Kulcinski and J.L. Brimhall, BNWL-1604, 80 (1971).

93. J.L. Brimhall, American Institute of Mining and Metallurgical Engineers' Fall Meeting, Detroit, Oct. 1974.

94. J.L. Brimhall and E.P. Simonen, Nucl. Technol., 29, 378 (1976).

95. A.T. Santhanam, Proceedings of the Fifth Symposium on Engineering Problems of Fusion Research, Princeton, NJ, Nov. 1973 p. 54.

96. A.T. Santhanam, A. Taylor and S.D. Harkness, Ref. 20, p. 302.

97. A.T. Santhanam, A.Taylor, B.J. Kestel and C. Steves, J. Vac. Sci. Technol., 12, 528 (1975).

98. S.C. Agarwal and A. Taylor, Ref. 22, p. I-150.

99. S.C. Agarwal, D.I. Potter and A. Taylor, Ref. 19, p. 298.

100. A. T. Santhanam, A. Taylor and S.D. Harkness, Paper presented at CTR Neutron Radiation Damage Coordination Meeting, Germantown, MD (1972).

101. S.C. Agarwal and A. Taylor, Proc. of Sec. Topical Meeting on The Technolgoy of Controlled Nuclear Fusion, Richland, WA, Sept. 1976, CONF-760935 p. III-949.

102. S.C. Agarwal, D.I. Potter and A. Taylor, Met. Trans., 9A, 569 (1978).

103. W.J. Weber, G.L. Kulcinski, R.G. Lott, P. Wilkes and H.V. Smith Jr., Ref. 22, p. I-130.

104. W.J. Weber, G.L. Kulcinski, H.V. Smith Jr. and P. Wilkes, Trans. Am. Nucl. Soc., 26, 182 (1977).

105. K. Ehrlich and D. Kaletta, Ref. 22, p. II-289.

106. The author wishes to acknowledge the work of Dr. R.E. Reed who provided the high purity vanadium stock for this study.

107. The author wishes to thank Dr. P. Okamoto of Argonne National laboratory for providing the V-1% Ni alloy.

108. The author wishes to thank Dr. D.I. Potter of Argonne National Laboratory for his assistance in preparing the V-1% N samples.

109. J.B. Whitley, Ph.D. Thesis, University of Wisconsin-Madison (1978).

110. H.V. Smith, Jr. and H.T. Richards, Nucl. Instr. and Meth., 125, 497 (1975).

111. J.H. Billen and H.T. Richards, Proc. of Symp. of Northeastern Accelerator Personnel, Oak Ridge National Laboratory, Oct. 1978, p. 137.

112. Proposed New Standard Recommended Practice for Neutron Radiation Damage Simulation by Charged Particale Irradiation, E521-00, (Prepared under the jurisdiction of ASTM Committee E-10) (1974).

113. J.M. Freeman and B.W. Hooton, Nucl. Instr. and Meth., 111, 501 (1973).

114. D.G. Westlake and W.R. Gray, Applied Physics Letters, 9, 3 (1966).

115. R.A. Spurling and C. Rhodes, J. Nucl. Mat., 44, 341 (1972).

116. The author wishes to recognize the work of Dr. S. Dahlgren and co-workers at Battelle Northwest Laboratory, who performed the sputter deposition of the vanadium specimens.

117. Thermophysical Properties of High Temperature Solid Materials, Y.S. Touloukian, Ed., 1, 720 (1967).

118. L.E. Rehn, S.C. Agarwal and F.V. Nolfi, Jr., Ref. 24, (to be published in J. Nucl. Mat.).

119. J.H. Evans to be published.

120. R.F. Peat, J. Phys. Chem. Solids, 26, 1853 (1965).

121. J. Pelleg, Phil. Mag., 29, 383 (1974).

122. H. Schultz, Scripta Met., 8, 721 (1974).

123. D.I. Bolef, J. Appl. Phys., 32, 100 (1961).